Optical Fusion Assay Based on Membrane-Coated Beads in a 2D Assembly

Dissertation

for the award of the degree
"Doctor rerum naturalium"
of the Georg-August-Universität Göttingen

within the doctoral program of chemistry
of the Georg-August University School of Science (GAUSS)

submitted by

Chunxiao Bao

from China

Göttingen, 2014

Thesis Committee

Prof. Dr. Andreas Janshoff
Institute of Physical Chemistry, Georg-August-Universität Göttingen

Prof. Dr. Philipp Vana
Institute of Physical Chemistry, Georg-August-Universität Göttingen

Members of the Examination Board

Reviewer: Prof. Dr. Andreas Janshoff
Institute of Physical Chemistry, Georg-August-Universität Göttingen

Second reviewer: Prof. Dr. Philipp Vana
Institute of Physical Chemistry, Georg-August-Universität Göttingen

Further members of the Examination Board

Prof. Dr. Burkhard Geil
Institute of Physical Chemistry, Georg-August-Universität Göttingen

Prof. Dr. Ulf Diederichsen
Institute of Organic and Bimolecular Chemistry, Georg-August-Universität Göttingen

Prof. Dr. Bert de Groot
Max Planck Institute for Biophysical Chemistry

Dr. Thomas Burg
Max Planck Institute for Biophysical Chemistry

Date of the oral examination: 2014-04-02

TABLE OF CONTENTS

1 INTRODUCTION

1.1 MEMBRANE FUSION

Membrane fusion, a key process in the life of eukaryotic cells, undergoes docking (outer bilayer leaflets contact), hemifusion (outer bilayer leaflets merge while inner leaflet membranes contact) and full fusion (both outer and inner bilayer leaflet merge resulting a continuous bilayer).[1-4] In this section, the basic definitions and functions of biological membranes are introduced followed by explaining the fundamental mechanism of membrane fusion.

1.1.1 LIPID BILAYER AND MEMBRANE[5, 6]

The cell membrane is a crucial part of the cell, which contains outer plasma membrane and internal membrane.[7-9] The plasma membrane defines the boundaries of the cell and physically separates the intracellular components from the extracellular environment. Inside the eukaryotic cell, the membrane of various organelles, such as Golgi apparatus and mitochondria, maintains their own functions, as well as the difference between the inner contents of the organelle and the outer cytosol (Figure 1-1a).[10-12] Despite their different functions, all biological membranes have the same common basic composition: a very thin film of lipid bilayer and associate proteins (Figure 1-1b).[8, 9] The lipid bilayer provides the basic fluid and dynamic structure of the biological membranes, while the membrane proteins are responsible for all the specialized biological activities, for example, catalyzing the membrane fusion process.

The lipid bilayer forms through the process of lipid assembly. Lipids (Greek *lipos* = fat) are amphiphilic molecules, which contain a hydrophilic (“water-loving”) head and a hydrophobic (“water-fearing”) tail, thus they are soluble in organic solvents such as chloroform and methanol but are only sparingly soluble in water.

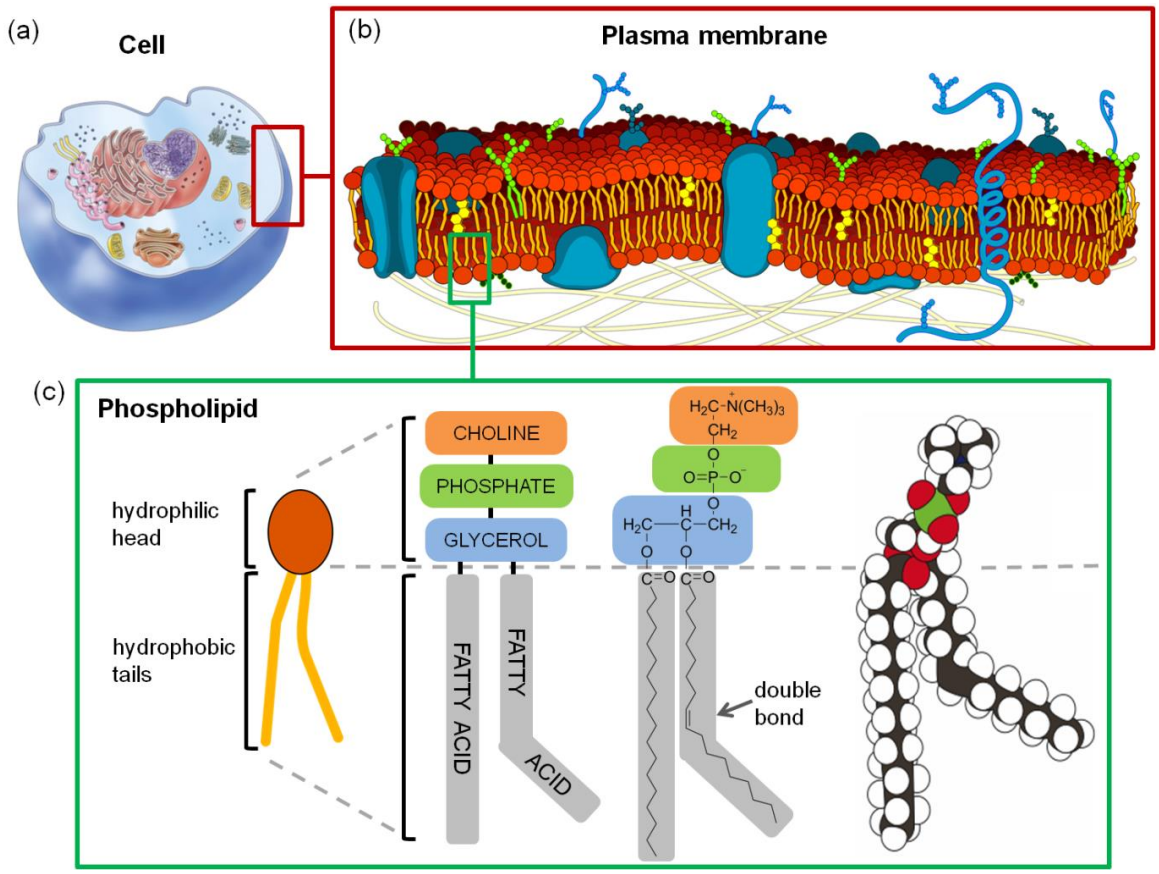

Figure 1-1 Schematic representation of a eukaryotic cell membrane (here refers to plasma membrane). (a) The anatomy of an animal cell.[1] (b) A detailed diagram of the plasma membrane mainly including a lipid bilayer and various membrane associated proteins. The polar head groups (orange) separate the nonpolar tails (yellow) from extracellular environments.[2] (c) The parts of phosphatidylcholine as an example of a phospholipid, represented as a symbol, schematically, by formula, as a space-filling model respectively (from left to right).[3]

The cell membrane consists of three kinds of lipids: phospholipids, glycolipids, and sterols, in which phospholipids are the most abundant ones.[13] The four major phospholipids in the plasma membrane are phosphatidylcholine (PC), phosphatidylethanolamine (PE), phosphatidylserine (PS), and sphingomyelin. Figure 1-1c shows the detailed structure of PC with different ways as an example of phospholipids.

[1] Figure 1-1a is taken from http://thescienceclassroom.org/wp-content/uploads/2013/02/Animal_cell_by_monstara.jpg.
[2] Figure 1-1b is taken from http://www.frontiers-in-genetics.org/pictures/cell-membrane_1.gif.
[3] Figure 1-1c is redrawn from Alberts, B., Bray, D., and Lewis, J. (2002) *Molecular biology of the cell*, P585

Most phospholipids have a phosphate head group and two hydrocarbon tails. The tails are usually fatty acids containing 14 to 24 carbons with/without *cis*-double bonds. Both of the length (number of carbons) and the degree of saturation of the fatty acid influence the fluidity of a bilayer hence the characteristic phase transition temperature (T_m), which is defined as the temperature required to induce a transition of a bilayer from the ordered gel phase to crystalline liquid phase (Table 1-1).[14] A shorter fatty acid reduces the interaction between tails and *cis*-double bonds produce kinks that disrupts the package of lipids, so that bilayer remain fluid as lower temperature.

Table 1-1 Phase transition temperature (T_m) of common used PC lipids influenced by length and degree of saturation of fatty acids.[4]

Name, abbreviation and chemical structure	Saturation	T_m / °C
1,2-dioleoyl-*sn*-glycero-3-phosphocholine (DOPC) 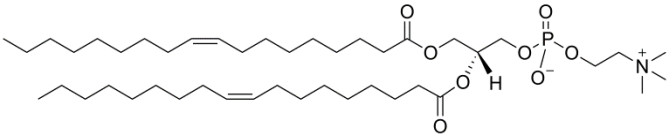	18:1 18:1	-20
1-palmitoyl-2-oleoyl-*sn*-glycero-3-phosphocholine (POPC) 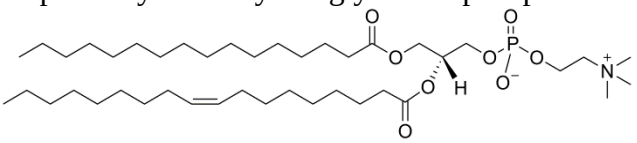	16:0 18:1	-2
1,2-dimyristoyl-*sn*-glycero-3-phosphocholine (DMPC) 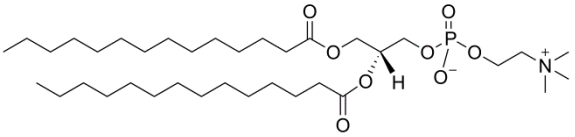	14:0 14:0	23
1,2-dipalmitoyl-*sn*-glycero-3-phosphocholine (DPPC) 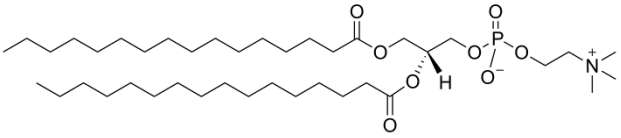	16:0 16:0	41

[4] The phase transition temperatures are extracted from http://www.avantilipids.com.

1.1.2 MECHANISM OF MEMBRANE FUSION

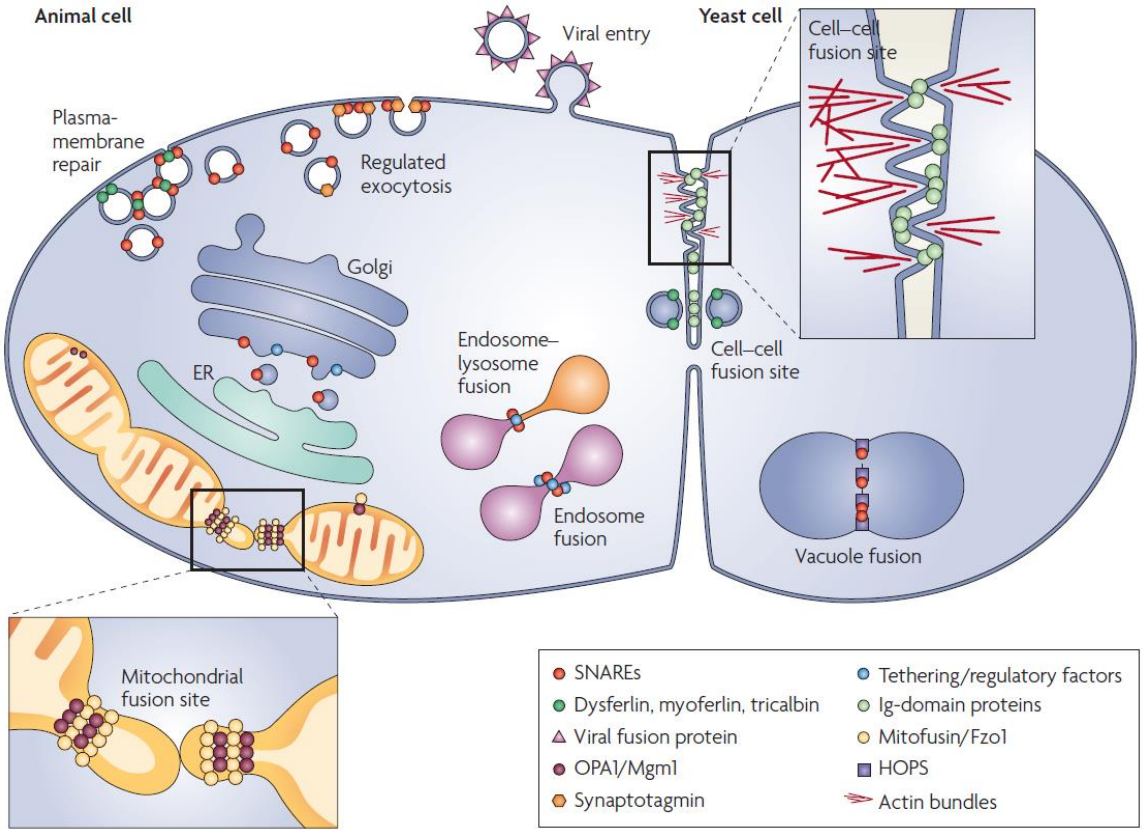

Figure 1-2 The broad spectrum of membrane fusion events. Membrane fusion can occur between cells (*e.g.* yeast mating), between intracellular compartments (*e.g.*, mitochondrial fusion, endosome-endosome fusion), between intracellular compartment and plasma membrane (*e.g.*, synaptic vesicle exocytosis) and between extracellular particles and plasma membrane (*e.g.*, during the viral entry).[5]

Membrane fusion, where two separate bilayers merge into one continuous bilayer, is a fundamental reaction in all living eukaryotic cells. Fusion reactions with different functions can vary vastly in space and time, such as cell-cell fusion in fertilization, intracellular fusion in exocytosis, intra- and extracellular fusion in viral entry (Figure 1-2).[3, 4, 14-16] Despite this diversity, all fusion reactions undergo the process involving the

[5] Figure is taken from Martens, S., and McMahon, H. T. (2008) Mechanisms of membrane fusion: disparate players and common principles, *Nat Rev Mol Cell Bio 9*, 543-55.

general steps shown in Figure 1-3. The natural distance between two membranes is at least 10-20 nm, because of the electrostatic repulsive force between the charged bilayers. Thus, the first step is to bring the membranes into close contact to overcome the electrostatic and hydration forces and the inner bilayer leaflets can interact (Figure 1-3a). This close contact is accompanied by instability of boundary between the hydrophilic and hydrophobic part of the bilayer (Figure 1-3b), leading to the formation of a stalk structure (Figure 1-3c), the inner leaflet merged but the outer leaflet not.[17, 18] Hemifusion diaphragm is induced by stalk expansion; in this case, the two aqueous compartments are separated only by inner leaflets contact (Figure 1-3d). Finally, lipids rearrange a small pore, which enlarges rapidly and form a connection of two aqueous compartments. The content of compartments mixing represents full fusion (Figure 1-3e).

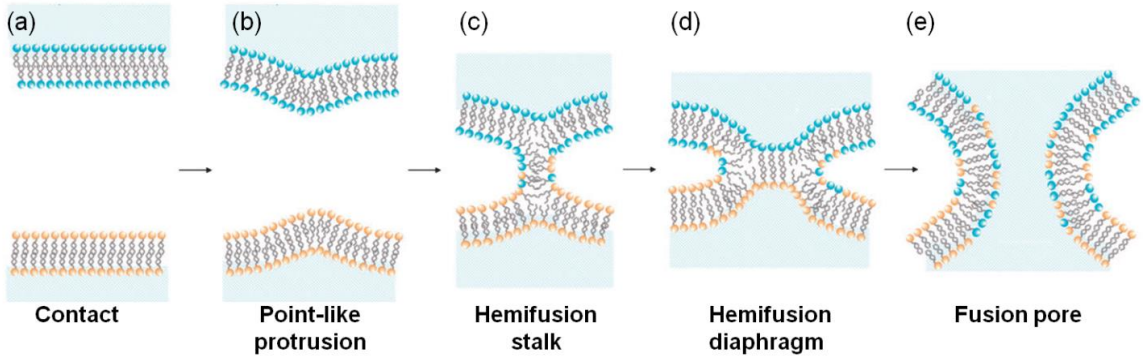

Figure 1-3 Elementary process of all membrane fusion reactions. (a) Pre-fusion contact. (b) A point-like membrane protrusion minimizes the energy of the hydration repulsion between the proximal leaflets of the membranes coming into immediate contact. (c) A hemifusion stalk with only proximal leaflets fused. (d) Stalk expansion induces the hemifusion diaphragm. (e) A fusion pore forms either from the hemifusion diaphragm or directly from the hemifusion stalk.[6]

Although all membrane fusion reactions involve the same basic procedures, various proteins trigger them. These proteins induce the initial recognition of the membranes and bring them into close proximity to initiate lipid mixing. A single protein may do everything in viral-cell fusion whereas protein complexes are needed in intracellular fusion. The mechanism of these two well-studied membrane fusion are introduced in the following sections.

[6] Figure is taken from Marsden, H. R., Tomatsu, I., and Kros, A. (2011) Model systems for membrane fusion, *Chem Soc Rev 40*, 1572-1585.

1.1.3 SNARE-MEDIATED FUSION

All intracellular membrane fusion events are proposed to be mediated by the formation of SNARE complexes (SNARE, soluble NSF attachment protein receptor where NSF stands for *N*-ethyl-maleimide-sensitive fusion protein).[4, 19-22] Since the SNARE proteins were first characterized in late 1980s, more than 100 family membranes have been found in different subcellular compartments and identified as key elements in membrane fusion.[23-36] In order to bring the two membranes into close proximity and fuse, energy is needed to overcome the electrostatic and hydration forces, SNARE proteins are excellent candidates since they can zip up into complexes during this process. Figure 1-4 shows a widely accepted model of SNARE-mediated membrane fusion.[14, 37-40] Firstly, the SNARE proteins zip up from the amino-terminal end forcing the two membranes to move close within 2-3 nm (Figure 1-4a, b). Afterwards, proceeding zipping creates high curvature and lateral tension in the membranes, thus stabilizing the transition state in which only the outer leaflets are merged, termed hemifusion (Figure 1-4c, d). Finally, the fusion pore opens and expands, causing full content mixing and membrane relaxation (Figure 1-4f). Although the SNARE proteins can vary considerably in structure and size during different types of membrane fusion, the core of the "zipper structure" was proved a four-helix coiled coil motif, called core SNARE complex.

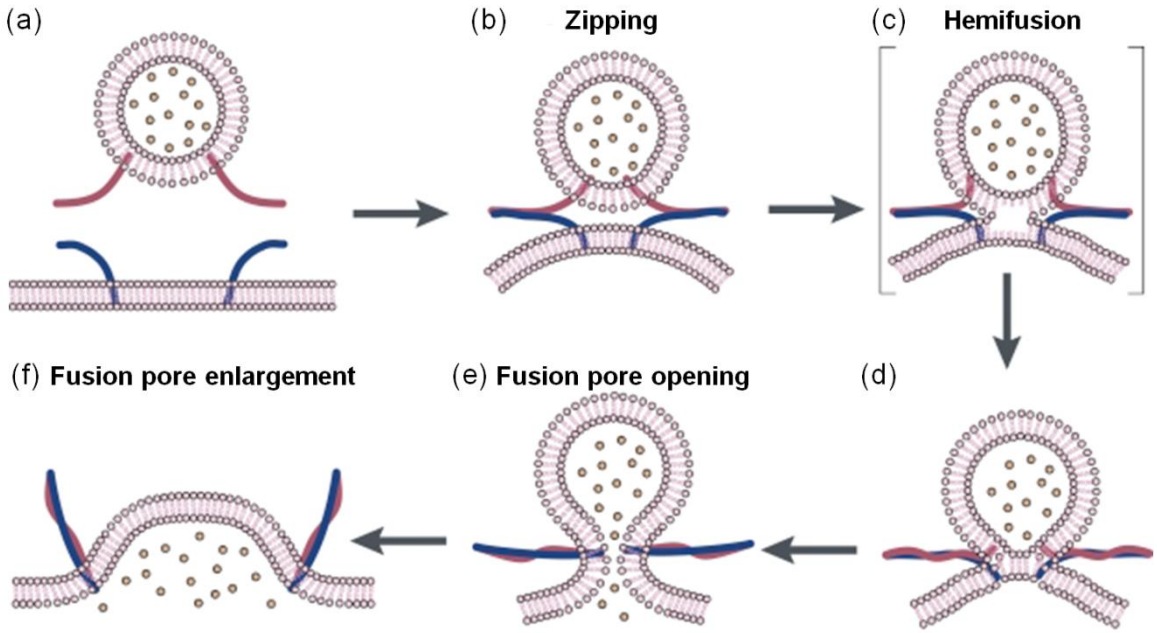

Figure 1-4 Model of SNARE-mediated membrane fusion. (a) The two membranes are in the vicinity but the SNAREs are not yet in contact. (b) SNARE complexes start zipping from the amino-terminal end, which forces the two membranes further towards each other. (c) Zipping proceeds, induces increased curvature and lateral tension of the membranes, exposing the bilayer interior. Spontaneous hemifusion occurs as the separation is sufficiently reduced. (d) The highly unfavorable void space at the membrane junction causes the establishment of contacts between the distal membrane leaflets. (e) The lateral tension in the transbilayer contact area induces membrane breakdown, yielding a tiny fusion pore. (f) The fusion pore expands and the membrane relaxes.[7]

1.1.4 VIRAL-CELL FUSION

Enveloped viruses such as HIV and influenza virus infect the host cell through fusion of the viral membrane and a target cell membrane. Viral fusion proteins catalyze this fusion process.[1-4, 41, 42] Although they vary greatly in structure, all seem to have a common mechanism involving an essential conformational change from native (non-fusogenic) to fusion-active (fusogenic) (Figure 1-5).[43-47] Before it interacts with the host cell membrane, the protein present on the viral surface is in an inactive state as a homotrimer with the non-helical fusion peptide or loop (light green) sequestered (Figure 1-5a). Upon appropriate trigger such as pH change, the protein undergoes a dramatic

[7] Figure is taken from Chen, Y. A., and Scheller, R. H. (2001) SNARE-mediated membrane fusion, *Nat Rev Mol Cell Bio 2*, 98-106.

conformational change, extending the fusion peptide or loop (helical) to inset into the target cell membrane (Figure 1-5b), resulting in a longer trimeric coiled coil structure. Afterwards, further conformational change occur: The protein folds back inducing the collapse of the intermediate, followed by the proximal leaflets merging into a hemifusion stalk (Figure 1-5c, d). Finally, the fusion pore opens resulting in the entry of viral content into the host cell (Figure 1-5e).

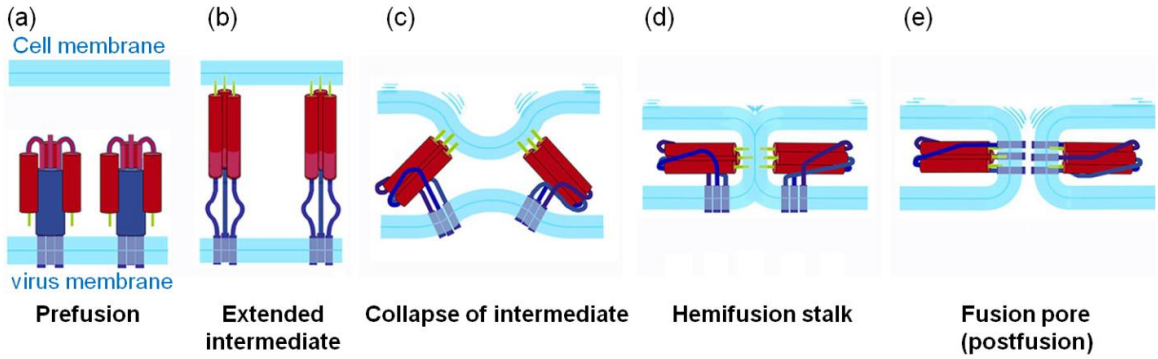

Figure 1-5 Model of membrane fusion trigged by a viral fusion protein. (a) The protein in the pre-fusion conformation, with its fusion peptide (green) sequestered. (b) Extended intermediate. The protein opens up at low pH (in the case of the influenza virus), extending the fusion peptide to interact with the target membrane. (c) Collapse of the extended intermediate. (d) The protein folds back bringing the membranes in closer proximity. The proximal leaflets merge into a hemifusion stalk. (e) Fusion pore formation.[8]

[8] Figure is taken from Harrison, S. C. (2008) Viral membrane fusion, *Nat Struct Mol Biol 15*, 690-698.

1.2 BULK PHASE FUSION ASSAY

Because of the complexity of living cells, reconstitution of protein-mediated membrane fusion events *in vitro* is a good alternative approach of cell-based assay towards mechanism understanding at molecular level. So far, several artificial model systems and methods have been established to study the mechanism of membrane fusion.[16] These models are predominately based on liposomes, consist of various types of liposomes and one or two fusogens generally. Fluorescence spectroscopy is common used to study such models in bulk phase solution, lipid mixing and content mixing can be identified from the change of fluorescence intensity.

1.2.1 LIPOSOMES AS A BASIS

Liposomes, or lipid vesicles, are artificially prepared spherical structures composed of one or a few lipid bilayers formed *in vitro* in an aqueous medium.[48, 49] This closed structure is energetically favorable because it avoids the exposure of the hydrophobic tails to water, which is unstable. Because of their similarity to the cells and vesicles in nature, they have been widely used as a model system in membrane science, drug delivery, as well as cell mimic study.[49-56]

Liposomes are often distinguished according to their number of lamellarity and size (Figure 1-6).[56-58] Depending on lamellarity, liposomes can be divided into unilamerllar vesicles and mutilamerllar vesicle. Generally, unilamellar vesicles are classified according to their size as small unilamellar vesicles (SUV, diameter < 100 nm), large unilamellar vesicles (LUV, diameter between 100-1000 nm) and giant unilamellar vesicles (GUV, diameter > 1 μm). Multilamellar vesicles (MLV) are onion-like structure and multivesicular vesicles (MVV) encapsulate smaller vesicles. The thickness of the membrane (phospholipid bilayer) measures approximately 4-5 nm.

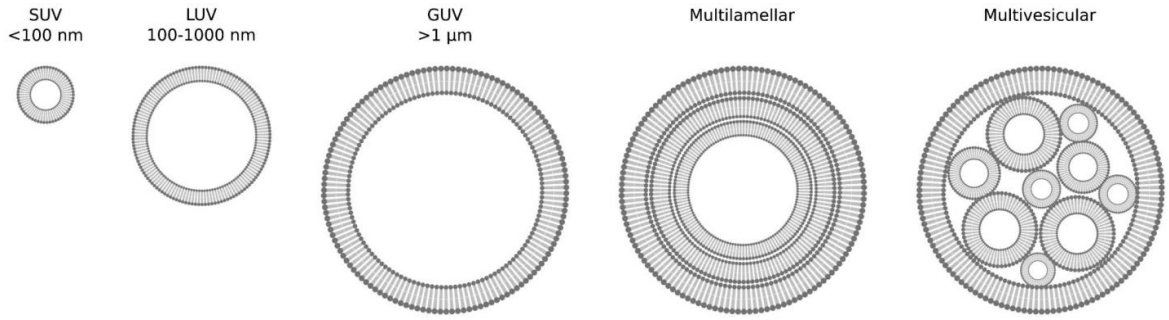

Figure 1-6 The common vesicle size and lamellarity classification system. Small unilamellar vesicles (SUV) are less than 100 nm in diameter; large unilamellar vesicles (LUV) are between 100 and 1000 nm; and giant unilamellar vesicles (GUV) are larger than 1 µm. Multilamellar vesicles have many membrane layers, and multivesicular vesicles encapsulate smaller vesicles.[9]

Various methods have been developed to prepare liposomes. However, despite the diversity of methods, the formation of all kinds of liposomes share the same mechanism except GUVs, which are mainly produced by electroformation (Figure 1-7).[49, 59-63] Firstly, a lipid mixture of the desired composition is dissolved in organic solvent (usually chloroform with/without methanol) to assure a homogeneous mixture, and then remove the solvent to get dry lipid film. Hydration of the dry lipid film is accomplished simply by adding an aqueous solution and agitating above the transition temperature of lipids, forming MLVs of different size distributions. Once a stable MLV suspension forms, the vesicles can be downsized by extrusion or sonication. Extrusion through a polycarbonate filter with defined pore size can produce LUVs of desired size. Sonication can disrupt the suspension to yield bilayer fragments and assembly into SUVs finally.

[9] Figure is taken from van Swaay, D., and deMello, A. (2013) Microfluidic methods for forming liposomes, *Lab Chip 13*, 752-767.

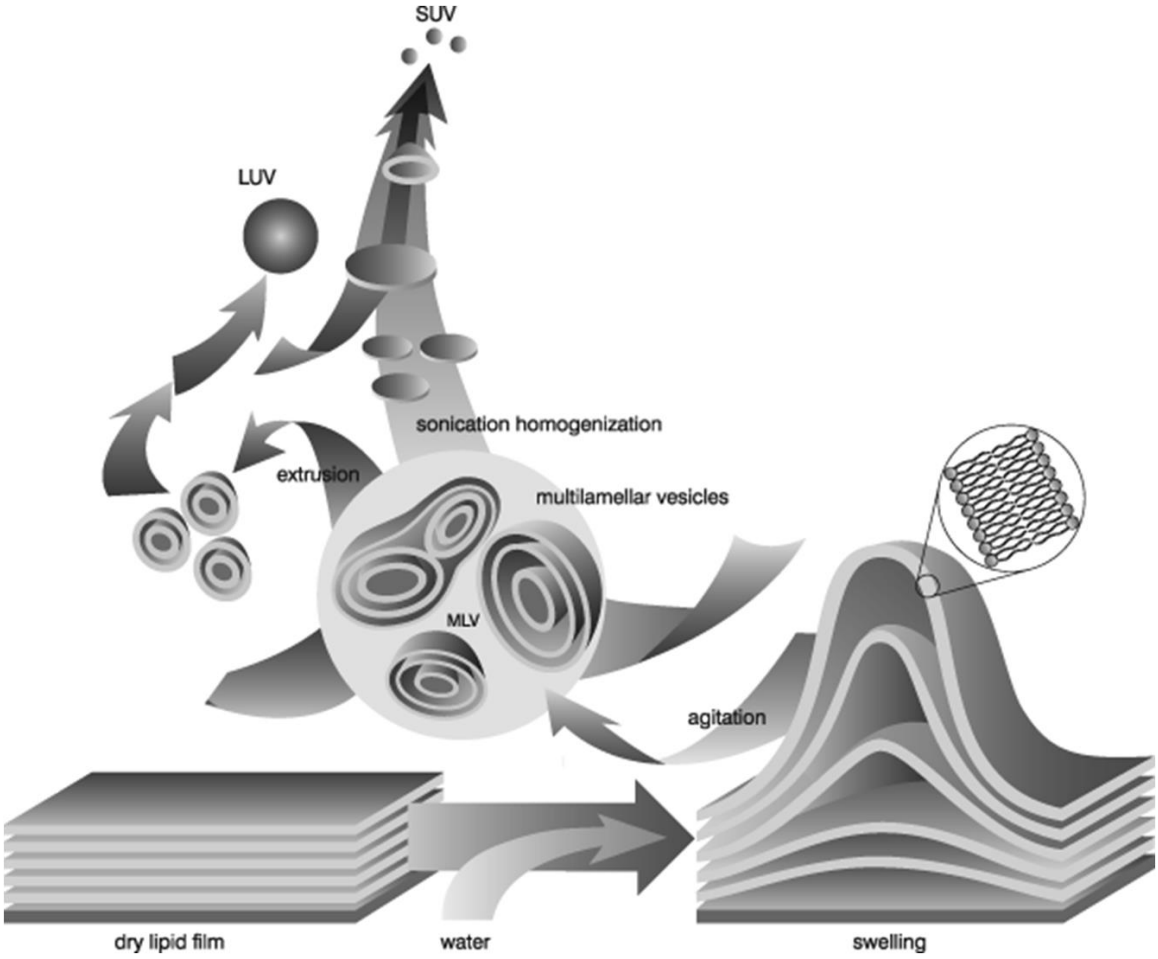

Figure 1-7 Illustration of the mechanism of liposome formation. Liposomes form from the dry lipid film, which detaches from the support upon hydration. Afterwards, the swelling film self-closes to form large multilamellar vesicles (MLVs) during agitation in order to prevent interaction of water with the hydrocarbon core of the bilayer at the edges. Finally, energy is input to reduce the size of the MLVs in the form of sonic energy (sonication) or mechanical energy (extrusion), resulting in LUVs and SUVs, respectively.[10]

Typically, membrane fusion assay is always based on bulk solution of SUVs or LUVs because the composition, size, surface charge and other properties of liposomes can be controlled easily. Besides, the liposomes can be functionalized with desired ligands such as peptides, DNAs and small molecules to introduce a certain specific function.

[10] Figure is taken from http://www.avantilipid.com, technical support, preparation of liposomes.

1.2.2 LIPID MIXING[16, 64]

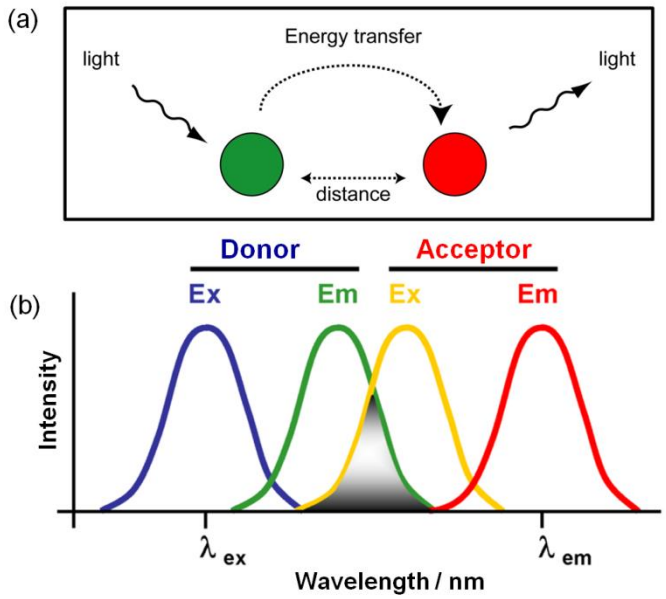

Figure 1-8 Mechanism of fluorescence resonance energy transfer (FRET). (a) Mode of energy transfer between different flurophores.[11] (b) Schematic representation of the FRET spectral overlap integral.[12]

Fluorescence resonance energy transfer (FRET) is a distance-dependent interaction between "donor fluorophore" and "acceptor fluorophore" in which excitation can transfer from donor to acceptor.[65] Therefore, in order to observe efficient FRET, the emission spectrum of donor must overlap the absorption spectrum of acceptor, and the distance between donor and accepter must be in appropriate distance (typically 10-100 Å) (Figure 1-8).

Struck and co-workers firstly applied FRET experiment to measure lipid mixing.[65] The assay was performed by labeling liposomes with both a donor fluorophore NBD (N-(7-nitro-2,1,3-benzoxadiazol-4-yl)) and an acceptor fluorophore rhodamine at an appropriate distance, resulting efficient FRET. When labeled liposomes fuse with

[11] Figure 1-8a is adapted from http://www.molecular-beacons.org/toto/Marras_energy_transfer.html.
[12] Figure 1-8b is adapted from http://de.wikipedia.org/wiki/Föster-Resonanzenergietransfer.

unlabeled liposomes, the increasing of average distance between donor and acceptor induces decreasing FRET efficiency. This FRET based lipid mixing assay is currently the most widely used assay.

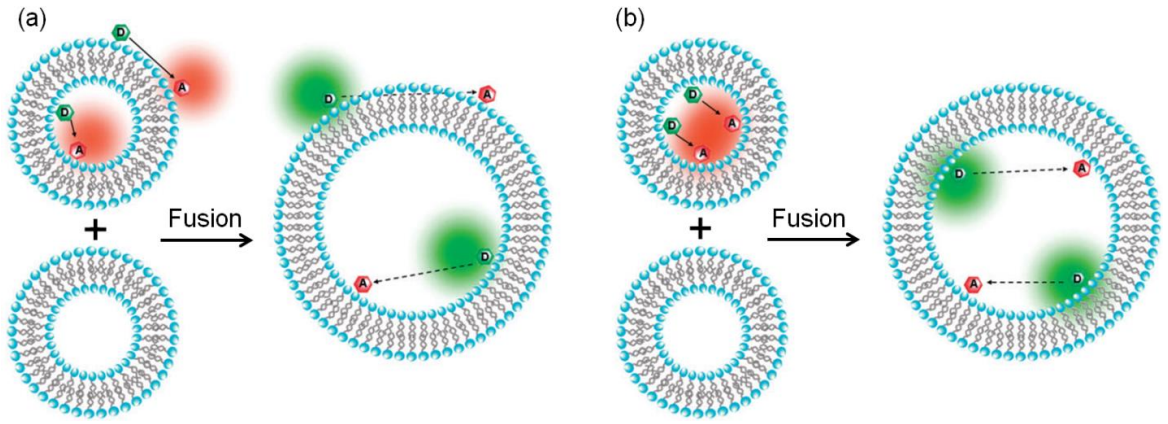

Figure 1-9 (a) Total lipid mixing and (b) inner leaflet mixing assay based on fluorescence resonance energy transfer (FRET). The average distance of the donor and acceptor fluorophore increases upon fusion of labeled membrane with unlabeled membrane, resulting in decreased FRET efficiency. Decreased FRET efficiency is registered by increased donor fluorescence intensity (green) and decreased acceptor fluorescence intensity (red). [13]

Hemifusion has been defined as lipid mixing without content mixing or as outer leaflets merge but not the inner leaflets of the two bilayers. Therefore, inner leaflet-mixing test is a necessary complement of content mixing results in the case of fusion process terminated in hemifusion.

An inner leaflet mixing assay is achieved by treating the NBD-labeled liposomes with sodium dithionite.[66, 67] Because sodium dithionite cannot penetrate the lipid bilayer, the fluorescence of the outer leaflet is selectivity eliminated. If decreased FRET is observed when mixing these liposomes with plain liposomes, inner leaflet mixing did occur.[68, 69]

Another widely used method to investigate lipid-mixing, based on self-quenching of octadecyl rhodamine B, was also original described by Hoekstra and co-workers.[70, 71] When the concentration of this fluorophore is up to 9 mol% of total lipid, the self-quenching efficiency is proportional to its surface intensity, therefore, if the labeled

[13] Figure is taken from Marsden, H. R., Tomatsu, I., and Kros, A. (2011) Model systems for membrane fusion, *Chem Soc Rev 40*, 1572-1585.

liposome fuse with non-labeled liposomes, the dilution of fluorophore causes a proportional increasing in fluorescence intensity (Figure 1-10).

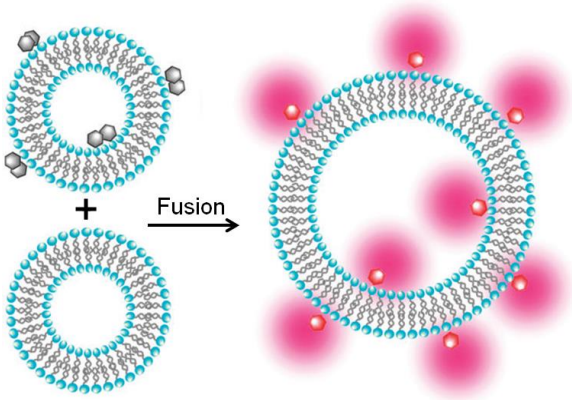

Figure 1-10 Lipid mixing assay based on fluorescence self-quenching. Fluorescence of the fluorophore is quenched at high concentration due to fluorophore-fluorophore interactions. Fusion with unlabeled liposomes causes dilution of the fluorophore, resulting increasing fluorescence (red). [14]

1.2.3 CONTENT MIXING AND LEAKAGE

Content mixing of liposomes is the most important criterion for fusion, which can be detected fluorometrically using low molecular weight soluble tracers. The most common used methods is the fluorescence quenching assay relaying on complex formation of a fluorophore and a quencher, for example, the polyanionic fluorophore ANTS and cationic quencher DPX, which introduced by Smolarsky and co-workers to determine complement-mediated liposome immune lysis (Figure 1-11a).[72, 73] Liposome populations are loaded with ANTS and DPX separately, content mixing results in quenching of ANTS fluorescence. This method is always performed at acidic conditions and with high concentration of both fluorophore and quencher.[74-78]

[14] Figure is taken from Marsden, H. R., Tomatsu, I., and Kros, A. (2011) Model systems for membrane fusion, *Chem Soc Re 40*, 1572-1585.

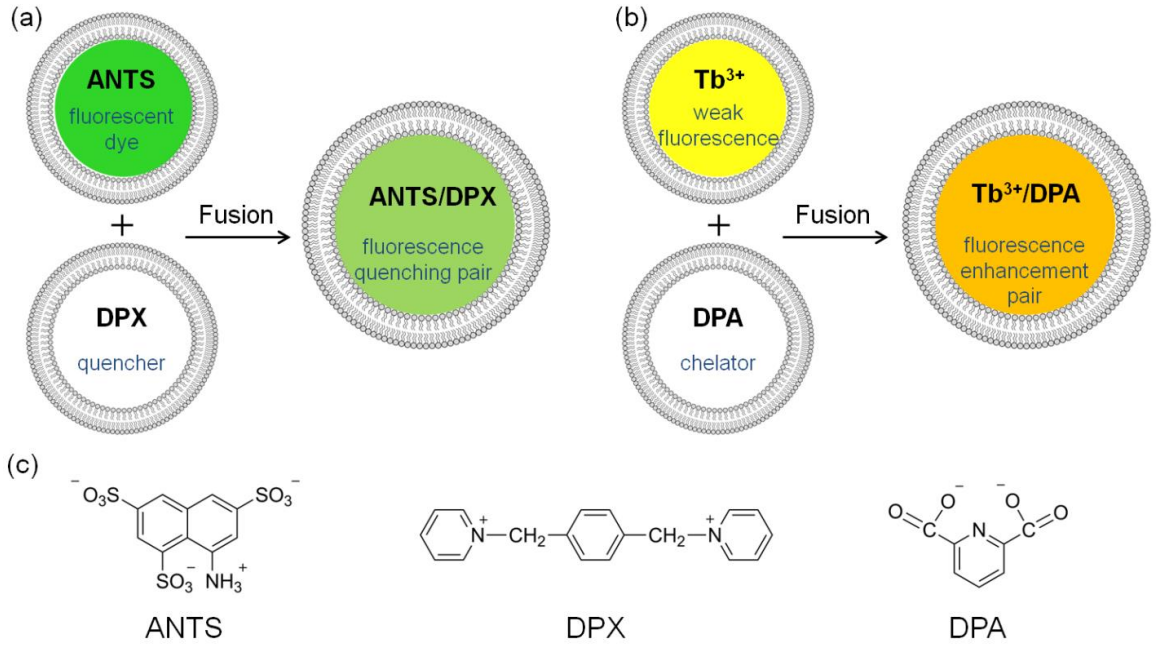

Figure 1-11 Content mixing assay. (a) Representation of the ANTS/DPX fluorescence quenching assay. (b) Representation of the terbium/dipicolinic acid (DPA) fluorescence enhancement assay for vesicle fusion. (c) Chemical structure of ANTS, DPX and DPA.

Another method is the fluorescence enhancement assay with terbium ions (Tb^{3+})/dipicolinic acid (DPA), which was originally described by Wilschut and co-workers (Figure 1-11b).[79, 80] This assay is based on the interaction between Tb^{3+} and DPA, that the chelates of Tb^{3+}/DPA can produce 10000 times more fluorescent than free Tb^{3+}.[81, 82] Therefore, in this assay, $TbCl_3$ is encapsulated in one population of liposomes and DPA is in the other, greatly enhanced fluorescence can be detected upon content mixing.

Besides, the self-quenching assay with fluorescein derivatives is an effective method.[83, 84] Fluorescence of fluorescein derivatives is more than 95% self-quenched at concentrations higher than 100 mM. Concentrated solutions of these water-soluble fluorophores are loaded in liposomes, upon fusion with plain liposomes, the dilution of fluorophore is accompanied by an increasing fluorescence.

Liposome fusion may be accompanied by leakage of content that may be slower or faster than fusion depending on the types of liposomes.[64] All of the above-mentioned three methods can be also applied to investigate content leakage.[72, 83, 85-87]

1.3 SINGLE-VESICLE ASSAY BASED ON FLUORESCENCE MICROSCOPY[88]

In typical fusion assays, as described in the last section, two populations of liposomes are treated differently so that membrane fusion will cause changes in fluorescence intensity due to FRET, self-quenching, *etc*. The experiments are usually performed in a cuvette with bulk mixture of liposomes, where total fluorescence is monitored over time by a fluorescence spectrometer.[64, 89] However, the amount of docking cannot be detected with these fusion assays. Besides, the change in fluorescence intensity in these assays is due to lipid mixing including hemifusion as well as full fusion, which cannot be distinguished and quantified in one single experiment. Furthermore, another drawback of liposome based fusion assays is the relatively high amount of fluorophore needed in the liposomes, leading to a substantial demand for less labeling. In order to overcome the limitations of the typical bulk fusion assay, a number of single-vesicle assays have recently been developed to investigate fusion events.[40, 90-99] These assays allow researchers observing the individual fusion event in real time, hence obtain quantitative data of the fusion process.

1.3.1 SINGLE-VESICLE FLUORESCENCE MICROSCOPY

Fluorescence microscopy has been a powerful tool to study biophysical systems via its real-time observation. Single-vesicle fluorescence imaging has proven to be a useful method for observing and analyzing the fusion dynamic, because the acquired fluorescence signal can provide a direct readout for the fusion process including all the transitions.[100] A common fluorescence microscope used to study membrane fusion is total internal reflection fluorescence (TIRF) microscope.[101-103] TIRF microscopy uses the evanescent wave to illuminate and excite fluorophores.[104-106] The evanescent field decays exponentially and extends only a few hundred nanometers from the interface, thus, TIRF microscopy enables a selective visualization of near the interface such as biological membranes which are within the illumination volume. The key advantage of TIRF microscopy is increasing the contrast hence the signal-to-noise ratio of the images

compare to the conventional microscopy since it excludes the background fluorescence from elsewhere of the sample. Recently, this technique is gaining popularity among biologists and neuroscientists to study membrane fusion. Confocal laser scanning microscopy (CLSM) can also be used, which is a scanning imaging technique that can obtain high-resolution optical images with depth selectivity.[94]

Various steps of the fusion process can be real-time monitored by fluorescence microscopy, modern electromultiplying charge-coupled device (EM-CCD) are always used to collect the images (excluding CLSM) at a very high frame rate. Three basic visualization strategies are depicted in Figure 1-12. Three-dimensional fluorescence profiles are generated from the grayscale images taken by the EM-CCD camera, thus fluorescence signal transfer can be shown in a "fluorescence intensity vs time" diagrams. Figure 1-12a shows the simplest lipid mixing between single vesicle and supported lipid bilayer (SLB) based on self-quenching. The vesicle is labeled with fluorophores at a high self-quenched concentration. When fusing with unlabeled SLB, the intensity rapidly increases due to dequenching. Content mixing and fusion pore formation can be easily detected through dequenching of water-soluble fluorophore loaded in vesicles (Figure 1-12b). When labeled content mixes with unlabeled buffer, a decreased intensity can be observed. FRET imaging strategy is shown in Figure 1-12c in which two populations of vesicles are labeled with a FRET pair respectively. Independent excitation of donor and acceptor fluorophore allows for visualization of each of the overlapping vesicles. Because FRET occurs when donor and acceptor fluorophores are at an appropriate distance, thus the acceptor vesicle only can be observed via excitation of donor after fusion, inducing an increasing intensity limited by the acceptor.

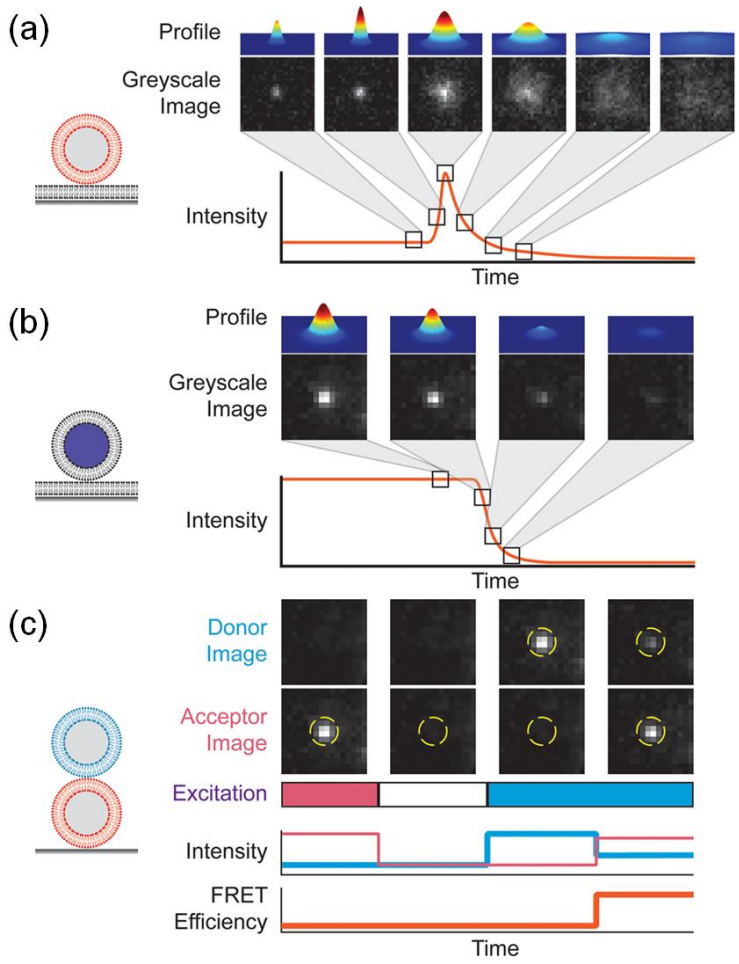

Figure 1-12 Visualizing membrane fusion through fluorescence microscopy. (a) Dequenching upon hemifusion to a large, planar bilayer (plain) with outward diffusion of fluorophore (red) from the fusion site. (b) Dissipative fluorescence loss upon escape of an aqueous fluorescence signal (purple) from the lumen of a fusogenic particle through the fusion pore. (c) FRET-based detection of hemifusion between two immobilized and labeled fusogenic vesicles (red and cyan).[15]

1.3.2 KINETIC STUDY OF SINGLE VESICLE FUSION

In vitro studies attempting to reconstitute the protein-mediated membrane fusion have been traditionally performed in bulk phase. Recently, more scientists are interested in visually single-vesicle fusion assay no matter whether viral membrane fusion or SNARE-mediated fusion. The single-vesicle assays can be classified as single vesicle-SLB assays

[15] Figure is thake from Otterstrom, J., and van Oijen, A. M. (2013) Visualization of membrane fusion, one particle at a time, *Biochemistry 52*, 1654-1668.

(Figure 1-13a,b) and single vesicle-vesicle assays (Figure 1-13c). Both can offer various kinetic information of fusion and can be applied to various conditions such as different fusogens, fluorophores and substrates.

Single vesicle-SLB assay is performed between labeled vesicles and plain SLBs on silica or quartz, *etc*.[96, 99, 102, 107-109] In the simplest lipid-mixing assay, the kinetics from docking and hemifuion can be obtained, including the residency time between docking and the dequenching fusion signal (t_{Res}), the lateral diffusion constant of the fluorophore away from the site of fusion, and, sometimes, the time between fusion and the onset of outward fluorophore diffusion (t_{Delay}).

Based on lipid-mixing, content mixing can be detected simultaneously via loading the free vesicles with fluorophore such as SPB and preparing polymer cushion-supported bilayer (Figure 1-13b).[101] This strategy is suitable for studying transitions from triggering fusion to full fusion. The following kinetics were obtained: the time between fusion trigger and hemifusion (t_H); the time between trigger and full fusion (t_F); and the time between hemifusion and full fusion (t_{HL}), which is the lifetime of the hemifused state.

Recently, a single vesicle-vesicle assay derived from single vesicle-SLB assay was established (Figure 1-13c).[92, 95, 97, 100, 110] The glass or quartz substrates are coated with a PEG/biotin-PEG layer to reduce the nonspecific interaction and immobilize vesicles through avidin-biotin interaction. Accessible kinetics are similar to those in the second strategy.

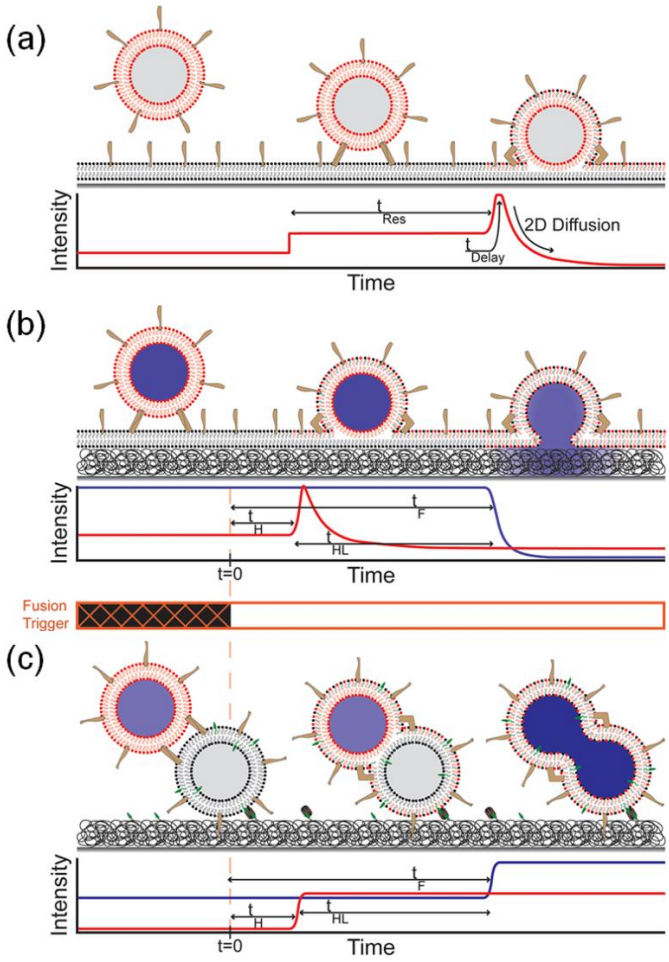

Figure 1-13 Observing kinetic the single-vesicle fusion process via fluorescence microscopy. (a) Observation of the transitions from particle docking to hemifusion. (b) Transitions from triggering fusion to full fusion with a polymer cushion-supported (black mesh below lipids) planar bilayer. (c) Transitions from triggering fusion to full fusion to an immobilized target vesicle.[16]

[16] Figure is taken from Otterstrom, J., and van Oijen, A. M. (2013) Visualization of membrane fusion, one particle at a time, *Biochemistry 52*, 1654-1668.

1.4 SYNTHETIC MEMBRANE FUSION MODEL SYSTEMS[16]

Several artificial model systems have been established to mimic the highly controlled *in vivo* membrane fusion process. Commonly, these model systems are based on different kinds of liposomes and equipped with one or two fusogens. The artificial model systems must fulfill several requirements, for example, the specific molecular recognition between two opposed membranes. Bottom-up approach is always used to investigate *in vitro* membrane fusion: using synthetic analogues sharing the key features of the native fusogens to gain insight into complex natural fusion machinery, such as peptides, DNAs and small molecules.[68, 111-114] These simple experimental model systems are powerful tools for developing understanding of the mechanism of membrane fusion because the chemical structure and composition of synthetic analogues can be systematically varied in order to study the influence of each segment on the fusion process. In this section, the existing studies about construction of *in vitro* artificial fusion systems are introduced.

1.4.1 SMALL MOLECULE-BASED MODELS

In vitro membrane fusion may be induced by small molecule recognition between synthetic fusogens. Bong and co-workers described such controlled selective membrane fusion and studied the functional determinants of this artificial fusion system.[111, 112] The well-studied small-molecule recognition pair–vancomycin glycopeptide and its native binding target, D-Ala-D-Ala dipeptides–was used to trigger liposome fusion (Figure 1-14). Recognition occurs via formation of five hydrogen bonds between vancomycin and the free *C*-terminus of D-Ala-D-Ala at micromolar concentration.[115, 116] A positively charged peptide, magainin II, is used to anchor vancomycin because its membrane-binding mode is well known and it is able to perturb membranes in a concentration dependent manner while D-Ala-D-Ala is membrane anchored by modifying Lys-D-Ala-D-Ala with lipid POPE (1-palmitoyl-2-oleoyl-*sn*-glycero-3-phosphoethanolamine).

The experiment was performed by mixing the two populations of LUVs bearing magainin-vancomycin conjugate (MV) and LUVs with lipid-attached D-Ala-D-Ala

(Kaa-POPE), respectively. Interestingly, rapid size increasing was detected by dynamic light scattering and full fusion was investigated by FRET. Notably, the fusion process can be efficiently inhibited by adding free vancomycin, which blocks all the available surface D-Ala-D-Ala sites.

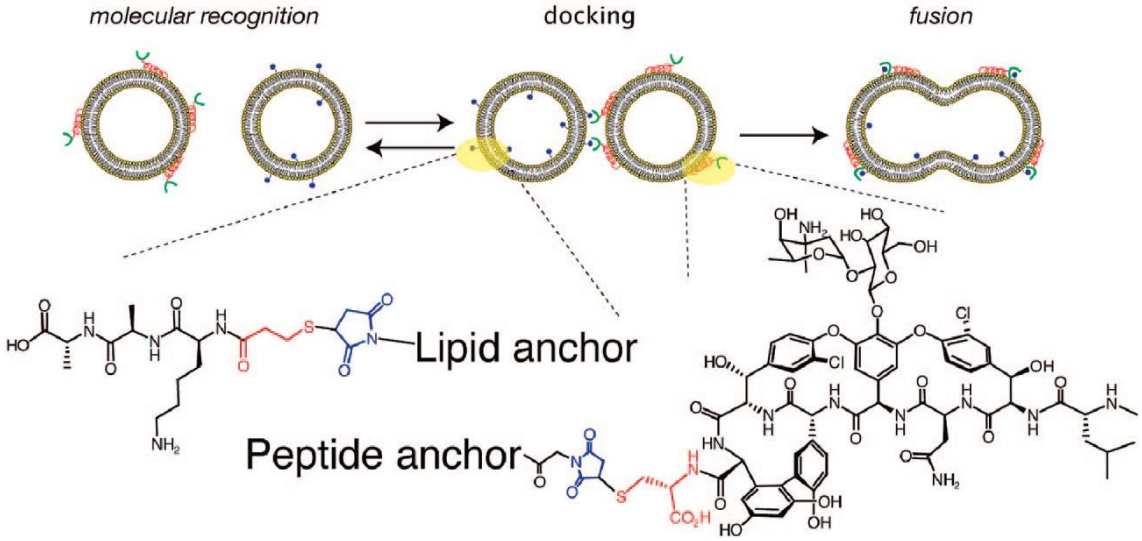

Figure 1-14 Illustration of selective vesicle fusion driven by recognition between vancomycin and D-Ala-D-Ala.[17]

1.4.2 DNA-BASED MODELS

DNA strands have been frequently used to induce membrane fusion, because of the high selectivity between two strands and the diversity of design and synthesis.[117-120] Stengel and co-workers first used DNA strands as recognition motifs and fusogens for selective membrane fusion.[68] This method takes advantages of the encoding potential of DNA and provides a novel model for mimicking membrane fusion *in vivo*.

[17] Figure is taken from Gong, Y., Ma, M., Luo, Y., and Bong, D. (2008) Functional determinants of a synthetic vesicle fusion system, *J Am Chem Soc 130*, 6196-6205.

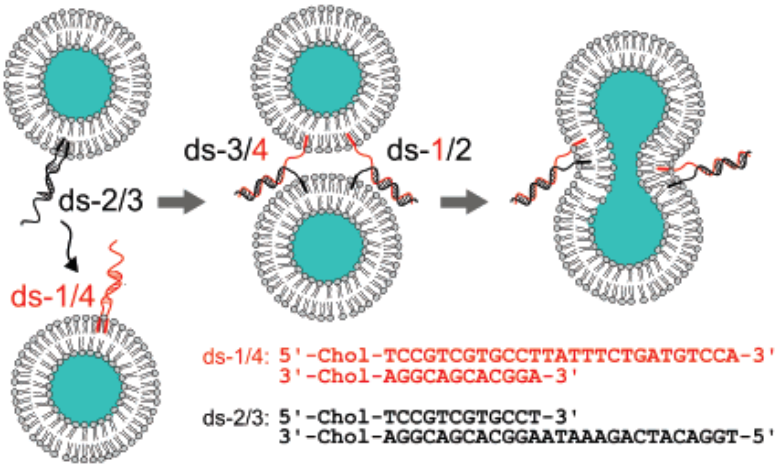

Figure 1-15 DNA induced vesicle fusion. Initially, vesicles are modified with the double CH terminated DNA strands ds-1/4 and ds-2/3 (left side). As ds-1/4 and ds-2/3 encounter each other, they hybridize in a zipperlike fashion, thereby forming blunt-ended duplexes with 27 base pairs (ds-1/2) and 12 base pairs (ds-3/4) (middle). In this geometry, the bilayers are thought to contact each other, which eventually enables opening of the fusion pore (right side).[18]

Inspired by the zipper fashion geometry of SNARE complexes during membrane fusion, cholesterol (CH) modified DNA (CH-DNA) strands were used to drive membrane fuison. Firstly, the hydrophobic CH anchor can spontaneously incorporate into the bilayer; secondly, double standed DNA has stronger affinity to egg PC compare to single standed DNA; at last, the orientation of the CH-DNA strands was designed that hydridization occurs in a zipper-like fashion, which can force the vesicles modified with complementary DNA into close proximity.[121] The membrane fusion process was monitored by FRET. Both inner and outer leaflet mixing were measured to conclude that at least one-third of the observed total lipid mixing represents complete vesicle fusion. Based on these preliminary results, the determinants for such CH-DNA induced membrane fusion was investigated in the following study, including varying the length and number of DNA strands as well as the number (one or two) CH groups for membrane anchoring of DNA.[120]

Because it is easy to control the sequence, binding geometry and length, Boxer and co-workers developed the DNA-based model as a powerful surrogate for the SNARE

[18] Figure is taken from Stengel, G., Zahn, R., and Höök, F. (2007) DNA-induced programmable fusion of phospholipid vesicles, *J Am Chem Soc 129*, 9584-9585.

machinery.[117, 122, 123] Recently, they applied this model to the single vesicle-SLB assay and observed all the transitions including docking, hemifusion and full fusion.[118]

1.4.3 PEPTIDE-BASED MODELS

Membrane fusion is a thermodynamically favorable reaction, but with a very high kinetic barrier. All kinds of fusogens can lower the barrier, SNAREs do this by complex formation whereas viral fusion proteins by changing the protein conformation during the fusion process. In both fusion processes, the coiled coil formation, that was found to play an important role to overcome the energy barrier, brings the two membranes into close proximity allowing fusion to occur. Therefore, synthetic peptides with coiled coil formation have been a popular model system for mimicking protein-mediated fusion.

The coiled coils are protein structural motifs commonly found in nature, formed by assembly of at least two α-helices wrapping around each other.[124, 125] Kros and co-workers designed a synthetic model based on two lipidated oligopeptide hybrids (LPE and LPK), where E and K are the shortest known coiled coil pair (Figure 1-16a).[126-129] The transmembrane domain of fusogen is mimicked by phospholipid tails (DOPE); the flexible spacer connecting peptides and DOPE is poly(ethylene glycol) chain (PEG_{12}) which allows the extension of E/K peptides from the surface of the vesicles.

Two population of vesicles modified with LPE/LPK were mixed, inducing a rapid increasing of both hydrodynamic diameter measured by DLS and ellipiticity ratios measured by CD, suggesting the coiled coil formation and the aggregation of vesicles. Both inner and outer leaflet mixing as well as content mixing were studied via typical fluorescence assay, proving that this model was able to induce membrane fusion without content leakage. Besides, the same assays were performed with various length of peptides to investigate the relation between the rate of membrane fusion and the length of the peptide.[128] The results showed that the stability of coiled coils increases with the length of the complementary peptides, leading to increased rates of membrane fusion. In the latest study, it was surprisingly observed that efficient membrane fusion was induced even when coiled coils formed in a non-zipper like (antiparallel) orientation.[127]

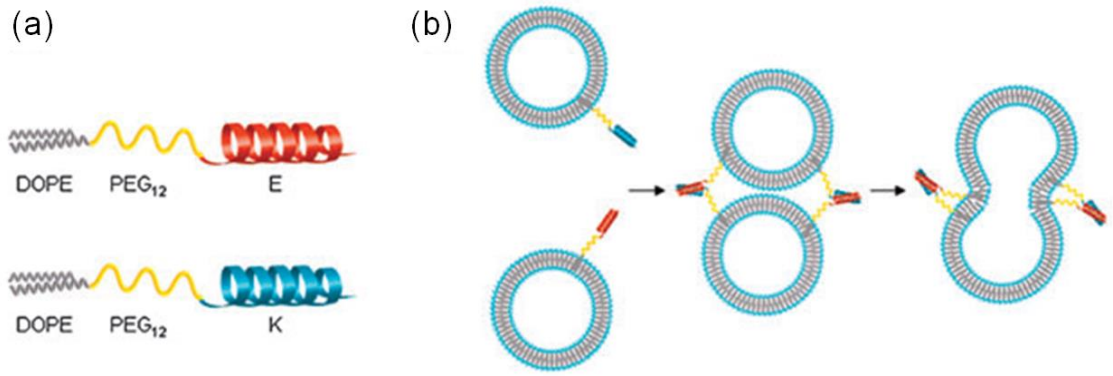

Figure 1-16 (a) Schematic illustrations of LPE and LPK. (b) Liposomes are decorated with LPE or LPK and coiled-coil formation occurs upon mixing. This brings the liposomes into close proximity and induces fusion.[19]

The peptide-based model shares the key characteristics of native protein-mediated fusion via the synthetic coiled coil motif. Considering the ease design and synthesis of coiled coils, the similar peptide model was used in the experimental work of this thesis.

[19] Figure is taken from Marsden, H. R., and Kros, A. (2010) Self-assembly of coiled coils in synthetic biology: inspiration and progress, *Angew Chem Int Ed 49*, 2988-3005.

1.5 SLBs AS MODEL MEMBRANES

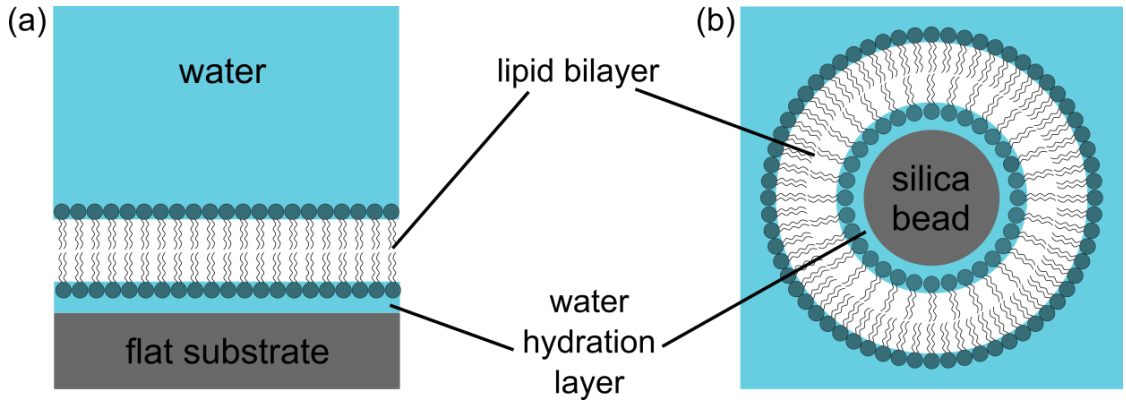

Figure 1-17 Schematic representation of a solid supported bilayer. The lipid bilayer is created on (a) a flat substrate and (b) a silica bead. The thin water hydration layer separates the bilayer from the supports hence maintains the natural lateral fluidity of the membrane.

The properties and functions of biological membranes are notoriously difficult to study at the molecular level due to their complex composition, sensitivity to the environment, *etc.* As a result, a lot of effort has been spent to establish the artificial model membranes, which can mimic the cellular membrane but with less complexity. Except for liposomes introduced in the previous section, solid supported bilayers (SLBs) have proven to be a successful model system with a number of applications in lateral diffusion of lipids, membrane protein chemistry, membrane-membrane interactions, *etc.*[130-137]

1.5.1 SLBs ON FLAT SUBSTRATES

The preparation of SLBs was pioneered by Brian and co-workers, who presented a simple route to spread vesicles from solution onto planar hydrophilic glass substrate.[131] This one-step method is attractive due to its simplicity and reproducibility so that it is widely studied for creating SLBs with different lipid composition, solid supports and biological applications.[133, 136, 138-142] Traditionally, flat supports are used including mica, silica wafer, glass and certain metals. The resulting membrane is separated from the underlying substrate by a very thin layer of hydration water (1 nm), thus, it retains the

natural fluidity and biological functions (Figure 1-17a).[143] In this case, the surface characterization requires elaborate techniques with limited sensitivity such as surface plasmon resonance (SPR), ellipsometry, atomic force microscopy (AFM) and quartz crystal microbalance (QCM).

The mechanism of SLB formation has been investigated by both theoretical and experimental work showing that the process includes two critical steps, vesicle rupture and the integration of supported bilayer patches.[144-150] When a hydrophilic substrate is incubated in a vesicle bulk solution, the vesicles absorb onto the support and rupture spontaneously driven by support-induced deformation, hence supported bilayer patches form with their edges exposed to water. Because the edges of the patches are energetically unfavorable, these patches tend to interact with the neighboring lipids, adjacent patches or vesicles in the solution to form a complete and continuous SLB.

1.5.2 SLBS ON SILICA BEADS

In 2004, Baksh and co-workers created SLBs on silica microbeads (5 μm in diameter) by essentially the same vesicle spreading process on flat support (Figure 1-17b).[151, 152] They established method to investigate protein-membrane interaction via two-dimensional distribution of membrane-coated beads.[153]

In an aqueous solution, the beads with incorporated ligands in the membrane settle gravitationally in microwells plates and assemble into an ordered condensed phase. Upon addition of proteins that react with the ligand, this ordered structure is disrupted and the beads start to move apart from each other, resulting a dispersed distribution. This dramatic phase transition could be detected by collecting bright field images at different locations in the same sample through a simple inverted microscope, and the degree of order depends on the strength of the interactions.

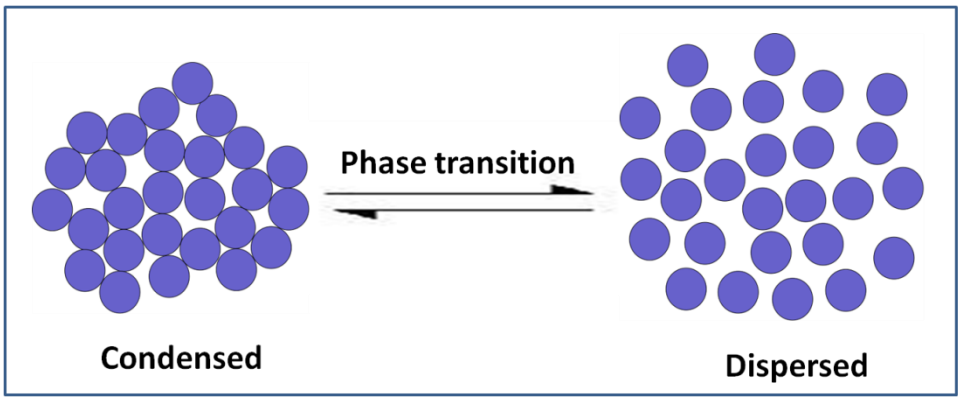

Figure 1-18 Schematic phase transition of membrane-coated beads. In an aqueous solution, membrane-coated beads can assemble into an ordered condensed phase or dispersed phase. The conversion between them is termed phase transition. In Basksh's work, the distribution of beads is governed by ligand-protein interactions, and the degree of order depends on the strength of the interactions.

This work gives some inspiration towards the study of membrane chemistry although the physical origins of the system behavior are not fully understood. This assay enables label-free investigation and can work in extremely low protein concentration (in the pico- to nanomolar range). The microscope can directly observe the behavior of the beads, thus, the experiments can be performed in any standard-equipped biological laboratory. This work may open a door to widespread the idea that membrane-coated beads can be served as model membranes for other applications.

1.6 MOTIVATION AND SCOPE

The mechanistic knowledge of *in vivo* membrane fusion remains far from complete, although many *in vitro* models and techniques have been established to simplify the native fusion environment and study the mechanism on a molecular lever. Inspired by the idea of Baksh *et al.* and considering the advantages of single vesicle-vesicle assays, a new fusion assay was established in this thesis to investigate membrane mixing.

Membrane-coated beads were used as model membranes representing native vesicles and cells instead of traditional lipid vesicles; a similar strategy as the single vesicle-vesicle assay was employed but with simpler operation since the micrometer size of silica beads allows direct observation and size-discrimination ensuring the distinction of various fusion stages including docking, hemifusion and full fusion. This method was firstly applied to the extensively studied membrane fusion system triggered by coiled coil formation of E and K peptides since the results obtained can be easily compared with traditional assays.

There are two main objectives of this work: creation and application of the proposed fusion assay.

The first part of the experimental work was focused on establishing the method to study membrane fusion, including experimental methods and data analytical methods. Preparation of monodisperse membrane-coated beads was the key for this work and the protocol was improved by studying SLB formation on silicon wafer via ellipsometry. For characterizations, a normal optical microscope was used to visualize the dispersion of bead collection and to obtain statistic data of fusion events, while imaging by CLSM was used to determine the fusion events by fluorescence intensity analysis. FRAP was performed to check for the lateral fluidity and connection of membranes to confirm the successful membrane fusion events.

The second part of the experimental work was aimed at applying this method to study membrane fusion triggered by coiled coil formation. Four strategies were investigated including the basic fusion assay in deionized water, Ca^{2+} triggered fusion and inhibition with/without Ca^{2+}. Besides, different amounts of the fusogens and the orientation of the coiled coil structure were considered. Additionally, Monte Carlo simulations were used to

model the lipid diffusion across the contact zone since the lipid diffusion between two beads of a pair is slower than within a bilayer with unrestricted geometry.

1.7 REFERENCE

[1]. Blumenthal, R., Clague, M. J., Durell, S. R., and Epand, R. M. (2003) Membrane Fusion, *Chem Rev 103*, 53-69.

[2]. Jahn, R., Lang, T., and Südhof, T. C. (2003) Membrane Fusion, *Cell 112*, 519-533.

[3]. Jahn, R., and Grubmuller, H. (2002) Membrane Fusion, *Curr Opin Cell Biol 14*, 488-495.

[4]. Wickner, W., and Schekman, R. (2008) Membrane Fusion, *Nat Struct Mol Biol 15*, 658-664.

[5]. Alberts, B., Bray, D., and Lewis, J. (2002) *Molecular Biology of the Cell*, Vol. 10, 4th ed.

[6]. Voet, D., and Voet, J. G. (1995) *Biochemistry*, 2nd ed.

[7]. Boesze-Battaglia, K., and Schimmel, R. J. (1997) Cell Membrane Lipid Composition and Distribution: Implications for Cell Function and Lessons Learned from Photoreceptors and Platelets, *J Exp Biol 200*, 2927-2936.

[8]. Jacobson, K., Sheets, E. D., and Simson, R. (1995) Revisiting the Fluid Mosaic Model of Membranes, *Science 268*, 1441-1442.

[9]. Singer, S. J., and Nicolson, G. L. (1972) The Fluid Mosaic Model of the Structure of Cell Membranes, *Science 175*, 720-731.

[10]. Linden, C. D., and Fox, C. F. (1975) Membrane Physical State and Function, *Acc Chem Res 8*, 321-327.

[11]. van Meer, G., Voelker, D. R., and Feigenson, G. W. (2008) Membrane Lipids: Where They Are and How They Behave, *Nat Rev Mol Cell Bio 9*, 112-124.

[12]. Bevers, E. M., Comfurius, P., Dekkers, D. W. C., and Zwaal, R. F. A. (1999) Lipid Translocation across the Plasma Membrane of Mammalian Cells, *BBA-Mol Cell Biol L 1439*, 317-330.

[13]. Suomalai.H, and Nurminen, T. (1970) Lipid Composition of Cell Wall and Plasma Membrane of Bakers Yeast, *Chem Phys Lipids 4*, 247-256.

[14]. Martens, S., and McMahon, H. T. (2008) Mechanisms of Membrane Fusion: Disparate Players and Common Principles, *Nat Rev Mol Cell Bio 9*, 543-556.

[15]. Chernomordik, L. V., and Kozlov, M. M. (2008) Mechanics of Membrane Fusion, *Nat Struct Mol Biol 15*, 675-683.

[16]. Marsden, H. R., Tomatsu, I., and Kros, A. (2011) Model Systems for Membrane Fusion, *Chem Soc Rev 40*, 1572-1585.

[17]. Kozlov, M. M., and Markin, V. S. (1983) Possible Mechanism of Membrane Fusion, *Biofizika 28*, 242-247.

[18]. Kozlov, M. M., Leikin, S. L., Chernomordik, L. V., Markin, V. S., and Chizmadzhev, Y. A. (1989) Stalk Mechanism of Vesicle Fusion - Intermixing of Aqueous Contents, *Eur Biophys J Biophy 17*, 121-129.

[19]. Jahn, R., and Scheller, R. H. (2006) SNAREs-Engines for Membrane Fusion, *Nat Rev Mol Cell Biol 7*, 631-643.

[20]. Chen, Y. A., and Scheller, R. H. (2001) SNARE-Mediated Membrane Fusion, *Nat Rev Mol Cell Biol 2*, 98-106.

[21]. Rizo, J., and Rosenmund, C. (2008) Synaptic Vesicle Fusion, *Nat Struct Mol Biol 15*, 665-674.

[22]. Scales, S. J., Finley, M. F. A., and Scheller, R. H. (2001) Cell Biology - Fusion without SNAREs?, *Science 294*, 1015-1016.

[23]. Blasi, J., Chapman, E. R., Link, E., Binz, T., Yamasaki, S., *et al.* (1993) Botulinum Neurotoxin-a Selectively Cleaves the Synaptic Protein Snap-25, *Nature 365*, 160-163.

[24]. Blasi, J., Chapman, E. R., Yamasaki, S., Binz, T., Niemann, H., *et al.* (1993) Botulinum Neurotoxin-C1 Blocks Neurotransmitter Release by Means of Cleaving Hpc-1/Syntaxin, *Embo J 12*, 4821-4828.

[25]. Eakle, K. A., Bernstein, M., and Emr, S. D. (1988) Characterization of a Component of the Yeast Secretion Machinery - Identification of the Sec18 Gene-Product, *Mol Cell Biol 8*, 4098-4109.

[26]. Wilson, D. W., Wilcox, C. A., Flynn, G. C., Chen, E., Kuang, W. J., *et al.* (1989) A Fusion Protein Required for Vesicle-Mediated Transport in Both Mammalian-Cells and Yeast, *Nature 339*, 355-359.

[27]. Dascher, C., Ossig, R., Gallwitz, D., and Schmitt, H. D. (1991) Identification and Structure of Four Yeast Genes (Sly) That Are Able to Suppress the Functional Loss of Ypt1, a Member of the Ras Superfamily, *Mol Cell Biol 11*, 872-885.

[28]. Novick, P., Field, C., and Schekman, R. (1980) Identification of 23 Complementation Groups Required for Post-Translational Events in the Yeast Secretory Pathway, *Cell 21*, 205-215.

[29]. Bennett, M. K., and Scheller, R. H. (1993) The Molecular Machinery for Secretion Is Conserved from Yeast to Neurons, *Proc Nat Acad Sci USA 90*, 2559-2563.

[30]. Sollner, T., Whitehart, S. W., Brunner, M., Erdjumentbromage, H., Geromanos, S., *et al.* (1993) Snap Receptors Implicated in Vesicle Targeting and Fusion, *Nature 362*, 318-324.

[31]. Clary, D. O., Griff, I. C., and Rothman, J. E. (1990) Snaps, a Family of Nsf Attachment Proteins Involved in Intracellular Membrane-Fusion in Animals and Yeast, *Cell 61*, 709-721.

[32]. Gerst, J. E., Rodgers, L., Riggs, M., and Wigler, M. (1992) Snc1, a Yeast Homolog of the Synaptic Vesicle-Associated Membrane-Protein Synaptobrevin Gene Family - Genetic Interactions with the Ras and Cap Genes, *Proc Nat Acad Sci USA 89*, 4338-4342.

[33]. Baumert, M., Maycox, P. R., Navone, F., De Camilli, P., and Jahn, R. (1989) Synaptobrevin: An Integral Membrane Protein of 18,000 Daltons Present in Small Synaptic Vesicles of Rat Brain, *Embo J 8*, 379-384.

[34]. Bennett, M. K., Calakos, N., and Scheller, R. H. (1992) Syntaxin - a Synaptic Protein Implicated in Docking of Synaptic Vesicles at Presynaptic Active Zones, *Science 257*, 255-259.

[35]. Schiavo, G., Benfenati, F., Poulain, B., Rossetto, O., Delaureto, P. P., *et al.* (1992) Tetanus and Botulinum-B Neurotoxins Block Neurotransmitter Release by Proteolytic Cleavage of Synaptobrevin, *Nature 359*, 832-835.

[36]. Trimble, W. S., Cowan, D. M., and Scheller, R. H. (1988) Vamp-1 - a Synaptic Vesicle-Associated Integral Membrane-Protein, *Proc Nat Acad Sci USA 85*, 4538-4542.

[37]. Jahn, R., and Südhof, T. C. (1999) Membrane Fusion and Exocytosis, *Annu Rev Biochem 68*, 863-911.

[38]. Monck, J. R., and Fernandez, J. M. (1996) The Fusion Pore and Mechanisms of Biological Membrane Fusion, *Curr Opin Cell Biol 8*, 524-533.

[39]. Lee, J., and Lentz, B. R. (1997) Evolution of Lipidic Structures During Model Membrane Fusion and the Relation of This Process to Cell Membrane Fusion, *Biochemistry 36*, 6251-6259.

[40]. Brunger, A. T., Weninger, K., Bowen, M., and Chu, S. (2009) Single-Molecule Studies of the Neuronal SNARE Fusion Machinery, *Annu Rev Biochem 78*, 903-928.

[41]. Harrison, S. C. (2008) Viral Membrane Fusion, *Nat Struct Mol Biol 15*, 690-698.

[42]. Harrison, S. C. (2005) Mechanism of Membrane Fusion by Viral Envelope Proteins, *Virus Structure and Assembly 64*, 231-261.

[43]. Colman, P. M., and Lawrence, M. C. (2003) The Structural Biology of Type I Viral Membrane Fusion, *Nat Rev Mol Cell Bio 4*, 309-319.

[44]. Backovic, M., and Jardetzky, T. S. (2009) Class Iii Viral Membrane Fusion Proteins, *Curr Opin Struc Biol 19*, 189-196.

[45]. White, J. M. (1990) Viral and Cellular Membrane-Fusion Proteins, *Annu Rev Physiol 52*, 675-697.

[46]. Eckert, D. M., and Kim, P. S. (2001) Mechanisms of Viral Membrane Fusion and Its Inhibition, *Annu Rev Biochem 70*, 777-810.

[47]. Chan, D. C., Fass, D., Berger, J. M., and Kim, P. S. (1997) Core Structure of Gp41 from the HIV Envelope Glycoprotein, *Cell 89*, 263-273.

[48]. van Swaay, D., and deMello, A. (2013) Microfluidic Methods for Forming Liposomes, *Lab Chip 13*, 752-767.

[49]. Jesorka, A., and Orwar, O. (2008) Liposomes: Technologies and Analytical Applications, *Annu Rev Anal Chem 1*, 801-832.

[50]. Lipowsky, R. (1991) The Conformation of Membranes, *Nature 349*, 475-481.

[51]. Shen, Y. Q., Jin, E. L., Zhang, B., Murphy, C. J., Sui, M. H., *et al.* (2010) Prodrugs Forming High Drug Loading Multifunctional Nanocapsules for Intracellular Cancer Drug Delivery, *J Am Chem Soc 132*, 4259-4265.

[52]. Allen, T. M., and Cullis, P. R. (2013) Liposomal Drug Delivery Systems: From Concept to Clinical Applications, *Adv Drug Deliver Rev 65*, 36-48.

[53]. Lorenz, B., Alvarez de Cienfuegos, L., Oelkers, M., Kriemen, E., Brand, C., *et al.* (2012) Model System for Cell Adhesion Mediated by Weak Carbohydrate-Carbohydrate Interactions, *J Am Chem Soc 134*, 3326-3329.

[54]. Antonietti, M., and Forster, S. (2003) Vesicles and Liposomes: A Self-Assembly Principle Beyond Lipids, *Adv Mater 15*, 1323-1333.

[55]. Immordino, M. L., Dosio, F., and Cattel, L. (2006) Stealth Liposomes: Review of the Basic Science, Rationale, and Clinical Applications, Existing and Potential, *Int J Nanomed 1*, 297-315.

[56]. Szoka, F., and Papahadjopoulos, D. (1980) Comparative Properties and Methods of Preparation of Lipid Vesicles (Liposomes), *Annu Rev Biophys Bio 9*, 467-508.

[57]. Walde, P., Cosentino, K., Engel, H., and Stano, P. (2010) Giant Vesicles: Preparations and Applications, *Chembiochem 11*, 848-865.

[58]. Lasic, D. D. (1988) The Mechanism of Vesicle Formation, *Biochem J 256*, 1-11.

[59]. Angelova, M. I., and Dimitrov, D. S. (1986) Liposome Electroformation, *Faraday Discuss 81*, 303-311.

[60]. Meleard, P., Bagatolli, L. A., and Pott, T. (2009) Giant Unilamellar Vesicle Electroformation: From Lipid Mixtures to Native Membranes under Physiological Conditions, *Methods in Enzymology Liposomes, Pt G 465*, 161-176.

[61]. Montes, L. R., Alonso, A., Goni, F. M., and Bagatolli, L. A. (2007) Giant Unilamellar Vesicles Electroformed from Native Membranes and Organic Lipid Mixtures under Physiological Conditions, *Biophys J 93*, 3548-3554.

[62]. Wesolowska, O., Michalak, K., Maniewska, J., and Hendrich, A. B. (2009) Giant Unilamellar Vesicles - a Perfect Tool to Visualize Phase Separation and Lipid Rafts in Model Systems, *Acta Biochim Pol 56*, 33-39.

[63]. Akashi, K., Miyata, H., Itoh, H., and Kinosita, K. (1996) Preparation of Giant Liposomes in Physiological Conditions and Their Characterization under an Optical Microscope, *Biophys J 71*, 3242-3250.

[64]. Düzgünes, N. (2003) Fluorescence Assays for Liposome Fusion, *Liposomes, Pt B 372*, 260-274.

[65]. Struck, D. K., Hoekstra, D., and Pagano, R. E. (1981) Use of Resonance Energy-Transfer to Monitor Membrane-Fusion, *Biochemistry 20*, 4093-4099.

[66]. McIntyre, J. C., and Sleight, R. G. (1991) Fluorescence Assay for Phospholipid Membrane Asymmetry, *Biochemistry 30*, 11819-11827.

[67]. Meers, P., Ali, S., Erukulla, R., and Janoff, A. S. (2000) Novel Inner Monolayer Fusion Assays Reveal Differential Monolayer Mixing Associated with Cation-Dependent Membrane Fusion, *BBA-Biomembranes 1467*, 227-243.

[68]. Stengel, G., Zahn, R., and Höök, F. (2007) DNA-Induced Programmable Fusion of Phospholipid Vesicles, *J Am Chem Soc 129*, 9584-9585.

[69]. Lygina, A. S., Meyenberg, K., Jahn, R., and Diederichsen, U. (2011) Transmembrane Domain Peptide/Peptide Nucleic Acid Hybrid as a Model of a SNARE Protein in Vesicle Fusion, *Angew Chem Int Ed 50*, 8597-8601.

[70]. Hoekstra, D., Klappe, K., Hoff, H., and Nir, S. (1989) Mechanism of Fusion of Sendai Virus - Role of Hydrophobic Interactions and Mobility Constraints of Viral Membrane-Proteins - Effects of Polyethylene-Glycol, *J Biol Chem 264*, 6786-6792.

[71]. Macdonald, R. I. (1990) Characteristics of Self-Quenching of the Fluorescence of Lipid-Conjugated Rhodamine in Membranes, *J Biol Chem 265*, 13533-13539.

[72]. Ellens, H., Bentz, J., and Szoka, F. C. (1985) H^+- and Ca^{2+}-Induced Fusion and Destabilization of Liposomes, *Biochemistry 24*, 3099-3106.

[73]. Smolarsky, M., Teitelbaum, D., Sela, M., and Gitler, C. (1977) A Simple Fluorescent Method to Determine Complement-Mediated Liposome Immune Lysis, *J Immunol Methods 15*, 255-265.

[74]. Bailey, A. L., and Cullis, P. R. (1994) Modulation of Membrane-Fusion by Asymmetric Transbilayer Distributions of Amino Lipids, *Biochemistry 33*, 12573-12580.

[75]. Eastman, S. J., Hope, M. J., Wong, K. F., and Cullis, P. R. (1992) Influence of Phospholipid Asymmetry on Fusion between Large Unilamellar Vesicles, *Biochemistry 31*, 4262-4268.

[76]. Epand, R. M., Nir, S., Parolin, M., and Flanagan, T. D. (1995) The Role of the Ganglioside-G(D1a) as a Receptor for Sendai Virus, *Biochemistry 34*, 1084-1089.

[77]. Hoekstra, D., Buistarkema, R., Klappe, K., and Reutelingsperger, C. P. M. (1993) Interaction of Annexins with Membranes - the N-Terminus as a Governing Parameter as Revealed with a Chimeric Annexin, *Biochemistry 32*, 14194-14202.

[78]. Nieva, J. L., Nir, S., Muga, A., Goni, F. M., and Wilschut, J. (1994) Interaction of the HIV-1 Fusion Peptide with Phospholipid-Vesicles - Different Structural Requirements for Fusion and Leakage, *Biochemistry 33*, 3201-3209.

[79]. Wilschut, J., and Papahadjopoulos, D. (1979) Ca^{2+}-Induced Fusion of Phospholipid-Vesicles Monitored by Mixing of Aqueous Contents, *Nature 281*, 690-692.

[80]. Wilschut, J., Düzgünes, N., and Papahadjopoulos, D. (1981) Calcium/Magnesium Specificity in Membrane Fusion: Kinetics of Aggregation and Fusion of Phosphatidylserine Vesicles and the Role of Bilayer Curvature, *Biochemistry 20*, 3126-3133.

[81]. Barela, T. D., and Sherry, A. D. (1976) Simple, One-Step Fluorometric Method for Determination of Nanomolar Concentrations of Terbium, *Anal Biochem 71*, 351-357.

[82]. Thomas, D. D., Carlsen, W. F., and Stryer, L. (1978) Fluorescence Energy-Transfer in Rapid-Diffusion Limit, *Proc Nat Acad Sci USA 75*, 5746-5750.

[83]. Weinstein, J. N., Yoshikami, S., Henkart, P., Blumenthal, R., and Hagins, W. A. (1977) Liposome-Cell Interaction - Transfer and Intracellular Release of a Trapped Fluorescent Marker, *Science 195*, 489-492.

[84]. Ravoo, B. J., Weringa, W. D., and Engberts, J. B. F. N. (1999) Membrane Fusion in Vesicles of Oligomerizable Lipids, *Biophys J 76*, 374-386.

[85]. Straubinger, R. M., Hong, K., Friend, D. S., and Papahadjopoulos, D. (1983) Endocytosis of Liposomes and Intracellular Fate of Encapsulated Molecules - Encounter with a Low pH Compartment after Internalization in Coated Vesicles, *Cell 32*, 1069-1079.

[86]. Bentz, J., Düzgünes, N., and Nir, S. (1983) Kinetics of Divalent-Cation Induced Fusion of Phosphatidylserine Vesicles - Correlation between Fusogenic Capacities and Binding Affinities, *Biochemistry 22*, 3320-3330.

[87]. Nir, S., Düzgünes, N., and Bentz, J. (1983) Binding of Mono-Valent Cations to Phosphatidylserine and Modulation of Ca^{2+}-Induced and Mg^{2+}-Induced Vesicle Fusion, *BBA 735*, 160-172.

[88]. Otterstrom, J., and van Oijen, A. M. (2013) Visualization of Membrane Fusion, One Particle at a Time, *Biochemistry 52*, 1654-1668.

[89]. Scott, B. L., Van Komen, J., Liu, S., Weber, T., Melia, T. J., *et al.* (2003) Liposome Fusion Assay to Monitor Intracellular Membrane Fusion Machines, *Liposomes, Pt B 372*, 274-300.

[90]. Lee, H. K., Yang, Y., Su, Z. L., Hyeon, C., Lee, T. S., *et al.* (2010) Dynamic Ca^{2+}-Dependent Stimulation of Vesicle Fusion by Membrane-Anchored Synaptotagmin 1, *Science 328*, 760-763.

[91]. Johnson, J. M., Ha, T., Chu, S., and Boxer, S. G. (2002) Early Steps of Supported Bilayer Formation Probed by Single Vesicle Fluorescence Assays, *Biophys J 83*, 3371-3379.

[92]. Kyoung, M., Srivastava, A., Zhang, Y. X., Diao, J. J., Vrljic, M., *et al.* (2011) In Vitro System Capable of Differentiating Fast Ca^{2+}-Triggered Content Mixing from Lipid Exchange for Mechanistic Studies of Neurotransmitter Release, *Proc Nat Acad Sci USA 108*, 304-313.

[93]. Bowen, M. E., Weninger, K., Brunger, A. T., and Chu, S. (2004) Single Molecule Observation of Liposome-Bilayer Fusion Thermally Induced by Soluble N-Ethyl Maleimide Sensitive-Factor Attachment Protein Receptors (SNAREs), *Biophys J 87*, 3569-3584.

[94]. Christensen, S. M., Mortensen, M. W., and Stamou, D. G. (2011) Single Vesicle Assaying of SNARE-Synaptotagmin-Driven Fusion Reveals Fast and Slow Modes

of Both Docking and Fusion and Intrasample Heterogeneity, *Biophys J 100*, 957-967.

[95]. Diao, J. J., Ishitsuka, Y., Lee, H., Joo, C., Su, Z. L., *et al.* (2012) A Single Vesicle-Vesicle Fusion Assay for in Vitro Studies of SNAREs and Accessory Proteins, *Nat Protoc 7*, 921-934.

[96]. Liu, T. T., Tucker, W. C., Bhalla, A., Chapman, E. R., and Weisshaar, J. C. (2005) SNARE-Driven, 25-Millisecond Vesicle Fusion in Vitro, *Biophys J 89*, 2458-2472.

[97]. Kyoung, M. J., Zhang, Y. X., Diao, J. J., Chu, S., and Brunger, A. T. (2013) Studying Calcium-Triggered Vesicle Fusion in a Single Vesicle-Vesicle Content and Lipid-Mixing System, *Nat Protoc 8*, 1-16.

[98]. Diao, J., Grob, P., Cipriano, D. J., Kyoung, M., Zhang, Y., *et al.* (2012) Synaptic Proteins Promote Calcium-Triggered Fast Transition from Point Contact to Full Fusion, *Elife 1*, e00109.

[99]. Wang, T. T., Smith, E. A., Chapman, E. R., and Weisshaar, J. C. (2009) Lipid Mixing and Content Release in Single-Vesicle, SNARE-Driven Fusion Assay with 1-5 ms Resolution, *Biophys J 96*, 4122-4131.

[100]. Yoon, T. Y., Okumus, B., Zhang, F., Shin, Y. K., and Ha, T. (2006) Multiple Intermediates in SNARE-Induced Membrane Fusion, *Proc Nat Acad Sci USA 103*, 19731-19736.

[101]. Floyd, D. L., Ragains, J. R., Skehel, J. J., Harrison, S. C., and van Oijen, A. M. (2008) Single-Particle Kinetics of Influenza Virus Membrane Fusion, *Proc Nat Acad Sci USA 105*, 15382-15387.

[102]. Wessels, L., Elting, M. W., Scimeca, D., and Weninger, K. (2007) Rapid Membrane Fusion of Individual Virus Particles with Supported Lipid Bilayers, *Biophys J 93*, 526-538.

[103]. Ivanovic, T., Rozendaal, R., Floyd, D. L., Popovic, M., van Oijen, A. M., *et al.* (2012) Kinetics of Proton Transport into Influenza Virions by the Viral M2 Channel, *Plos One 7*, e31566.

[104]. Axelrod, D. (1984) Total Internal-Reflection Fluorescence in Biological-Systems, *J Lumin 31-2*, 881-884.

[105]. Axelrod, D., Burghardt, T. P., and Thompson, N. L. (1984) Total Internal-Reflection Fluorescence, *Annu Rev Biophys Bio 13*, 247-268.

[106]. Axelrod, D. (2003) Total Internal Reflection Fluorescence Microscopy in Cell Biology, *Methods in enzymology 361*, 1-33.

[107]. Domanska, M. K., Kiessling, V., Stein, A., Fasshauer, D., and Tamm, L. K. (2009) Single Vesicle Millisecond Fusion Kinetics Reveals Number of SNARE Complexes Optimal for Fast SNARE-Mediated Membrane Fusion, *J Biol Chem 284*, 32158-32166.

[108]. Kiessling, V., Domanska, M. K., and Tamm, L. K. (2010) Single SNARE-Mediated Vesicle Fusion Observed in Vitro by Polarized Tirfm, *Biophys J 99*, 4047-4055.

[109]. Liu, T., Wang, T., Chapman, E. R., and Weisshaar, J. C. (2008) Productive Hemifusion Intermediates in Fast Vesicle Fusion Driven by Neuronal SNAREs, *Biophys J 94*, 1303-1314.

[110]. van den Bogaart, G., and Jahn, R. (2011) Inside Insight to Membrane Fusion, *Proc Nat Acad Sci USA 108*, 11729-11730.

[111]. Gong, Y., Luo, Y. M., and Bong, D. (2006) Membrane Activation: Selective Vesicle Fusion Via Small Molecule Recognition, *J Am Chem Soc 128*, 14430-14431.

[112]. Gong, Y., Ma, M., Luo, Y., and Bong, D. (2008) Functional Determinants of a Synthetic Vesicle Fusion System, *J Am Chem Soc 130*, 6196-6205.

[113]. Ma, M., and Bong, D. (2013) Controlled Fusion of Synthetic Lipid Membrane Vesicles, *Acc Chem Res 46*, 2988-2997.

[114]. Rawle, R. J., van Lengerich, B., Bendix, P. M., Chung, M., and Boxer, S. G. (2012) DNA-Mediated Fusion between Small Vesicles and a Planar, Tethered Bilayer Patch, *Biophys J 102*, 605a-605a.

[115]. Walsh, C. T. (1993) Vancomycin Resistance - Decoding the Molecular Logic, *Science 261*, 308-309.

[116]. Kahne, D., Leimkuhler, C., Wei, L., and Walsh, C. (2005) Glycopeptide and Lipoglycopeptide Antibiotics, *Chem Rev 105*, 425-448.

[117]. Chan, Y. H. M., van Lengerich, B., and Boxer, S. G. (2009) Effects of Linker Sequences on Vesicle Fusion Mediated by Lipid-Anchored DNA Oligonucleotides, *Proc Nat Acad Sci USA 106*, 979-984.

[118]. van Lengerich, B., Rawle, R. J., Bendix, P. M., and Boxer, S. G. (2013) Individual Vesicle Fusion Events Mediated by Lipid-Anchored DNA, *Biophys J 105*, 409-419.

[119]. Simonsson, L., Jonsson, P., Stengel, G., and Höök, F. (2010) Site-Specific DNA-Controlled Fusion of Single Lipid Vesicles to Supported Lipid Bilayers, *Chemphyschem 11*, 1011-1017.

[120]. Stengel, G., Simonsson, L., Campbell, R. A., and Höök, F. (2008) Determinants for Membrane Fusion Induced by Cholesterol-Modified DNA Zippers, *J Phys Chem B 112*, 8264-8274.

[121]. Pfeiffer, I., and Höök, F. (2004) Bivalent Cholesterol-Based Coupling of Oligonucletides to Lipid Membrane Assemblies, *J Am Chem Soc 126*, 10224-10225.

[122]. Chan, Y. H. M., Lenz, P., and Boxer, S. G. (2007) Kinetics of DNA-Mediated Docking Reactions between Vesicles Tethered to Supported Lipid Bilayers, *Proc Nat Acad Sci USA 104*, 18913-18918.

[123]. Rawle, R. J., van Lengerich, B., Chung, M., Bendix, P. M., and Boxer, S. G. (2011) Vesicle Fusion Observed by Content Transfer across a Tethered Lipid Bilayer, *Biophys J 101*, L37-L39.

[124]. Marsden, H. R., and Kros, A. (2010) Self-Assembly of Coiled Coils in Synthetic Biology: Inspiration and Progress, *Angew Chem Int Ed 49*, 2988-3005.

[125]. Apostolovic, B., Danial, M., and Klok, H. A. (2010) Coiled Coils: Attractive Protein Folding Motifs for the Fabrication of Self-Assembled, Responsive and Bioactive Materials, *Chem Soc Rev 39*, 3541-3575.

[126]. Marsden, H. R., Elbers, N. A., Bomans, P. H. H., Sommerdijk, N. A. J. M., and Kros, A. (2009) A Reduced SNARE Model for Membrane Fusion, *Angew Chem Int Ed 48*, 2330-2333.

[127]. Versluis, F., Dominguez, J., Voskuhl, J., and Kros, A. (2013) Coiled-Coil Driven Membrane Fusion: Zipperlike Vs. Non-Zipper-Like Peptide Orientation, *Faraday Discuss 166*, 349-359.

[128]. Zheng, T. T., Voskuhl, J., Versluis, F., Zope, H. R., Tomatsu, I., *et al.* (2013) Controlling the Rate of Coiled Coil Driven Membrane Fusion, *Chem Commun 49*, 3649-3651.

[129]. Versluis, F., Voskuhl, J., van Kolck, B., Zope, H., Bremmer, M., *et al.* (2013) In Situ Modification of Plain Liposomes with Lipidated Coiled Coil Forming Peptides Induces Membrane Fusion, *J Am Chem Soc 135*, 8057-8062.

[130]. Sackmann, E. (1996) Supported Membranes: Scientific and Practical Applications, *Science 271*, 43-48.

[131]. Brian, A. A., and McConnell, H. M. (1984) Allogeneic Stimulation of Cytotoxic T Cells by Supported Planar Membranes, *Proc Natl Acad Sci U S A 81*, 6159-6163.

[132]. Salafsky, J., Groves, J. T., and Boxer, S. G. (1996) Architecture and Function of Membrane Proteins in Planar Supported Bilayers: A Study with Photosynthetic Reaction Centers, *Biochemistry 35*, 14773-14781.

[133]. Tamm, L. K., and Mcconnell, H. M. (1985) Supported Phospholipid-Bilayers, *Biophys J 47*, 105-113.

[134]. Garcia-Manyes, S., Redondo-Morata, L., Oncins, G., and Sanz, F. (2010) Nanomechanics of Lipid Bilayers: Heads or Tails?, *J Am Chem Soc 132*, 12874-12886.

[135]. Fang, Y., Frutos, A. G., and Lahiri, J. (2002) Membrane Protein Microarrays, *J Am Chem Soc 124*, 2394-2395.

[136]. Mcconnell, H. M., Watts, T. H., Weis, R. M., and Brian, A. A. (1986) Supported Planar Membranes in Studies of Cell-Cell Recognition in the Immune-System, *BBA 864*, 95-106.

[137]. Groves, J. T., and Dustin, M. L. (2003) Supported Planar Bilayers in Studies on Immune Cell Adhesion and Communication, *J Immunol Methods 278*, 19-32.

[138]. Watts, T. H., Brian, A. A., Kappler, J. W., Marrack, P., and Mcconnell, H. M. (1984) Antigen Presentation by Supported Planar Membranes Containing Affinity-Purified I-Ad, *Proc Nat Acad Sci-Biol 81*, 7564-7568.

[139]. Richter, R. P., Berat, R., and Brisson, A. R. (2006) Formation of Solid-Supported Lipid Bilayers: An Integrated View, *Langmuir 22*, 3497-3505.

[140]. Cremer, P. S., and Boxer, S. G. (1999) Formation and Spreading of Lipid Bilayers on Planar Glass Supports, *J Phys Chem B 103*, 2554-2559.

[141]. Reviakine, I., and Brisson, A. (2001) Streptavidin 2D Crystals on Supported Phospholipid Bilayers: Toward Constructing Anchored Phospholipid Bilayers, *Langmuir 17*, 8293-8299.

[142]. Schonherr, H., Johnson, J. M., Lenz, P., Frank, C. W., and Boxer, S. G. (2004) Vesicle Adsorption and Lipid Bilayer Formation on Glass Studied by Atomic Force Microscopy, *Langmuir 20*, 11600-11606.

[143]. van Oudenaarden, A., Groves, J. T., and Boxer, S. G. (1999) Geometrical Brownian Ratchets: A Supported Lipid Bilayer on a Microfabricated Array of Diffusion Barriers, *Biophys J 76*, A11-A11.

[144]. Richter, R., Mukhopadhyay, A., and Brisson, A. (2003) Pathways of Lipid Vesicle Deposition on Solid Surfaces: A Combined QCM-D and AFM Study, *Biophys J 85*, 3035-3047.

[145]. Richter, R. P., and Brisson, A. R. (2005) Following the Formation of Supported Lipid Bilayers on Mica: A Study Combining AFM, QCM-D, and Ellipsometry, *Biophys J 88*, 3422-3433.

[146]. Seifert, U., and Lipowsky, R. (1990) Adhesion of Vesicles, *Phys Rev A 42*, 4768-4771.

[147]. Seifert, U. (1997) Configurations of Fluid Membranes and Vesicles, *Adv Phys 46*, 13-137.

[148]. Zhdanov, V. P., and Kasemo, B. (2001) Comments on Rupture of Absorbed Vesicles, *Langmuir 17*, 3518-3521.

[149]. Keller, C. A., Glasmastar, K., Zhdanov, V. P., and Kasemo, B. (2000) Formation of Supported Membranes from Vesicles, *Phys Rev Lett 84*, 5443-5446.

[150]. Zhdanov, V. P., Keller, C. A., Glasmastar, K., and Kasemo, B. (2000) Simulation of Adsorption Kinetics of Lipid Vesicles, *J Chem Phys 112*, 900-909.

[151]. Bayerl, T. M. (2004) A Glass Bead Game, *Nature 427*, 105-106.

[152]. Baksh, M. M., Jaros, M., and Groves, J. T. (2004) Detection of Molecular Interactions at Membrane Surfaces through Colloid Phase Transitions, *Nature 427*, 139-141.

[153]. Winter, E. M., and Groves, J. T. (2006) Surface Binding Affinity Measurements from Order Transitions of Lipid Membrane-Coated Colloidal Particles, *Anal Chem 78*, 174-180.

2 EXPERIMENTAL AND ANALYTICAL METHODS

2.1 INSTRUMENTS

Microscopy is a well-known optical technology to study objects or specimens that are too small to be seen with naked eye. Microscopes are specialized optical instruments designed to fulfill the study of microscopy by producing magnified images.[1] The main well-known branches of microscopy are optical, electron, and scanning probe microscopy. Among them, optical microcopy is the most common one and many techniques are available such as bright field microscopy, fluorescence microscopy and confocal microscopy, which were extensively used in this work. Besides, another optical technique, ellipsometry, was used for optimizing the conditions for preparing membrane bilayers on silica wafer. The details of these techniques used in this work are discussed in the following text.

2.1.1 OPTICAL MICROSCOPY

Bright field microscopy is the most elementary form of all optical microscopy illumination techniques for the past 300 years. The specimen illumination is transmitted white light and the contrast of the image is due to the absorbance of the transmitted light in the sample. Therefore, the typical appearance of a bright field microscopy image is a dark specimen on a bright background, hence the name. The light path of common bright field microscopy is extremely simple. The light source illuminates the specimen from below and the condenser lens focuses the light onto the specimen, finally, objectives and oculars are used to observe the specimen from above.

In contrast to normal trans-illuminated light microscopy, the specimen is illuminated with light of a specific wavelength in fluorescence microscopy. The fluorophore in the specimen absorbs this light and re-emit light of a longer wavelength, hence make up the images with color. In order to observe this fluorescence, specific filters are applied to isolate the excitation and emission wavelength of the fluorophore.

In this work, inverted fluorescence microscope was used for taking both common bright field images and fluorescence images. An inverted microscope shares the same theory with common microscope but with its light source and condenser on the top, and objective are below the specimen. Inverted microscopes are useful for observing specimen at the bottom of a container.

2.1.2 CONFOCAL LASER SCANNING MICROSCOPY

Confocal laser scanning microscopy (CLSM) is a powerful tool for obtaining high resolution and high contrast fluorescence images with depth selectivity.[2-4] Specimen is excited by point like light and images are acquired point by point in the in-focus plane of interest from selected depth then reconstructed with a computer. Compared to conventional fluorescence microscopy, different light source and detector are used. However, the major development is the introduction of pinhole apertures that are the key devices to reduce the background information.

Figure 2-1 shows the basic principle of CLSM. A pinhole aperture is placed between the light source and specimen, which presents a point illumination on the specimen in a focus plane when excited light passes though. Laser is used as light source since a mercury light would be too weak for point illumination. Once the excited light interacts with the fluorophore in the specimen, the secondary fluorescence emission is separated by the dichromatic mirror and barrier filter. A second detecting pinhole is positioned in a conjugated plan to the focus plane in front of the detector. Therefore, only the secondary fluorescence from focal plane is allowed to pass and reach the detector. Obviously, the majority of the out-of-focus (background) information is blocked by the pinhole, hence the image quality is significantly improved instead of observing the images directly by eyepieces in traditional fluorescence microscopy, electronic detectors (usually photomultipliers) are always used for sensitive and fast signal point registration in CLSM. A computer is necessary for acquisition, processing, analysis, and display of images. Besides, CLSM can also built three-dimensional (3D) reconstruction by computationally assembling the stacks of images from various focal planes (z-stack) of a thick specimen.[5]

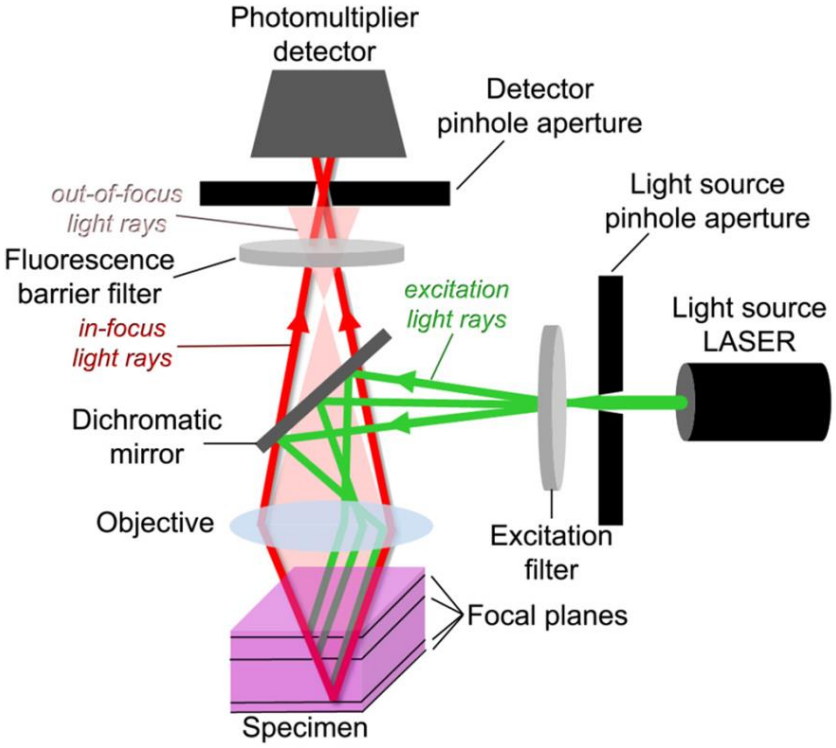

Figure 2-1 Schematic setup of a confocal laser scanning microscope.[20]

In addition to observe fluorescent labeled specimen, fluorescence recovery after photobleaching (FRAP) experiments can be performed with CLSM. FRAP denotes a method measuring two-dimensional lateral diffusion rates of membranes with/without associated molecules such as proteins.[6-10]

[20] Figure is taken from Dr. Marta Kocun's doctoral thesis (2011) Mechanical properties of pore-spanning membranes prepared from giant vesicles, University of Göttingen, Germany.

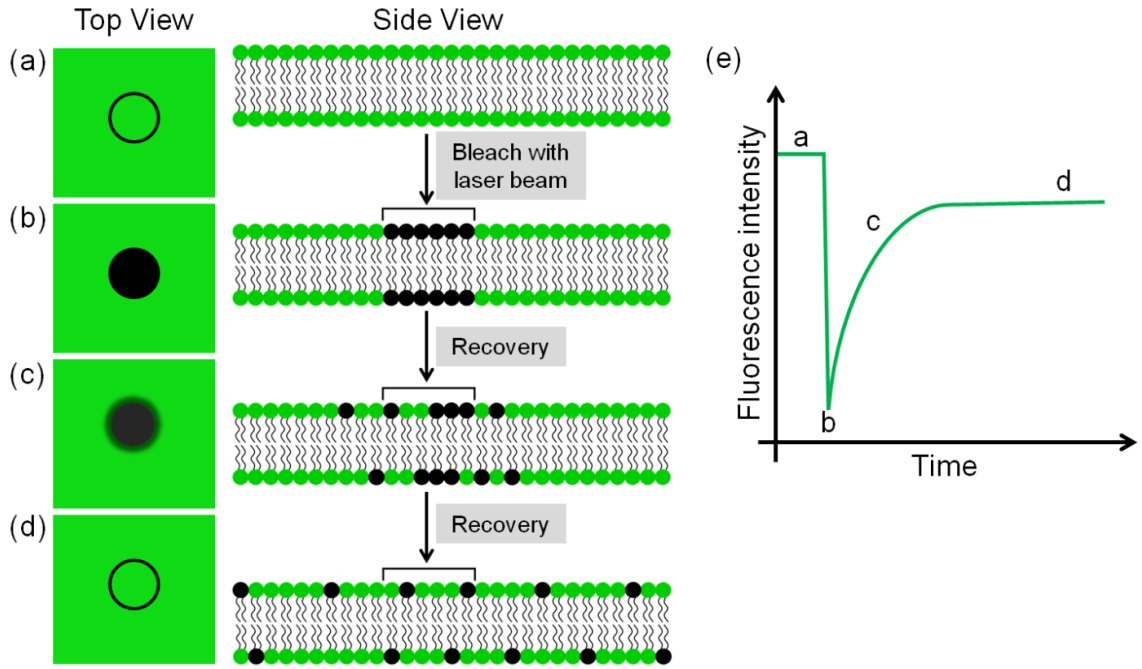

Figure 2-2 Schematic representation of fluorescence recovery after photobleaching (FRAP) experiment on a lipid bilayer. A pulse laser is used to bleach a region of interest (black circle), and the fluorescence intensity recovers as the bleached molecules diffuse away and the unbleached molecules diffuse into the region (shown here in top and side views). The series photographs and fluorescence intensity are simultaneously recorded of this in this process, which involves (a) before bleaching, (b) after bleaching, (c) partial recovery and (d) full recovery, generating a curve of fluorescence intensity as a function of time (e).[21]

Lipids are highly mobile in the plane of the bilayer over transition temperature (lateral diffusion). FRAP assay begins by taking a background image (baseline) of fluorescently labeled specimen (Figure 2-2a). The fluorophore is then bleached in a very tiny area (ROI, region of interest) by high intensity laser pulses, forming a dark spot and fluorescence intensity decreases sharply (Figure 2-2b). As the adjacent unbleached lipids diffusing into the bleached area, the dark spot recovers as well as the fluorescence intensity, this recovery is monitored by the same, but attenuated laser beam (Figure 2-2c, d). Fluorescence recovery curve is generated by plotting the fluorescence intensity of ROI as a function of time (Figure 2-2e). The rate of fluorescent recovery is determined by the rate of lipid diffusion, termed diffusion coefficient *D*. Assuming a Gaussian profile for the

[21]Figure is adapted from http://en.wikipedia.org/wiki/Fluorescence_recovery_after_photobleaching.

bleaching beam and a circular bleached area, the diffusion coefficient *D* can be simply calculated from:

$$D = \frac{\omega^2}{4t_{1/2}}$$

where ω is the approximate radius of the bleached region and $t_{1/2}$ is the "Characteristic" diffusion time after which fluorescence intensity recovered to half of the original.

2.1.3 ELLIPSOMETRY

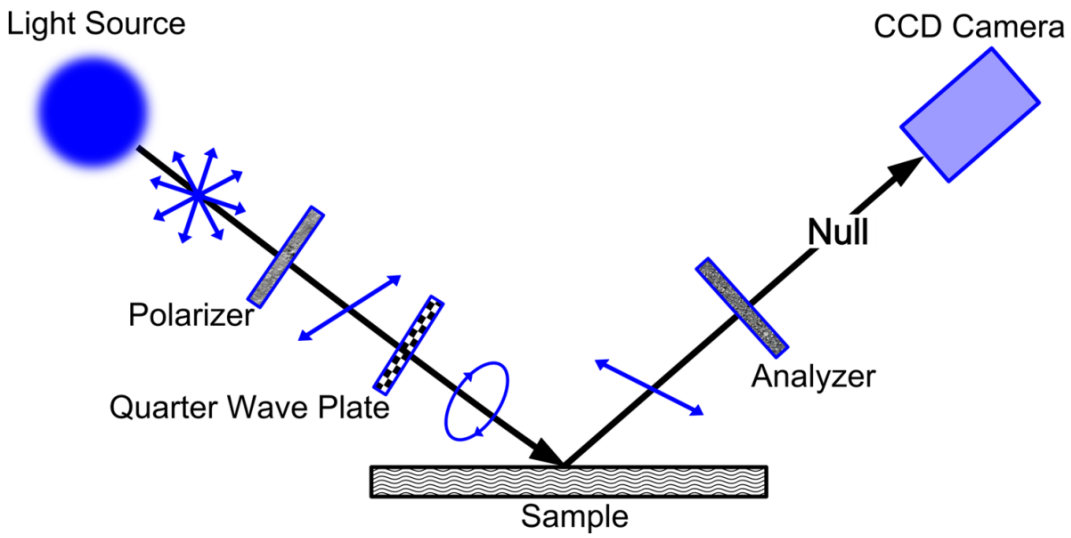

Figure 2-3 Schematic representation of the ellipsometer used in this work.

Ellipsometry is an extremely sensitive optical technique to investigate the properties of thin films. It is based on the measurement of polarization change caused by reflection or transmission from a material structure. Paul Drude invented ellipsometry and derived the fundamental equations in 1880's, and then Alexandre Rothe termed the method ellipsomety in 1945 for measuring the thickness of thin film with a sensitivity of 0.3 Å.[11, 12] So far, ellipsometry can be also used to get refractive index, extinction coefficient and reflectivity, *etc*.

In this work, null ellipsometry was used to monitor the process of vesicle spreading on flat substrate based on thickness characterization, hence optimize the experimental conditions of preparation of membrane-coated beads.

The principle of setup in this work is show in Figure 2-3. Nd:YAG laser emits unpolarized and monochromatic (λ = 532 nm) light which is then sent through a linearly polarizer, forming a linear polarized light. After passing through a compensator (quarter wave plate), the resulting elliptically polarized light reflects from the surface of the sample, it becomes linearly polarized again and the analyzer is adjusted so that the light is extinguished (nulling). Finally, the light is detected with a CCD camera, which converts light to electronic signal to determine the reflected polarization. Compare to input polarization, the change in amplitude (*del, Δ*) and phase (psi, Ψ) of the reflected light causing by the sample are obtained, which are directly related to the complex reflectance ratio, ρ:

$$\rho = \tan(\Psi)\, e^{j\Delta}$$

Because ellipsometry is an indirect method, that the measured Δ and Ψ cannot offer any optical properties directly, thus different models are needed for various experiments. In this work, the model for calculating the thickness was employed. However, for thin layers (< 50 nm) Δ is linearly decreasing with increasing layer thickness, hence, the dynamic process of vesicle spreading can be monitored by plotting *del* via time, and thickness of deposited layers can be estimated from *del*.

2.2 MATERIALS

Lipids, buffers and silica beads are common used materials in this work. Details of all these materials and some other materials such as silica wafer for elliposometry are introduced in this section.

2.2.1 LIPIDS

Table 2-1 Abbreviation, name, and charge of lipids used in this work

Abbreviation	Name	Charge
DOPC	1,2-dioleoyl-*sn*-glycero-3-phosphocholine	Neutral
DMOPC	1,2-dimyristoleoyl-*sn*-glycero-3-phosphocholine	Neutral
DOEPC	1,2-dioleoyl-*sn*-glycero-3-ethylphosphocholine	+
MCC-DOPE	1,2-dioleoyl-*sn*-glycero-3-phosphoethanolamine-N-[4-(p-maleimidomethyl)cyclohexane-carboxamide] (sodium salt)	–
Texas Red-DHPE	Texas Red-DHPE (N-(Texas Red sulfonyl)-1,2-dihexadecanoyl-*sn*-glycero-3-phosphoethanolamine, (triethylammonium salt)	–
NBD-DOPE	1,2-dioleoyl-*sn*-glycero-3-phosphoethanolamine-*N*-(7-nitro-2-1,3-benzoxadiazol-4-yl) (ammonium salt)	–
G_{M1}	Monosialoganglioside G_{M1}	–

All lipids were used without further purification. DOPC, DMOPC, DOEPC, MCC-DOPE and NBD-DOPE were purchased from Avanti Polar Lipids (Alabaster, AL, USA). Texas Red-DHPE was purchased from Biotium (Hayward, CA, USA). G_{M1} (Monosialoganglioside G_{M1}) was purchased from Sigma-Aldrich. Among them, NBD-

DOPE and Texas Red-DHPE are head group labeled lipids for fluorescence detection (Figure 2-4).

All lipids were dissolved and stored in chloroform stock solutions (c_{lipids} = 1-10 mg / mL) in a freezer at -20 °C.

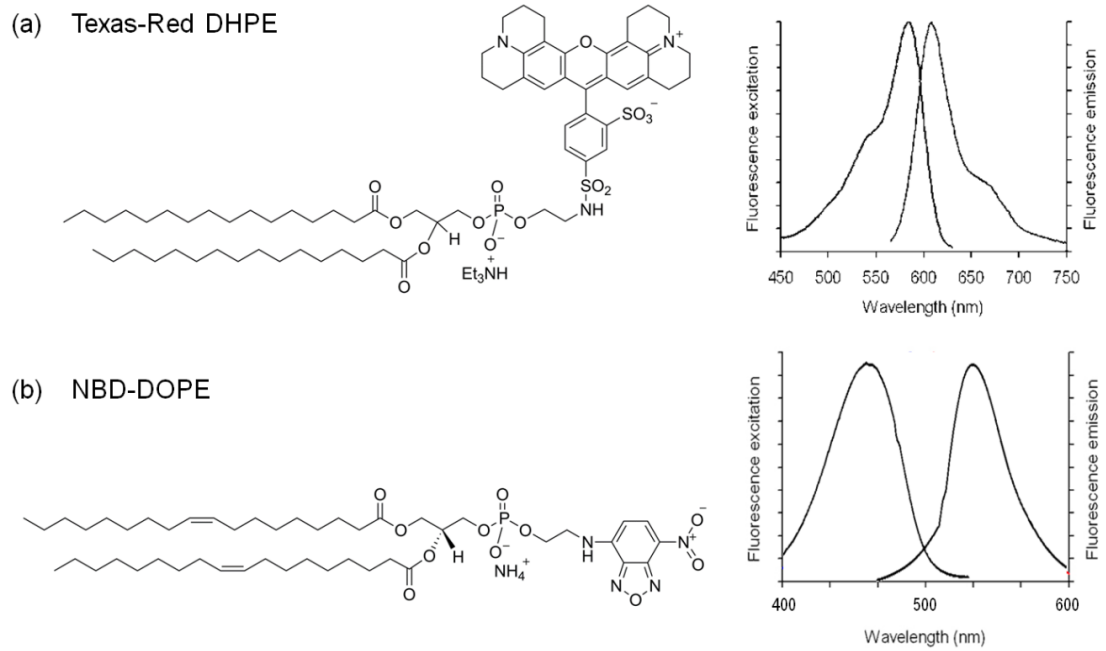

Figure 2-4 Structure (left) and spectrum (right) of fluorophore used in this work. (a) Texas red-DHPE. Excitation/Emission: 595/615 nm.[22] (b) NBD-DOPE. Excitation/Emission: 460/535 nm.[23]

2.2.2 CHEMICALS

All the chemicals were high-grade and used without further purification. Chloroform ($CHCl_3$), hydrofluoric acid solution (HF, 35 wt% in water), ammonium hydroxide solution ($NH_3 \cdot H_2O$, 25% in water), hydrogen peroxide solution (H_2O_2, 30 wt% in water), tris-(hydroxymethyl) aminomethane hydrochloride (Tris/HCl), sodium chloride (NaCl), potassium chloride (KCl), calcium chloride ($CaCl_2$) and 4-(2-Hydroxyethyl)piperazine-1-ethanesulfonic acid (HEPES) were purchased from Sigma-Aldrich. Sodium phosphate dibasic anhydrous ($Na_2HPO_4 \cdot 2H_2O$) was bought from AppliChem (Gatersleben, Saxony-Anhalt, Germany).

[22] Spectrum is taken from http://probes.invitrogen.com/media/spectra/1395lip.jpg.
[23] Spectrum is taken from http://www.avantilipids.com/images/Spectra/810145_Spectra.gif.

Deionized (DI) water used for all experiments was filtered by a Millipore system (MilliQ System from Millipore, Molsheim, France; resistance > 18 MΩ cm^{-1}).

2.2.3 BUFFER

Table 2-2 Abbreviation, compositions, pH value of buffers or solutions used for different applications.

Abbreviation	Composition	pH	Application
PB buffer	Na_2HPO_4 50 mM	6.8	Peptide modification; Fix the beads for CLSM
Tris buffer	Tris/HCl 10 mM NaCl 50/100/300 mM	7.4	Elliposometry for parameter optimization
Tris buffer	Tris/HCl 10 mM NaCl 300 mM	7.4	Preparation of membrane-coated beads
HEPES buffer	HEPES 50 mM KCl 150 mM	7.4	Fixing the beads for CLSM; Reducing electrostatic repulsion between beads
$CaCl_2$ solution	$CaCl_2$ 100 mM		Ca^{2+} triggered membrane fusion

DI water was used for all the buffer and solution preparation. Besides, it is also used for lipid film hydration, rinsing of beads and standard solution for membrane fusion assay.

All the buffers or solutions in this work were degassed in case of introducing air bubbles that might exposure the bilayer to air and destroy it.

2.2.4 SILICA BEADS

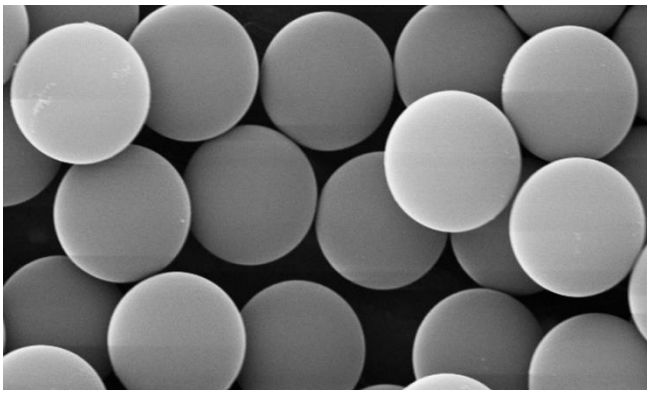

Figure 2-5 Scanning Electron Microscope image of Bangs Laboratories' (4.1 μm) silica microbeads.

Silica microbeads are frequently used as support for a variety of applications, including isolation of nucleic acids, cell separation, and immuno- and DNA-based assays.[13-15] In this work, the silica beads were used for preparing sealed supported bilayer, termed membrane-coated beads, as a model membrane.

These uniform, non-porous silica beads were obtained from Bangs Laboratories (Fisher, IN, USA) with mean diameters of 4.7 μm referred to as small beads (SBs), 6.5 μm classified so-called large beads (LBs) and 7.3 μm defined as LLB (Figure 2-5). Silica beads were stored in DI water at 4 °C and used as received without any further modification.

2.3 MEMBRANE-COATING OF BEADS

2.3.1 VESICLE PREPARATION

The vesicle preparation was carried out according to the protocol of Brian and McConnell.[16] The lipids with desired composition were first mixed in a glass test tube from chloroform stock solutions (c_{lipids} = 1-10 mg/mL). To form dry lipid films, mixture was put under a stream of nitrogen for about 30 min and in vacuum for at least 3 h to evaporate the solvent. Afterwards, the dry lipid film were hydrated in desired solvent (DI water) above the phase transition temperature for about 20 min and vortexes the suspension periodically, resulting a turbid MLV suspension. Finally, the MLVs were reduced in size by sonication (30 min, 50 W, 0.4 s pulse) in a vessel resonator (Sonoplus HD 2070, Bandelin, Berlin, Germany)**,** resulting in a clear and transparent SUV solution.

The lipid compositions are all given in mol% throughout the following text according to the different experiments and applications. LB was usually labeled with fluorophore (0.5% Texas Red-DHPE or 1.0% NBD-DOPE) while as SB not. In size-dependent assay, two populations of beads are labeled with NBD and Texas Red, respectively.

2.3.2 SLB ON SILICON WAFER

Elliposometry was used to monitor the process of SLB formation on silicon wafer with different compositions of lipids and various osmotic pressures of vesicles.

The silicon wafer (Active Business Company GmbH, Brunnthal, Germany; 525 nm thickness, 5.6-10.4 cm) was firstly cleaned by rinsing with isopropanol and deionized water. Afterwards, incubating the wafer in dilute HF solution (1%, *v/v*) for 15 min to remove the native SiO_2 layer from the surface and activated in $NH_3 \cdot H_2O/H_2O_2/H_2O$ (1:1:5, *v/v*) at 75 °C for 20 min, forming an active oxide layer. The hydrophilized wafer was rinsed with DI water thoroughly and used immediately. In order to enhance the hydrophilicity, oxygen plasma (plasma cleaner, Harrick, NY) can be applied for 1 min just before usage.

Because the purpose of this experiment is to optimize the experimental conditions of preparing membrane-coated beads rather than to study mechanism of SLB formation, which has been well investigated, thus the time regime of vesicle spreading is the only parameter of interest. Experiments were performed with a commercial ellipsometer (EP³-SW, Nanofilm Technology, Göttingen, Germany) as decribed obviously.[17, 18] All measurements were performed in a closed chamber with fixed incident angle of 60°. SLB was formed by spreading SUVs (0.2-0.3 mg/mL) in bulk solution onto silicon wafer. In order to change the osmotic pressure, different buffers were used for SUV preparation (inside of vesicles) and spreading (outside of vesicles), the detailed composition of buffer is described in chapter 3. The spreading buffer (Tris buffer) was used throughout the whole experiment. Data was collected with six data points/min. The following experimental procedure of preparing membrane-coated beads was based on the results of ellipsometry with optimized experimental condition.

2.3.3 PREPARATION OF SLB ON SILICA BEADS

Membrane-coated beads were prepared via the same vesicle adsorbing/spreading process as successfully applied to planar substrates and previously reported by Groves and coworkers.[19, 20] Bared silica microbeads were suspended in DI water with a final concentration of 10 wt%. Equal volumes (250 µL each) of a SUV solution (c_{SUV} = 1 mg/mL in DI water) and buffer (10 mM Tris, 300 mM NaCl, pH 7.4) were combined in a small centrifuge tube. Afterwards, 10 µL of the silica beads suspension (10 wt% of beads) were added and the resulted mixture was pulse vortexed for 20 min. During this time, a solid supported membrane was formed on the beads. Excess vesicles were removed by rinsing twice with DI water. For each rinsing step, the bead suspension was centrifuged using a mini centrifuge (LMS CONSULT, Brigachtal, Germany, maximum speed of 6000 rpm) and the supernatant was exchanged. The final volume was 200 µL; hence, the final concentration of resulting stock solution was 0.5 wt% of membrane-coated beads.

2.4 PEPTIDE MODIFICATION

2.4.1 PEPTIDE SYNTHESIS AND PURIFICATION[24]

Table 2-3 Schematic drawings, names and primary sequences of peptides.

Illustration	Name	*N*-Terminus	Sequence	*C*-terminus
	*i*-E3Cys	Ac-	$(KELAAIE)_3$	-GWGGGC-NH_2
	*i*-K3Cys	Ac-WG-	$(EKLAAIK)_3$	-GGGGC-NH_2
	K3Cys	Ac-WG-	$(KIAALKE)_3$	-GGGGC-NH_2

Solid phase peptide synthesis (SPPS), invented by Robert Bruce Merrifield in 1963, is an intensively used method in the lab for creating peptides.[21] In this work, all peptides were synthesized manually with Fmoc-strategy improved by as described obviously.[22, 23] Synthesis proceeded in a *C*-terminal to *N*-terminal fashion and amino acids with Fmoc group protected *N*-terminals were used. After cleaving the rude peptide from the polystyrene resin, reversed phase high-performance liquid chromatography (RP-HPLC) with linear gradient elusion was applied for purification. The resulting peptides were characterized by electrospray ionization mass spectrometry (ESI-MS).[18, 24] Using this protocol, a pair of coiled coil forming peptides *i*-E3Cys and *i*-K3Cys was synthesized as well as K3Cys that shares the inverted sequence of *i*-K3Cys. The detailed sequences of peptides are shown in Table 2-3.

[24] Dr. Gesa Pähler synthesized and purified the peptides in this work; the details are described in her doctoral thesis (2012): Lateral organization and thermodynamics of coiled-coil lipopeptides—implications for docking and fusion efficiency, University of Göttingen, Germany.

2.4.2 *IN SITU* COUPLING REACTION OF PEPTIDE

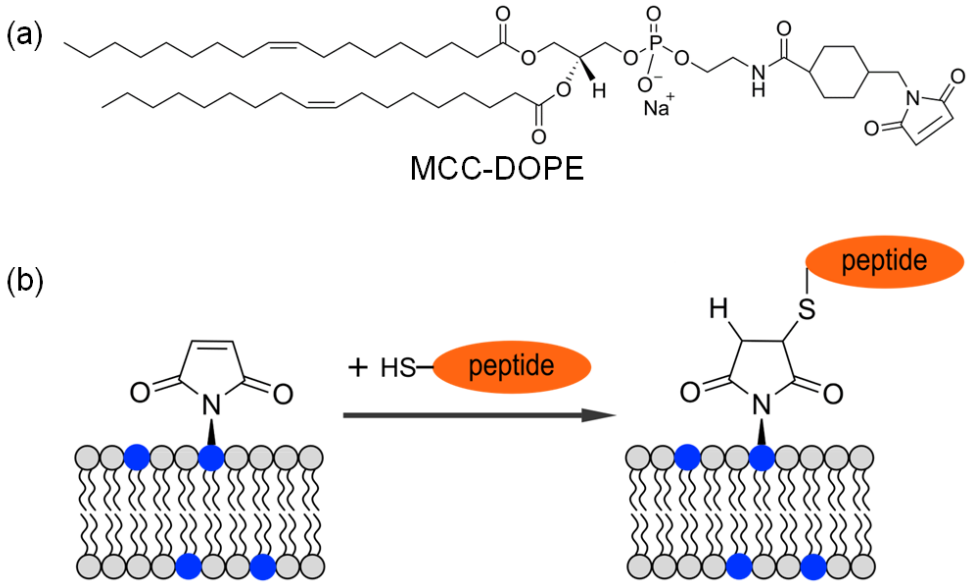

Figure 2-6 (a) Chemical structure of maleimide-functionalized lipid MCC-DOPE. (b) *In situ* coupling reaction of a peptide with a terminal cysteine moiety to a maleimide-functionalized lipid.

In situ coupling between terminal cysteine bearing peptides and maleimide-functionalized lipids have been intensively used for synthesis of lipopeptides, cell attachment, and modification of SLBs.[24-30] The reactions were based on Michael addition of free cysteine (exposing thiol group) to maleimide (thiol reactive group), which was one of the most widely used Michael acceptors in cysteine alkylation because of its high selectivity and reactivity under essentially neutral aqueous solution (Figure 2-6 a).[25, 31-33] Hence, the conjugation of cysteine-terminated peptides to maleimide-functionalized membranes provides a versatile and robust way to *in situ* modified membranes with peptides (Figure 2-6b).

In the former studies of membrane fusion, such conjugation strategy was employed to prepare fusogenic liposomes, while fusogenic membrane-coated beads were synthesized along the same way in this work.[18, 34] *In situ* coupling of peptides to planar SLBs were monitored with time-resolved ellipsometry in previous work of Dr. Pähler, hence, the

experimental procedure of preparing fusogentic membrane-coated beads in this work was developed according to the previous result.[18]

MCC-DOPE was used as maleimide-based lipid incorporated into the membranes on the beads (Figure 2-6a), and all peptide used in this work were cysteine-terminated peptides. The peptides were covalently coupled to the membrane-coated beads by incubating the beads with peptides (final $c_{peptide}$ = 100 µM) in phosphate buffer (50 mM Na_2HPO_4, pH 6.8) for 3 h at room temperature with gentle continuous mixing (vortexing). Excess peptide was removed by rinsing twice with DI water using a mini centrifuge.

2.5 DATA COLLECTION AND ANALYTICAL METHODS

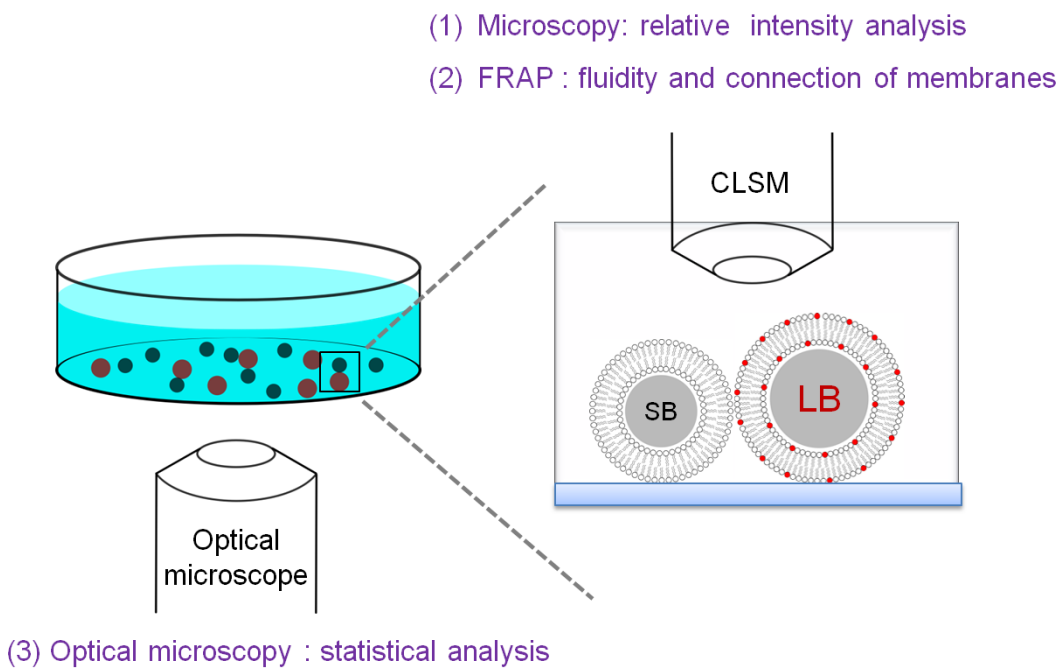

Figure 2-7 Schematic design of single fusion assay based on membrane-coated beads. CLSM, FRAP are used to determine and confirm the fusion events, while optical microscopy is employed to obtain statistical data on the fusion events.

Based on these monodisperse peptide-modified beads, a novel bead supported membrane fusion assay was established (Figure 2-7). In order to distinguish the two populations of beads with different fusogens, two sizes of beads were used so that only one fluorophore is enough in this case. Three kinds of characterization methods performed via CLSM and optical microscopy were applied to determine and quantify the fusion events for assay in various conditions. In this section, these three methods are introduced including detailed protocols and corresponding specific analytical method.

2.5.1 CLSM

CLSM was used to take fluorescent images and perform FRAP experiments in this work. In this section, the experimental protocol and relative intensity analysis are introduced.

2.5.1.1 PROTOCOLS

Peptide-modified stock solutions of LBs and SBs were first combined with the desired concentration in a centrifuge tube with DI water to prevent aggregation. Afterwards, the mixture of beads was transferred to a petri dish in DI water (total volume 3.5 mL). The petri dish was left undisturbed on the microscope stage for about 90 min, allowing the beads to settle down and find reaction partners by Brownian motion. However, the Brownian motion may produce unwanted drift of beads since imaging of CLSM is scanned line by line. Thus, HEPES buffer (0.5 mL) was adding 5 min before imaging to terminate the lateral mobility of the beads due to the electrostatic interaction between the beads and substrate. Note that ionic buffer must be added carefully in case of stirring up the beads and separating the connected beads.

Fluorescent images containing exactly one LB and one SB were taken by an upright confocal laser scanning microscope (CLSM) equipped with a water immersion objective at 63× magnification (LSM710, Zeiss, Jena, Germany). LB was labeled with 0.5% Texas Red-DHPE in this measurement while SB not. All the incubations and imaging were performed in the dark at room temperature.

2.5.1.2 RELATIVE INTENSITY ANALYSIS

In order to distinguish hemifusion and full fusion quantitatively, intensity analysis was applied to fluorescent images of a tethered pair analyzed by Image J software. Firstly, rotate the original image to horizontal position (the centers of beads are in a horizontal line) and select a rectangular profile crossing the pair with a width roughly equivalent to

the width of "visual" contact zone (the contact zone shown in the image other than the real contact zone of LB and SB which is unable to be seen). Afterwards, plot the profile displaying a two-dimensional graph of the intensities of pixels along the rectangular profile within the image, where the x-axis represents the horizontal distance through the selection and the y-axis is the vertically averaged pixel intensity. The peaks in the graph are corresponding to intensity of SB (I_{SB}), merged area and LB (I_{LB}). Here, only value of I_{SB} and I_{LB} are considered to calculate the relative intensity (I_{RI}) by equation

$$I_{RI} = \frac{I_{SB}}{I_{LB}}$$

In this work, the ideal I_{RI} values for hemifusion and full fusion are 0.4 and 1.0 respectively, the detailed calculation is described in the following text.

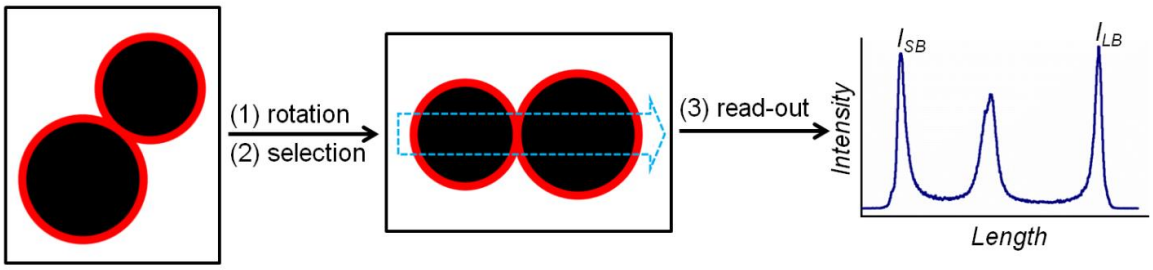

Figure 2-8 Schematic steps of intensity analysis by Image J.

2.5.1.3 IDEAL RELATIVE INTENSITY

The ratio of fluorescence intensities of SB and LB (relative intensity) after hemifusion and full fusion are generally computed based on the assumption that the system is under ideal conditions. For one thing, the lipid diffusion of both single leaflet and merged leaflet is "in equilibrium" meaning the distribution of fluorescent molecules is uniform; second, there is no detectable "flip-flop" between outer and inner leaflets.

Since after full fusion a merging of both leaflets occurred, which corresponds to an equal distribution of the fluorophore, the ratio of fluorescence intensity between SB and LB should be 1:1.

Hemifusion leads to a different picture. Here, the inner and outer leaflets of both beads need to be considered separately. Before the beads are in contact (t = 0 s), following intensities I can be defined:

$$I_{\mathrm{LB}}(0) = I_{\mathrm{LB}}^{out} + I_{\mathrm{LB}}^{in} = 1 \qquad with \qquad I_{\mathrm{LB}}^{out} = I_{\mathrm{LB}}^{in} = 0.5$$

$$I_{\mathrm{SB}}(0) = I_{\mathrm{SB}}^{out} + I_{\mathrm{SB}}^{in} = 0 \qquad with \qquad I_{\mathrm{SB}}^{out} = I_{\mathrm{SB}}^{in} = 0$$

Here, the subscripts indicate the bead size (LB or SB) while the superscripts refer to corresponding leaflet (*out* = outer leaflet, *in* = inner leaflet). Furthermore, it should be noted that before hemifusion, the intensities of outer and inner leaflet for SB and LB, respectively, are identical.

After hemifusion, the inner leaflets of the membrane remain unaltered in fluorescence intensity, while the outer leaflet of the membrane-coated LB undergoes dilution due to mixing with the outer leaflet of membrane-coated SB. Because of this dilution and the size difference between the two beads, the fluorescence intensity after hemifusion is different from 2:1. Since the area difference of the two populations of beads needs to be taken into account. The following calculation holds after merging of outer leaflets after without participation of inner leaflets:

$$I_{\mathrm{LB}}(t) = I_{\mathrm{LB}}^{out}(t) \cdot \frac{4\pi \cdot r_{\mathrm{LB}}^2}{4\pi \cdot (r_{\mathrm{LB}}^2 + r_{\mathrm{SB}}^2)} + I_{\mathrm{LB}}^{in} = 0.5 \cdot 0.65 + 0.5 = 0.83$$

$$I_{\mathrm{SB}}(t) = I_{\mathrm{LB}}^{out}(t) \cdot \frac{4\pi \cdot r_{\mathrm{LB}}^2}{4\pi \cdot (r_{\mathrm{LB}}^2 + r_{\mathrm{SB}}^2)} + I_{\mathrm{SB}}^{in} = 0.5 \cdot 0.65 + 0 = 0.33$$

From these calculations, a final fluorescence intensity ratio of 0.83:0.33 concerning LB to SB can be defined, that the SB irradiates at 40% of the intensity produced by the LB.

2.5.2 FRAP

FRAP experiments were originally intended to characterize the motion of fluorescently labeled molecules of a single cell membrane, but nowadays are used to study lateral diffusion of artificial lipid membranes. In this work, on the one hand, FRAP was used to measure the fluidity of lipid bilayer on single silica bead; on the other hand, it was applied to confirm that whether lipid-mixing (hemifusion/full fusion) did occur between LB and SB in a tethered pair. If recovery happens for lipid-mixing pair, meaning that the bilayers of the two beads are connected.

The sample preparation and instrument were the same as fluorescent imaging by CLSM but NBD-DOPE was used for LB labeling since Texas Red-DHPE is too photostable to be bleached.

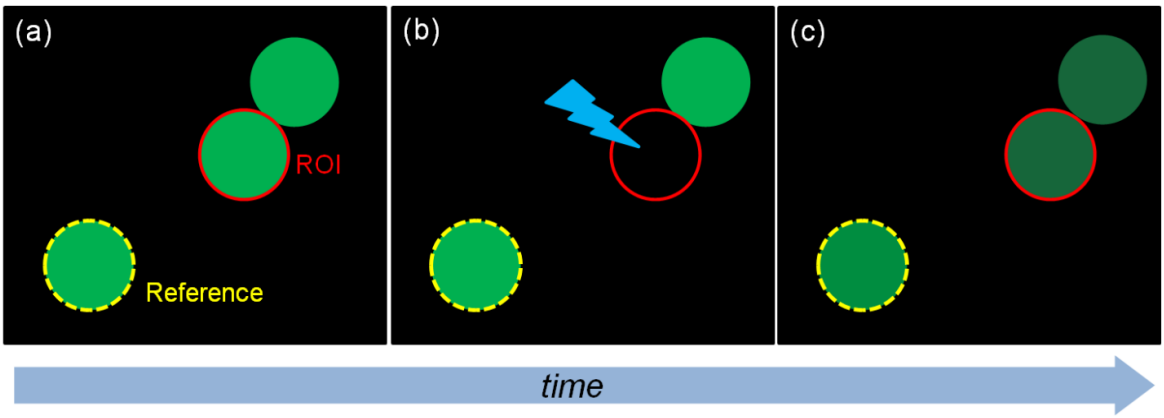

Figure 2-9 Schematic illustrating the FRAP experiment performed on a lipid-mixing (hemifusion or full fusion) pair of beads. A total SB is fully bleached (ROI, red circle) and a single bead far away is chosen as reference due to photobleaching. The time sequence fluorescent images (a) prior bleaching, (b) directly after bleaching and (c) after fluorescence recovery are recorded.

For FRAP on single bead, a tiny ROI was selected on the top of the bead and the similar area was chosen as reference on the other single bead. For FRAP on a lipid-mixing pair (hemifusion/full fusion), SB was bleached totally a single bead nearby was chosen as a reference for taking into account of photobleaching (Figure 2-9). For both of the cases, time-lapse images were taken and analyzed with supplier's ZEN 2008 software. Besides, the regime of recovery time of these two cases were compared to estimate the impact of contact zone on lipid diffusion between LB and SB in a lipid-mixing pair.

2.5.3 OPTICAL MICROSCOPY

2.5.3.1 PROTOCOLS

Peptide-modified stock solutions of LBs and SBs were uniformly mixed in a centrifuge tube and then the mixture (total volume 250 µL) was pipetted into one well of a 96-well-plates (TPP, Switzerland, 92696). Generally, the fill-height of bead solution in

one well is about 8 mm and the beads take around 15 min to gravitationally down to the bottom (diameter ~ 4.7 µm). Incubation time of 90 min was necessary that allowed a sufficient number of tethered pairs for the following statistic analysis. Both bright-field and fluorescence images at the same positions were acquired with 40× air objective, at room temperature using an inverted fluorescence microscope (Axiovert 200, Zeiss, Jena, Germany) equipped with a sCMOS camera (ORCA-Flash 2.8, Hamamatsu, Tokyo, Japan) read out with the proprietary HCImageLive acquisition software.

2.5.3.2 STATISTICAL ANALYSIS OF FUSION EVENTS

Even though the membranes on the SBs are not fluorescently labeled, both bead populations can be readily distinguished by size discrimination using an optical microscope (Figure 2-10a, left). The fluorescence label embedded in the lipid bilayer covering the LBs, allows us to detect fusion events by fluorescence microscopy of the same area (Figure 2-10a, right). This enables simultaneously quantification of docking, hemifusion, and full fusion.

The envisioned read-out of membrane fusion is illustrated in Figure 2-10b, which is corresponding to the experimental results shown in Figure 2-10a. Starting with two bead populations differing in size and lipid composition of membranes, all connected bead pairs consisting of exactly one LB and one SB are considered, which are called tethered pairs in the following. From these tethered pairs, the three main steps of membrane fusion, *e.g.* docking, hemifusion and full fusion, can be easily distinguished by reading out the fluorescence intensity of the lipid membranes covering connected LB and SB pairs, while simultaneously taken bright field microscopy images allow the detection of all beads. A fluorescent membrane on a LB in contact with a dark SB characterizes docking without fusion. In this thesis, the term “hemifusion” is used synonymously with merging of the two outer membrane leaflets. Therefore, this term is not thoroughly precise since the molecular organization concerning incipient stalk formation and a fully formed diaphragm-shaped hemifusion in the contact area is yet unknown.

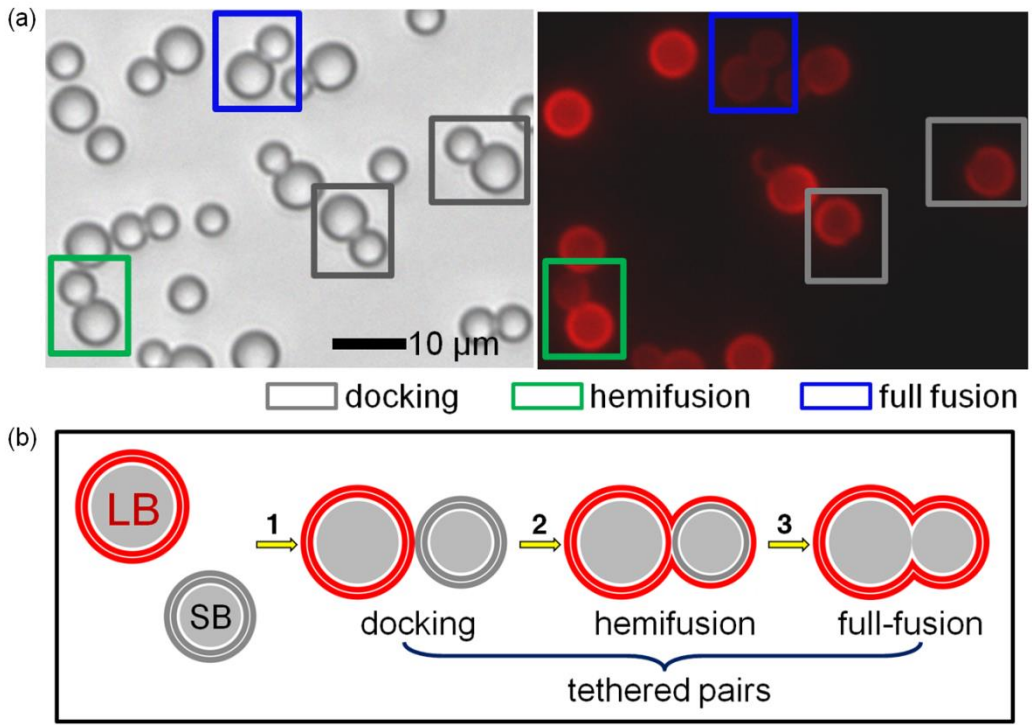

Figure 2-10 Principle of the 2D fusion assay based on membrane-coated beads. (a) Bright field (left) and corresponding fluorescence image (right) of LBs and SBs modified with coiled coil forming peptides. From the distribution of the fluorophore, docked pairs (grey box), hemifused pairs (green box) as well as fully fused pairs (blue box) can be clearly distinguished. (b) Schematic illustration of scenarios after mixing of LBs and SBs. Plain docking (1) followed by hemifusion (2) and eventually full fusion of the bilayer (3). All pairs consisting of exactly one LB and one SB, regardless of interaction state of the employed lipid bilayers, are considered as tethered pairs.[25]

Statistical analysis consisted of two steps. First, the number of tethered pairs ($N_{\text{tethering}}$) was counted manually in bright field images, and was compared with tethered pairs in the fluorescence image to distinguish the docked pairs (N_{docking}) from hemifused and fully fused pairs ($N_{\text{hemifusion}}$, $N_{\text{full fusion}}$). Naturally, $N_{\text{tethering}}$ is the sum of N_{docking}, $N_{\text{hemifusion}}$ and $N_{\text{full fusion}}$. Calculation of the tethering efficiency, hemifusion efficiency as well as full fusion efficiency proceeds as follows: docking efficiency = $N_{\text{docking}}/N_{\text{tethering}}$, hemifusion efficiency = $N_{\text{hemifusion}}/N_{\text{tethering}}$, full fusion efficiency = $N_{\text{full fusion}}/N_{\text{tethering}}$.

[25] Figure is taken from Bao, C. X., Pähler, G., Geil, B., and Janshoff, A. (2013) Optical fusion assay based on membrane-coated spheres in a 2D assembly, *J Am Chem Soc 135*, 12176-12179.

2.6 REFERENCE

[1]. Abramowitz, M., and Davidson, M. W. Introduction to Microscopy, *Molecular expressions*.

[2]. Schermelleh, L., Heintzmann, R., and Leonhardt, H. (2010) A Guide to Super-Resolution Fluorescence Microscopy, *J Cell Biol 190*, 165-175.

[3]. Cremer, C., and Cremer, T. (1978) Considerations on a Laser-Scanning-Microscope with High Resolution and Depth of Field, *Microsc Acta 81*, 31-44.

[4]. Fellers, T. J., and Davidson, M. W. Introduction to Confocal Microscopy, *Olympus Fluoview Resource Center*.

[5]. Conchello, J. A., and Lichtman, J. W. (2005) Optical Sectioning Microscopy, *Nat Methods 2*, 920-931.

[6]. Axelrod, D., Koppel, D. E., Schlessinger, J., Elson, E., and Webb, W. W. (1976) Mobility Measurement by Analysis of Fluorescence Photobleaching Recovery Kinetics, *Biophys J 16*, 1055-1069.

[7]. Liebman, P. A., and Entine, G. (1974) Lateral Diffusion of Visual Pigment in Photoreceptor Disk Membranes, *Science 185*, 457-459.

[8]. Poo, M., and Cone, R. A. (1974) Lateral Diffusion of Rhodopsin in the Photoreceptor Membrane, *Nature 247*, 438-441.

[9]. Schlessinger, J., Koppel, D. E., Axelrod, D., Jacobson, K., Webb, W. W., *et al.* (1976) Lateral Transport on Cell Membranes: Mobility of Concanavalin a Receptors on Myoblasts, *Proc Nat Acad Sci USA 73*, 2409-2413.

[10]. Alberts, B., Bray, D., and Lewis, J. (2002) *Molecular Biology of the Cell*, Vol. 10, 4th ed.

[11]. Drude, P. (1887) *Ueber Die Gesetze Der Reflexion Und Brechung Des Lichtes an Der Grenze Absorbirender Krystalle*, Druck von Metzger & Wittig, Leipzig,.

[12]. Rothen, A. (1945) The Ellipsometer, an Apparatus to Measure Thicknesses of Thin Surface Films, *Rev Sci Instrum 16*, 26-30.

[13]. Steinberg, G., Stromsborg, K., Thomas, L., Barker, D., and Zhao, C. F. (2004) Strategies for Covalent Attachment of DNA to Beads, *Biopolymers 73*, 597-605.

[14]. Walsh, M. K., Wang, X., and Weimer, B. C. (2001) Optimizing the Immobilization of Single-Stranded DNA onto Glass Beads, *J Biochem Biophys Methods 47*, 221-231.

[15]. van der Meulen, S. A., and Leunissen, M. E. (2013) Solid Colloids with Surface-Mobile DNA Linkers, *J Am Chem Soc 135*, 15129-15134.

[16]. Brian, A. A., and Mcconnell, H. M. (1984) Allogeneic Stimulation of Cyto-Toxic T-Cells by Supported Planar Membranes, *Proc Nat Acad Sci-Biol 81*, 6159-6163.

[17]. Faiss, S., Schuy, S., Weiskopf, D., Steinem, C., and Janshoff, A. (2007) Phase Transition of Individually Addressable Microstructured Membranes Visualized by Imaging Ellipsometry, *J Phys Chem B 111*, 13979-13986.

[18]. Pähler, G., Panse, C., Diederichsen, U., and Janshoff, A. (2012) Coiled-Coil Formation on Lipid Bilayers-Implications for Docking and Fusion Efficiency, *Biophys J 103*, 2295-2303.

[19]. Baksh, M. M., Jaros, M., and Groves, J. T. (2004) Detection of Molecular Interactions at Membrane Surfaces through Colloid Phase Transitions, *Nature 427*, 139-141.

[20]. Winter, E. M., and Groves, J. T. (2005) Surface Binding Affinity Measurements from Order Transitions of Lipid Membrane-Coated Colloidal Particles, *Anal. Chem. 78*, 174-180.

[21]. Merrifield, R. B. (1963) Solid Phase Peptide Synthesis .1. Synthesis of a Tetrapeptide, *J Am Chem Soc 85*, 2149-2154.

[22]. Pähler, G., Lorenz, B., and Janshoff, A. (2013) Impact of Peptide Clustering on Unbinding Forces in the Context of Fusion Mimetics, *Biochem Bioph Res Comm 430*, 938-943.

[23]. Schuy, S., Schäfer, E., Yoder, N. C., Kumar, K., Vogel, R., *et al.* (2009) Lipopeptides Derived from HIV and Siv Mimicking the Prehairpin Intermediate of Gp41 on Solid Supported Lipid Bilayers, *J Struct Biol 168*, 125-136.

[24]. Schuy, S., Treutlein, B., Pietuch, A., and Janshoff, A. (2008) In Situ Synthesis of Lipopeptides as Versatile Receptors for the Specific Binding of Nanoparticles and Liposomes to Solid-Supported Membranes, *Small 4*, 970-981.

[25]. Elliott, J. T., and Prestwich, G. D. (2000) Maleimide-Functionalized Lipids That Anchor Polypeptides to Lipid Bilayers and Membranes, *Bioconjugate Chem 11*, 832-841.

[26]. Svedhem, S., Dahlborg, D., Ekeroth, J., Kelly, J., Höök, F., *et al.* (2003) In Situ Peptide-Modified Supported Lipid Bilayers for Controlled Cell Attachment, *Langmuir 19*, 6730-6736.

[27]. Marsden, H. R., Elbers, N. A., Bomans, P. H. H., Sommerdijk, N. A. J. M., and Kros, A. (2009) A Reduced SNARE Model for Membrane Fusion, *Angew Chem Int Ed 48*, 2330-2333.

[28]. Schuy, S., Schäfer, E., Yoder, N. C., Hobe, S., Kumar, K., *et al.* (2009) Coiled-Coil Lipopeptides Mimicking the Prehairpin Intermediate of Glycoprotein Gp41, *Angew Chem Int Ed 48*, 751-754.

[29]. Zheng, T. T., Voskuhl, J., Versluis, F., Zope, H. R., Tomatsu, I., *et al.* (2013) Controlling the Rate of Coiled Coil Driven Membrane Fusion, *Chem Commun 49*, 3649-3651.

[30]. Cavalli, S., and Kros, A. (2008) Scope and Applications of Amphiphilic Alkyl- and Lipopeptides, *Adv Mater 20*, 627-631.

[31]. Chalker, J. M., Bernardes, G. J. L., Lin, Y. A., and Davis, B. G. (2009) Chemical Modification of Proteins at Cysteine: Opportunities in Chemistry and Biology, *Chem-Asian J 4*, 630-640.

[32]. Moore, J. E., and Ward, W. H. (1956) Cross-Linking of Bovine Plasma Albumin and Wool Keratin, *J Am Chem Soc 78*, 2414-2418.

[33]. Sechi, S., and Chait, B. T. (1998) Modification of Cysteine Residues by Alkylation. A Tool in Peptide Mapping and Protein Identification, *Anal Chem 70*, 5150-5158.

[34]. Versluis, F., Voskuhl, J., van Kolck, B., Zope, H., Bremmer, M., *et al.* (2013) In Situ Modification of Plain Liposomes with Lipidated Coiled Coil Forming Peptides Induces Membrane Fusion, *J Am Chem Soc 135*, 8057-8062.

3 RESULTS AND DISCUSSION

In this chapter, the results and discussion of both experimental and theoretical work are described, including (1) preparation and characterization of monodisperse membrane-coated beads; (2) the fusion assay under different conditions; (3) simulation of tiny contact zone between beads in a lipid mixing pairs; (4) cons and pros of this novel method compared to traditional assays.

3.1 SLB FORMATION ON SILICON SUBSTRATE

The preparation of monodisperse membrane-coated beads is the basis of this work. The planar SLB preparation has been well studied. The experiments were always performed by incubating planar substrates in desired vesicle buffer for minutes up to hours depending on the properties of both vesicles and substrate.[1-4] However, this protocol may cause problems for membrane-coated bead preparation although they share the same mechanism of vesicle spreading on a solid support. In this section, the optimization of experimental conditions for membrane-coated beads and its characterization including the Brownian motion are introduced.

3.1.1 HYPOTHESIS OF LIPID PATCH INTEGRATION ON BEADS

For planar substrates, once a bilayer patch has been formed accompany by an exposure edge. In order to minimize its edge length, it then interacts with the neighboring patches or vesicles, resulting a larger bilayer patch and finally a complete SLB.[5-9] However, the process of bilayer patch growth and coalescence is not exactly the case for SLB formation on silica beads (Figure 3-1). After mixing the SUVs and silica beads, the SUVs adsorb and rupture onto the surface of beads like on the planar substrates; but the patch propagation may occur in different ways depending on where the “neighboring patches” come from. The first way is that the patches coalesce with other patches on the same bead or vesicles in the solution, forming a complete sealed bilayer over the bead.

The resulting membrane-coated beads are the desired monodisperse beads because of the electrostatic repulsion between beads (Figure 3-1, pathway 1).

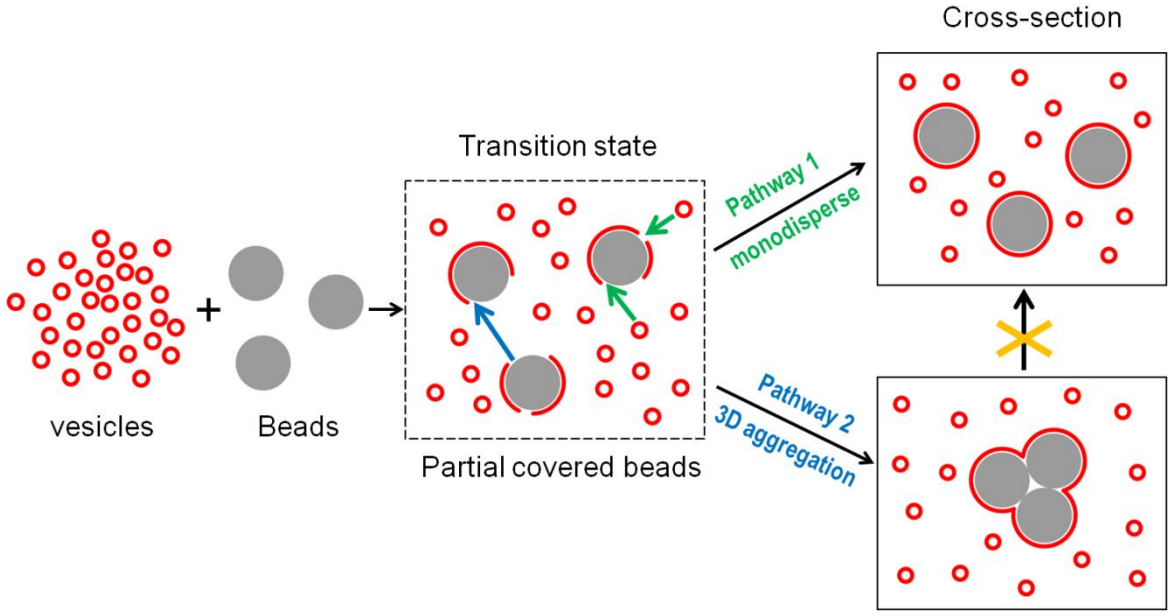

Figure 3-1. Illustration of hypothetic pathways of lipid patches integration on silica beads. Once vesicles and silica beads are mixed, there is a transition state during which the beads are partially covered by lipid patches (dashed box). The monodisperse membrane-coated beads are desirable (pathway 1, green) while three-dimensional (3D) aggregation may occur because the patches from different beads coalesce (pathway 2, blue) if the total surface area of vesicles is sufficient. The polydisperse bead collection cannot be converted into a monodisperse collection.

Alternatively, the existing patches extend by assembling the patches on other beads in bulk solution; this may cause irreversible three-dimensional (3D) aggregation that cannot be redispersed by sonication (Figure 3-1, pathway 2). This 3D aggregation is mainly caused by two factors. One factor is the total surface area of SUVs. If it is insufficient for covering the total surface of the beads, the patches on different partial-covered beads have to merge in order to reduce the edge effect, forming a multi-bead cluster covered with one continuous bilayer. Therefore, excess vesicles are always used in the experiments to offer sufficient bilayer area. The other factor is that the kinetic time of SLB formation is so long that the patch assembly occurs between different beads due to the random, fast and continuous bead collision.

In order to optimize the experimental conditions for preparing monodisperse membrane-coated beads, the investigation of vesicle spreading process on silica beads is

necessary. However, it is hard to perform experiments on silica beads via common methods such as QCM, SPR and ellipsometry. Therefore, silicon wafer was used as an alternative substrate because both have extremely similar surface chemistry. Ellipsometry was used to monitor the vesicle spreading process upon various lipid compositions, buffers, *etc.* The main goal of the ellipsometry experiments was to figure out the optimal experimental conditions for SLB formation, including vesicle adsorption, rupture, and lipid patch evolution. The faster the SLB forms on silica wafer, the better the monodisperse of membrane-coated beads is.

3.1.2 SLB FORMATION ON FLAT SUBSTRATE

3.1.2.1 PATHWAYS OF VESICLE DEPOSITION[5]

From the perspective of vesicle stability, Richter and co-workers classified four main pathways of vesicle deposition by dissipation monitoring of the process with QCM-D (Figure 3-2).[5, 8, 10-13] When a planar silica substrate is incubating in a vesicle bulk solution, the first scenario is that vesicle do not adsorb at all (Figure 3-2a). Besides, the vesicles adsorb onto the substrate either remain intact (Figure 3-2b) forming a supported vesicular layer (SVL) or give rise to a SLB when a large amount of vesicles adsorb as an intermediate state (Figure 3-2c). The last pathway is that the vesicles adsorb and rupture instantaneously, triggered by the interaction with the solid support (Figure 3-2d).

In general, which pathway will be taken is determined by the "nature of the support (surface charge, chemical composition, and roughness), the lipid vesicles (composition, charge, size, and physical state), as well as the aqueous environment (the pH and ionic strength)."[14] In this work, silicon wafer was used as support since it is the best alternative of silica beads; the role of vesicle with various charges and buffers with different ionic strength were studied.

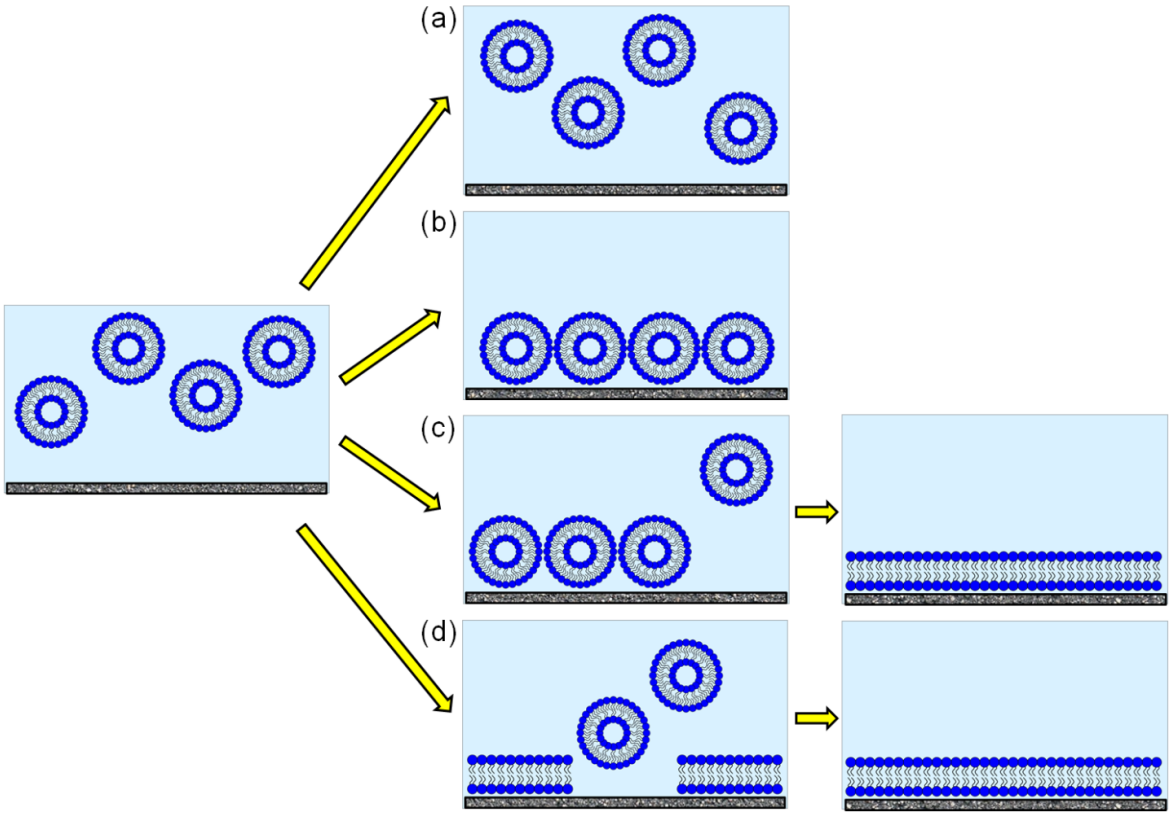

Figure 3-2 Schematic pathways of vesicle spreading on flat substrate. (a) Vesicles do not adsorb. (b) Vesicles adsorb but do not rupture, forming a supported vesicular layer (SVL). (c) Vesicles adsorb and rupture at high vesicular coverage, SLB forms. (d)Vesicles adsorb and rupture instantaneously, forming a continuous SLB.[26]

3.1.2.2 VESICLE SPREADING ON SILICON WAFER

Electrostatic interaction plays an important role in SLB formation, which has been studied by several research groups mainly based on the charge of support and vesicles as well as ionic strength of the solution.

The SLB formation using vesicles with different charges were first investigated. In these experiments, both inside and outside solution of the vesicles is DI water, hence there is no osmotic pressure. Figure 3-3 shows typical temporal variations of Δdel that is proportional to the thickness of the film. Obviously, the 10% negative vesicles (black

[26] Figure is adapted and redrawn from Richter, R. P., Berat, R., and Brisson, A. R. (2006) Formation of solid-supported lipid bilayers: an integrated view, *Langmuir 22*, 3497-3505.

curve) were almost not adsorbed over the whole time regime since the *Δdel* value did not change, due to the electrostatic repulsion between the negative vesicles and the negative substrate (pathway (a) in Figure 3-2a). When 0.5% positive vesicles were used, they initially adsorb without rupturing (for $t < t_1 \approx 15$ min) and start to rupture after reaching a critical vesicular coverage, then a lipid bilayer is formed (pathway in Figure 3-2c). The bilayer is saturated and stable at $t > t_2$, that is, the thickness is no longer increasing. When the positive charge increases up to 10%, the strong electrostatic attraction dominates the interaction between the vesicles and substrate hence the vesicle adsorb and rupture instantaneously ($t_1 \approx t_2$), the bilayer is complete after t_2 (pathway in Figure 3-2d). This is the desired pathway in this work since the process has the shortest time of vesicle adsorption ($t_1 \approx 3$ min), and of vesicle rupture and patches assembly ($\Delta t \approx t_2 - t_1 \approx 0$ min). It should therefore effectively prevent from aggregating. The ion strength of solution was investigated by using 0.5% positive charge vesicles (Figure 3-2b). Obviously, both of t_1 and t_2 are dramatically shortened in ionic buffer (10 mM Tris, 50 mM NaCl, pH 7.4) compare to DI water. This is because the increased ionic strength shrinks the electric double layers, which allows the vesicles to get closer without being repelled.

The above results clearly show that the vesicle to bilayer transformation is influenced by ion electrostatic interaction involving the charge of vesicles and the ion strength of buffer. Further investigations were performed on vesicles that were used in the following work for peptide modification (10% negative charge, DOPC/MCC-DOPE 90/10). Figure 3-3c shows results of vesicle spreading process in Tris buffer (10mM Tris, pH 7.4) but with different concentrations of NaCl (0-300 mM). The transformation time decreases as the ionic strength increases. 300 mM NaCl allows the fastest transformation and is therefore used in the following preparation of membrane-coated beads. Note that the ionic strength investigation in this work could also be considered as different osmotic pressure since the internal solution of vesicles is DI water for all experiments. Reimhult and co-workers proved that “osmotic pressure promotes bilayer formation, especially when the external salt concentration is higher than the internal one”.[12]

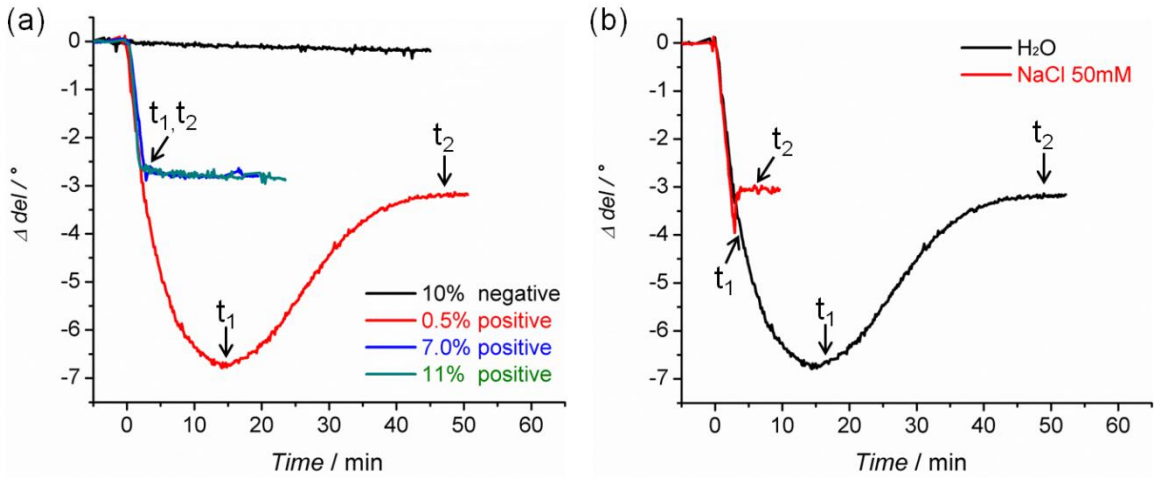

Figure 3-3 Kinetic process of vesicle deposition onto silicon wafer monitored by ellipsometer. Curves are presented for (a) vesicles carry various charges: 10% negative charge (MCC-DOPE/DOPC 10/90), 0.5% positive charge (DMOPC/DOEPC/Texas Red-DHPE/G_{M1} 97.5/1.5/0.5/0.5), 7.0% positive charge (DMOPC/DOEPC/Texas Red-DHPE 92.0/7.5/0.5) and 11.0% positive charge (DMOPC/DOEPC/Texas Red-DHPE 88/11.5/0.5). All fractions are given in mol% and both internal and external solution of vesicles are DI water. (b) Vesicles of 0.5% positive charge in different external buffer: DI water (black) and 10 mM Tris, 50 mM NaCl, pH 7.4), the internal buffer is DI water.

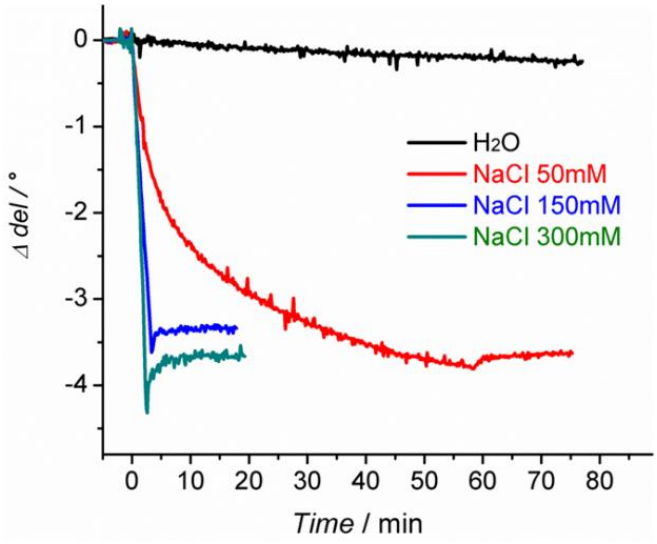

Figure 3-4 Kinetic process of vesicle deposition onto silicon wafer at four different bulk concentrations of NaCl (in Tris 10 mM, pH 7.4). The vesicles carried 10% negative charge and the solution inside the vesicles was DI water.

3.2 MONODISPERSE MEMBRANE-COATED BEADS[27]

The membrane-coated beads were characterized by bright field microscopy, fluorescence microscopy and FRAP. Microscopy was used to investigate the dispersion of bead collection and FRAP was used to proof the fluidity of the lipid bilayer coating.[15]

3.2.1 MICROSCOPY

In this work, bright field microscopy and fluorescent microscopy were used. Bright field microscopy offers the information of dispersion of bead collections while fluorescence microscopy gives membrane coating information. Sometimes, the comparison of both images is used to determine whether the beads really stick together.

In order to characterize the 2D dispersion of the sedimented beads, experiments were performed on peptide free beads of different sizes (LBs and SBs) in DI water (Figure 3-5). Since the SBs in this work are not fluorescence labeled, only bright field images are taken (Figure 3-5a). Obviously, both SBs and LBs have a good dispersion due to the electrostatic repulsion between the negatively charged bilayers. Since the source of lipid patches can come from different beads as described in last section (Figure 3-1), very a few dimmers are reasonable to be seen (yellow arrows). These dimmers do not separate into single beads over time and move as a whole. However, there are also some beads showing different behavior in bright field and fluorescence images (white arrows). Those are tethered like a dimer in bright field image but separated in the corresponding fluorescence image. This phenomenon is due to the Brownian motion during the very short interval (about ten seconds) between subsequently bright field and fluorescence images. The two beads just collide but are not coated by one complete bilayer, so called "apparent dimer". In all fusion assays, these "apparent dimers" (contains one LB and one SB) are common but can be distinguished easily when comparing bright field image and fluorescence

[27] Most of the data in this section has been published in Bao, C. X., Pahler, G., Geil, B., and Janshoff, A. (2013) Optical fusion assay based on membrane-coated spheres in a 2D assembly, *J Am Chem Soc 135*, 12176-12179.

image. Thus, they will not cause an error in statistical analysis that taking them as a tethered pair. Relatively, if the beads in a dimer maintain stick to each other in both images, the dimmer is considered as a tethered pair.

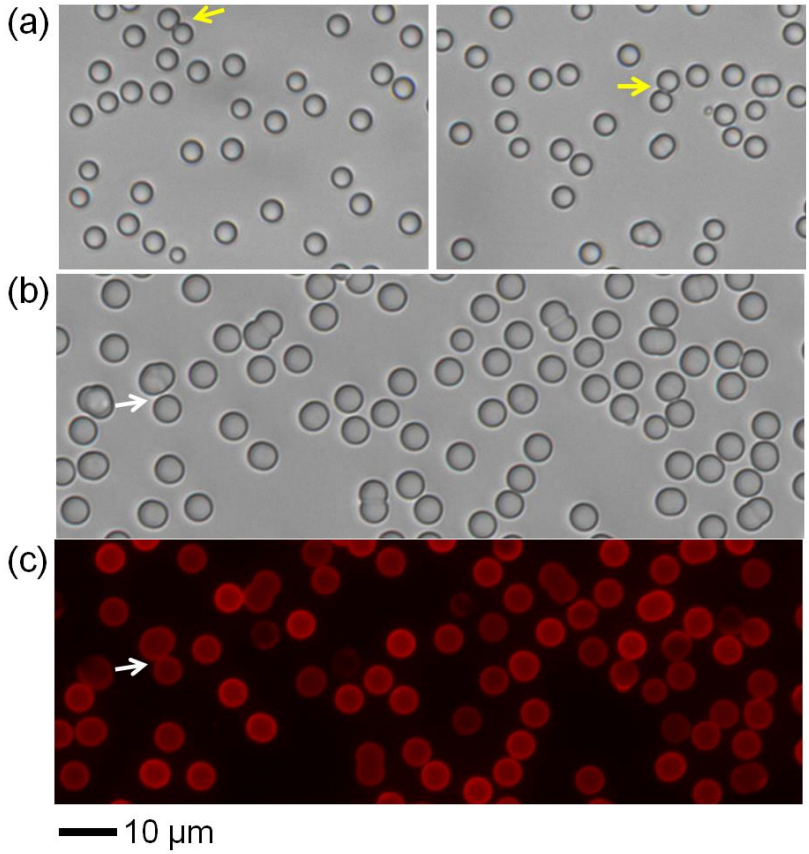

Figure 3-5 Microscopy of membrane-coated beads without peptide modification. Lipid composition of small beads (SBs) is DOPC/MCC-DOPE 90/10 while in large beads (LBs) it is DOPC/MCC-DOPE/Texas Red-DHPE 89.5/10/0.5. (a) Bright field images of SBs. The beads are monodisperse but with dimer occasionally. Two images are taken at different positions of the sample. (b) Bright field and (c) the corresponding fluorescence images of LBs. White arrows point to "apparent dimers" where two beads are detached in the bright field image but look like a dimer in the fluorescence image.

3.2.2 FRAP

In order to characterize the fluidity and continuity of the bilayer on the beads, FRAP experiments are performed on top of a single membrane-coated LB. In this case, the recovery of fluorescence is achieved around 10 s. The incomplete recovery is not only due to the immobile fraction of lipid bilayer but also originates from an exhausting membrane reservoir on the bead.[16] The resulting fluidity of membrane is as expected for solid supported lipid bilayers.[17, 18] This result indicates that the bilayer is separated from the underlying bead by the water film and the natural structure and biological functionality are conserved.[19]

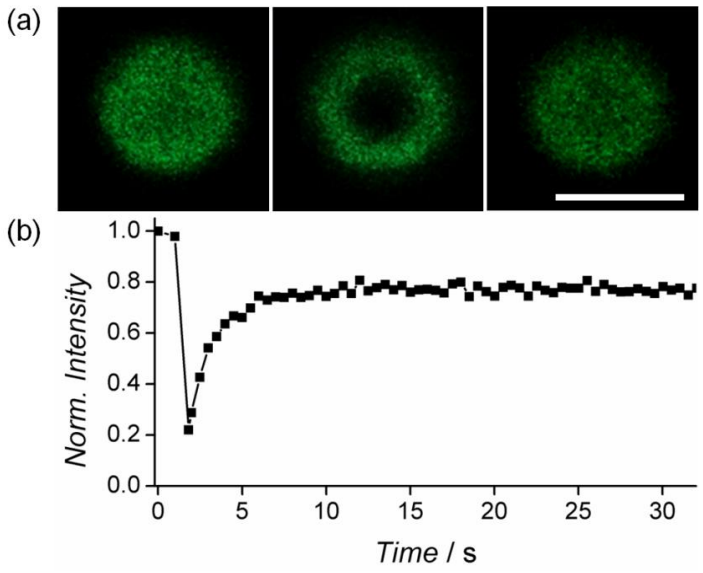

Figure 3-6 Fluorescence recovery after photobleaching (FRAP) experiment performed on single LB. (a) Fluorescence micrographs prior to bleaching the NBD fluorophore, directly after bleaching and after fluorescence recovery (from left to right). (b) Corresponding plot of the normalized fluorescence intensity of the bleached area as a function of time. Brownian motion of membrane-coated beads

Time sequences of micrographs showing membrane-coated beads in DI water are presented in Figure 3-7. The pictures were collected 20 min after the beads gravitationally rested on the bottom of a sample well. Since the incubation time of all experiments was set

to 90 min, the beads had enough time to interact. The images were taken slightly out–of–focus, which makes it easier for tracking the beads in self-written software.

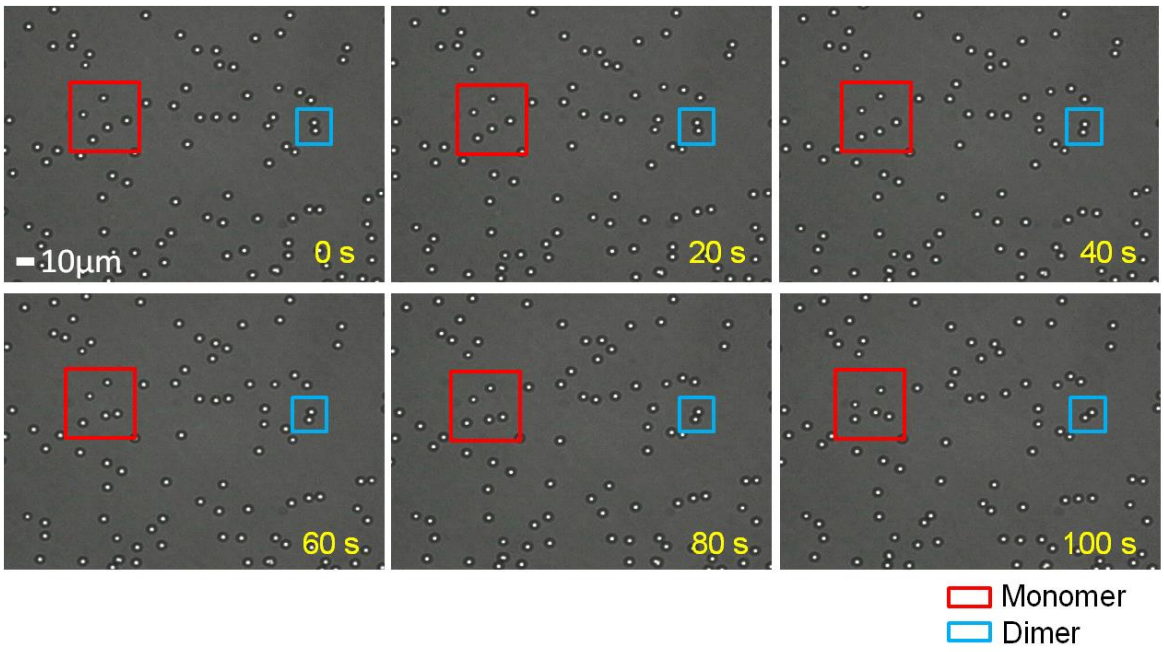

Figure 3-7 Time-dependent images from gravitationally sedimented membrane-coated beads in DI water. Size of bead is 4.7 µm (SB) and membrane composition is DOPC/MCC-DOPE/Texas Red-DHPE 89.5/10/0.5. Time of the image taken is given in the right corner of each micrograph (yellow). In the red rectangle, motion of single beads is highlighted, while in the blue rectangle the motion of a bead dimer is visible.

From the micrographs, collected in a time-span of 100 s, it becomes obvious that beads display Brownian motion, which allows them to self-assemble in a two dimensional way according to their interparticle-affinity. In the red box, single beads are highlighted during their movement. In the blue box, a bead dimer is highlighted. This dimer also undergoes Brownian motion (slowed down due to its increased size); however, the beads usually do not separate into single beads.

Brownian motion is dramatically decreased when ions are introduced into the medium due to the increasing electrostatic attraction between beads and substrate. The beads do not move at all in 10mM NaCl solution. Therefore, the fusion assay experiments are always performed in DI water in order to allow the beads to interact with others. If salt is necessary for the experiments, *e.g*, Ca^{2+} triggering fusion, the ions are always introduced after the beads settled down to the bottom and react with their partners (about 90 min).

Note that 3D aggregation is observed if the salt solution is injected to the bulk bead solution directly.

However, the immobile beads in salt solution offer an extremely simple strategy for fixing the beads comparing to the complex fixation method of SUVs or GUVs.[20-25] In those experiments, the vesicles were always tethered to PEG-coated substrate via biotin-avidin interactions. Therefore, salts are used in all CLSM/FRAP experiments to ensure that the beads cannot move during the measurement.

3.3 FUSION ASSAY BASED ON LB/SB[28]

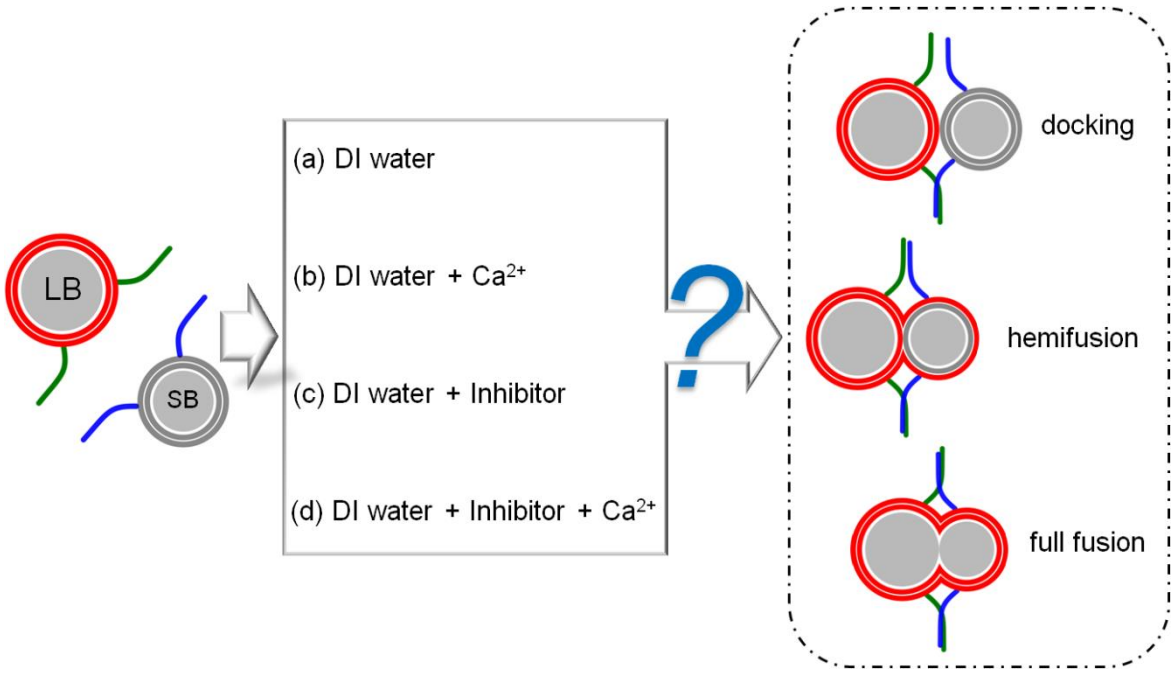

Figure 3-8 Schematic presentation of four strategies that can be employed by this new method. The experiments were performed (a) in DI water, (b) in the presence of Ca^{2+}, (c) with inhibitor and (d) in the presence of an inhibitor and Ca^{2+}. The LBs were modified with *i*-K3 (LB-*i*-K3) while the SBs were decorated with *i*-E3 (SB-*i*-E3). The zipping coiled coil of *i*-K3Cys and *i*-E3Cys could force the two beads into close proximity allowing fusion to occur.

Based on the new method introduced in last chapter, the detailed strategies can be employed by this method are described in this section, including basic fusion assay in DI water and external stimulation such as Ca^{2+} triggering or/and inhibition (Figure 3-8). Microscopy, intensity analysis, FRAP and statistical analysis were used to characterize the fusion events.

As a proof of concept, the well-established fusogenic E-peptides (*i*-E3Cys) and K-peptides (*i*-K3Cys) were coupled to the lipid anchor MCC-DOPE forming SB-*i*-E3 and

[28] Most of the data of this section have been published in Bao, C. X., Pahler, G., Geil, B., and Janshoff, A. (2013) Optical Fusion Assay Based on Membrane-Coated Spheres in a 2D Assembly, *J Am Chem Soc 135*, 12176-12179.

LB-*i*-K3 respectively. These peptides are known to form heterodimeric coiled coil structures, which initiate docking between two lipid bilayers and facilitate membrane fusion.[26-28] When SB-*i*-E3 and LB-*i*-K3 contacts, the coiled coil forms in zipping fashion that is the only coiled coil orientation when native membrane fusion occurs. The zipping orientation arises when parallel coiled coil formation take place between two peptides.

3.3.1 NEGATIVE CONTROL

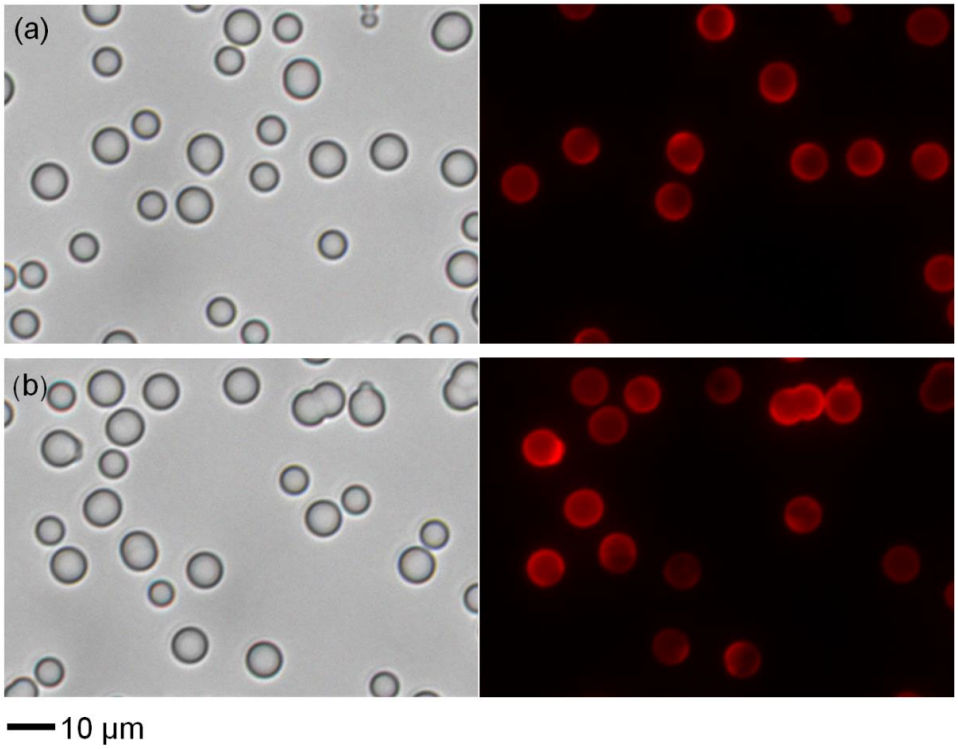

Figure 3-9 Bright field images (left) and corresponding fluorescence images (right) of LB-*i*-K3 and SB-*i*-E3 without peptides on their surface. (a) and (b) were taken in different positions of one sample.

Fusion assays based on beads without peptides are used in a negative control experiment. In Figure 3-9, the LBs and SBs are in a good dispersion. This indicates that the interaction between the two populations of beads is much smaller than the thermal motion. Furthermore, since the lipid MCC-DOPE carrying negative change, the electrostatic repulsion forces the beads separating from others.

3.3.2 FUSION ASSAY IN WATER

Membrane fusion assay based on peptide-modified, membrane-covered beads was firstly performed in DI water, which allows the most freely motion of beads.

3.3.2.1 MICROSCOPY

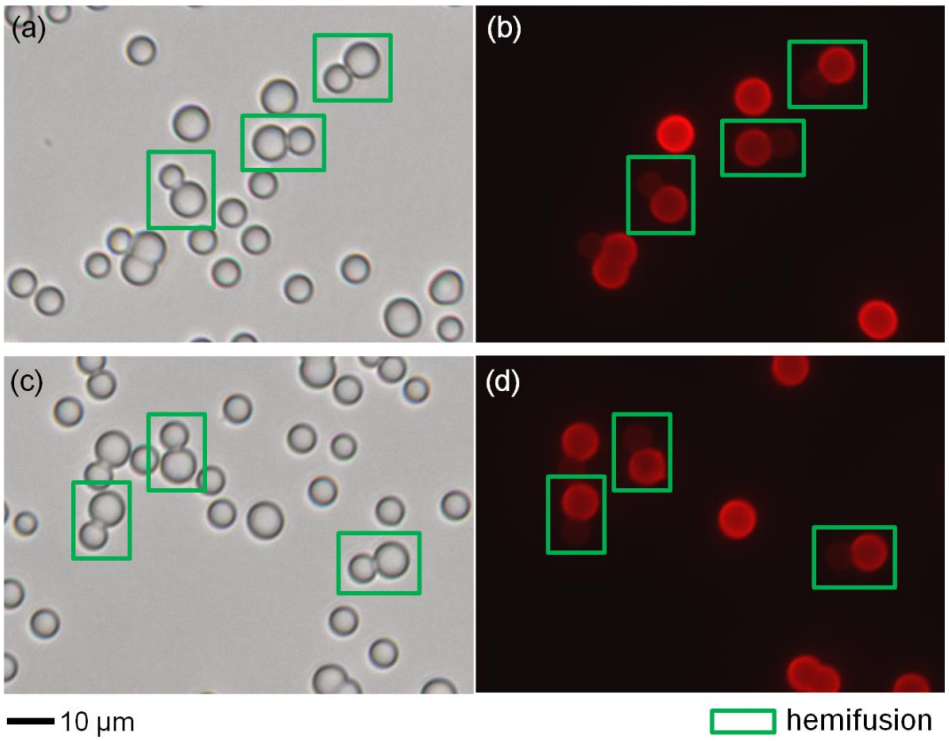

Figure 3-10 Bright field images (left) and corresponding fluorescence images (right) of LB-*i*-K3 and SB-*i*-E3 on a surface. From the distribution of the fluorophore, lipid-mixed pairs (green box) can be clearly identified and considered as hemifused pairs of beads. (a) and (b) were taken from different positions of one sample.

Optical microscope is standard equipment in common laboratory and it plays important role in this work. Even though the membranes on the SB-*i*-E3 are not fluorescently labeled, both bead populations can be readily distinguished by size discrimination using an optical microscope. The fluorescence label embedded in the lipid bilayer covering the LBs allows us to detect fusion events by fluorescence microscopy of

the same area (Figure 3-10). Obviously, lipid leaflets merged under this experimental condition since the SB-*i*-E3 could be seen in the fluorescent images the tethered pairs in green rectangular box. Interestingly, the fluorescence intensity of SB-*i*-E3 seems weaker than LB-*i*-K3, it is considered "hemifusion" that only outer leaflet merged.

3.3.2.2 RELATIVE INTENSITY ANALYSIS

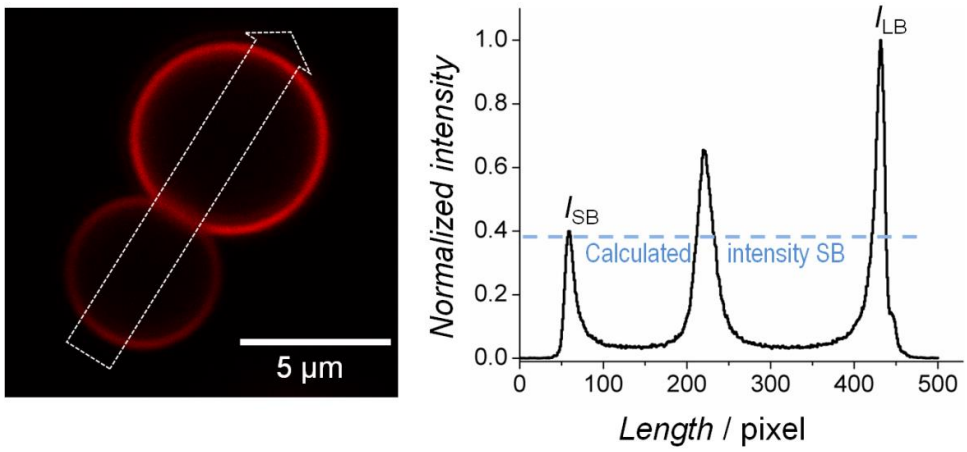

Figure 3-11 Intensity analysis using a broad line profile of a pair consisting of LB-*i*-K3/SB-*i*-E3 shown in fluorescence micrograph. White arrow indicates course of analyzed line profile shown in graph. Peaks correspond to relative fluorescence intensity of SB-*i*-E3 (I_{SB}), merged area and LB-*i*-K3 (I_{LB}). Scattered line shows calculated mean I_{SB} 0.43 ± 0.04 (16 hemifused pairs are considered).

The conclusion from the microscopy that hemifusion occur between LB-*i*-K3 and SB-*i*-E3 in DI water was proved by analyzing the fluorescence intensity. Unequivocal identification of docking, hemifusion, and full fusion was accomplished by intensity analysis across the corresponding LB-*i*-K3/SB-*i*-E3 pair. Based on the previous discussion, lipid fused pairs with a fluorescence intensity ratio of 0.4:1 (SB:LB) were assigned to hemifusion, while an intensity ratio of 1:1 was attributed to full fusion. However, in the case presented here, the average fluorescence intensity of SB-*i*-E3 was found to be 0.43 ± 0.04 (Figure 3-11).

In a previous study concerning fusogenicity of E- and K-peptides based on liposome fusion assays, the parallel coiled coil formation using lipopeptides made of *i*-E3Cys and *i*-K3Cys exhibited slight content mixing, which could not be found here in this 2D assay

that membrane merging arrested in the hemifused state.[1] This was attributed to an additional energy contribution needed to be supplied for detachment of the supported membrane from the beads and the lack of energy gain due to loss of binding energy upon fusion. This additional energy might be released from reducing the contact area between the hydrophobic acyl chains of the phospholipid monolayer pointing towards the aqueous phase and the van der Waals attraction between the two silica beads. Since the van der Waals energy scales with bead size, full fusion is expected to come into reach for larger beads.

3.3.2.3 FRAP

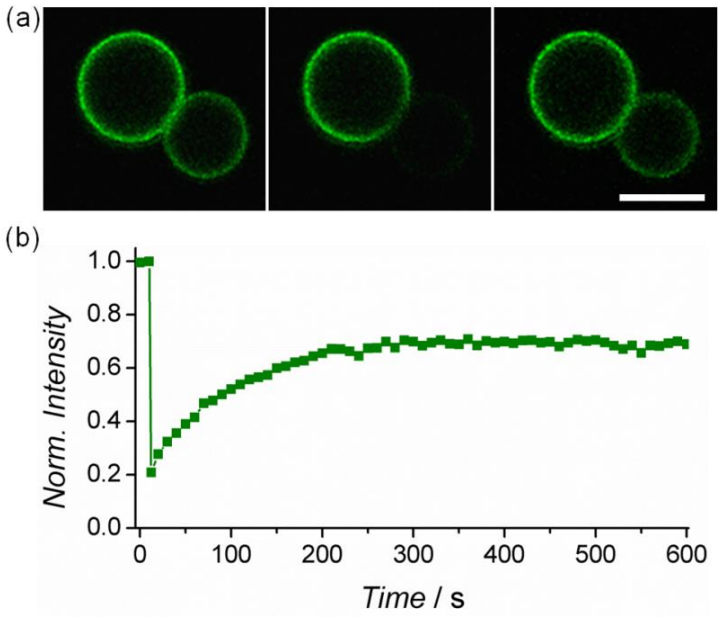

Figure 3-12. FRAP experiment proving membrane connection between LB-*i*-K3/SB-*i*-E3 in DI water. (a) Fluorescence images of LB-*i*-K3/SB-*i*-E3 before bleaching, shortly after bleaching and 10 min after bleaching the entire SB-*i*-E3. (b) Corresponding normalized fluorescence recovery of SB-*i*-E3 as a function of time.

In order to investigate the connection between LB-*i*-K3 and SB-*i*-E3 in a (hemi)fused pair, FRAP experiments are performed on SB-*i*-E3.

The formation of a continuous membrane structure along the contact zone as well as its fluidity could be studied by FRAP experiments (Figure 3-12). After fully bleaching the fluorophores on the SB-*i*-E3, the intensity of SB-*i*-E3 recovered to nearly 60% of its initial

fluorescence. Interestingly, the recovery process is slowed down by two orders of magnitude compared to the diffusion from geometrically unrestricted membranes, which is attributed to the small contact zone between the beads consisting of non-bilayer structures that form a bottleneck for lipid diffusion.[17, 18]

3.3.2.4 EFFICIENCIES OF FUSION EVENTS

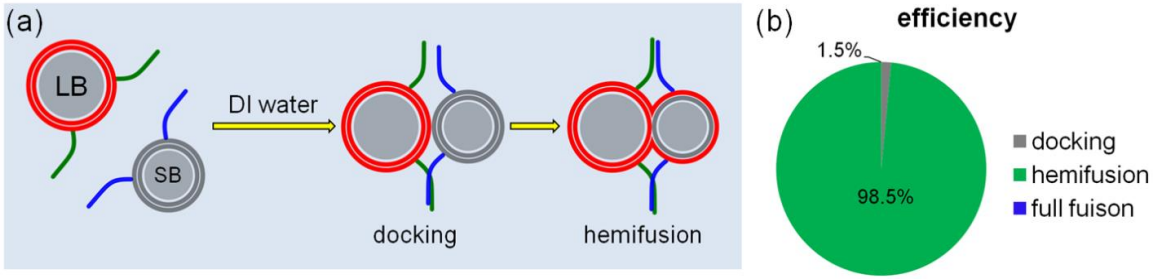

Figure 3-13 Illustration of 2D the fusion assay with LB-*i*-k3 and SB-*i*-E3 in DI water. (a) Schematic illustration of scenarios after mixing of LB-*i*-k3 and SB-*i*-E3. The membrane merging can be arrested in the docked or the hemifused state. (b) Corresponding statistical analysis shows the efficiency of various fusion events.

Fusion event efficiency is analyzed by comparing all docked LB-*i*-K3/SB-*i*-E3 pairs (N_{docking}) to hemifused pairs ($N_{\text{hemifusion}}$) and fully fused pairs ($N_{\text{full fusion}}$), respectively. However, in this experimental condition, the membrane merging process terminate at hemifusion (Figure 3-13a) hence the full fusion efficiency is 0. Figure 3-13b clearly shows that the hemifusion efficiency provided high values around 98.5%, implying that docking within the period of our experiments leads predominantly to hemifusion.

3.3.3 CALCIUM-TRIGGERED FULL FUSION

Ca^{2+} is known as the final trigger in many vesicle trafficking events that directs the complete fusion process.[29-33] However, the commonly used *in vitro* bulk assays only observe the average fluorescence intensity and cannot distinguish docking, hemifusion and fusion hence not allowed monitoring the exactly fusion transitions such as the process from hemifusion to full fusion triggered by Ca^{2+}. Single vesicle-vesicle assay overcome this limitation by monitoring both content and lipid-mixing starting from a metastable state of interacting vesicle pairs before the Ca^{2+} injection.[34, 35] A similar strategy can be achieved by the membrane-coated bead-based assay, which thus offers an alternative method to study Ca^{2+} triggered membrane fusion.

In this work, full fusion could be achieved if additionally Ca^{2+} ions were added, as was recently found to lead to content mixing in vesicle assays.[1] This was attributed to the described bridging effect of calcium ions binding to PC and non-reacted MCCDOPE carrying a negative charge. This is an important breakthrough for the bead assay since it can now distinguish docking from hemifusion and full membrane merging. The results of this 2D fusion assay applied to Ca^{2+} mediated fusion events are discussed in the following section.

3.3.3.1 MICROSCOPY

Prior to the addition of Ca^{2+}, only docking and hemifusion is observed. Surprisingly, all types of fusion events occur after addition of 12 mM Ca^{2+} including docking, hemifusion and full fusion (Figure 3-14). These different fusion events can be easily distinguished by the fluorescence intensity of SB-*i*-E3: in docked pairs (Figure 3-14, grey box), SB-*i*-E3 do not show fluorescence; in hemifused pairs (Figure 3-14, green box), SB-*i*-E3 show less fluorescence intensity compared to LB-*i*-K3; in full fused pairs (Figure 3-14, blue box), SB-*i*-E3 appears with similar fluorescence intensity as LB-*i*-K3.

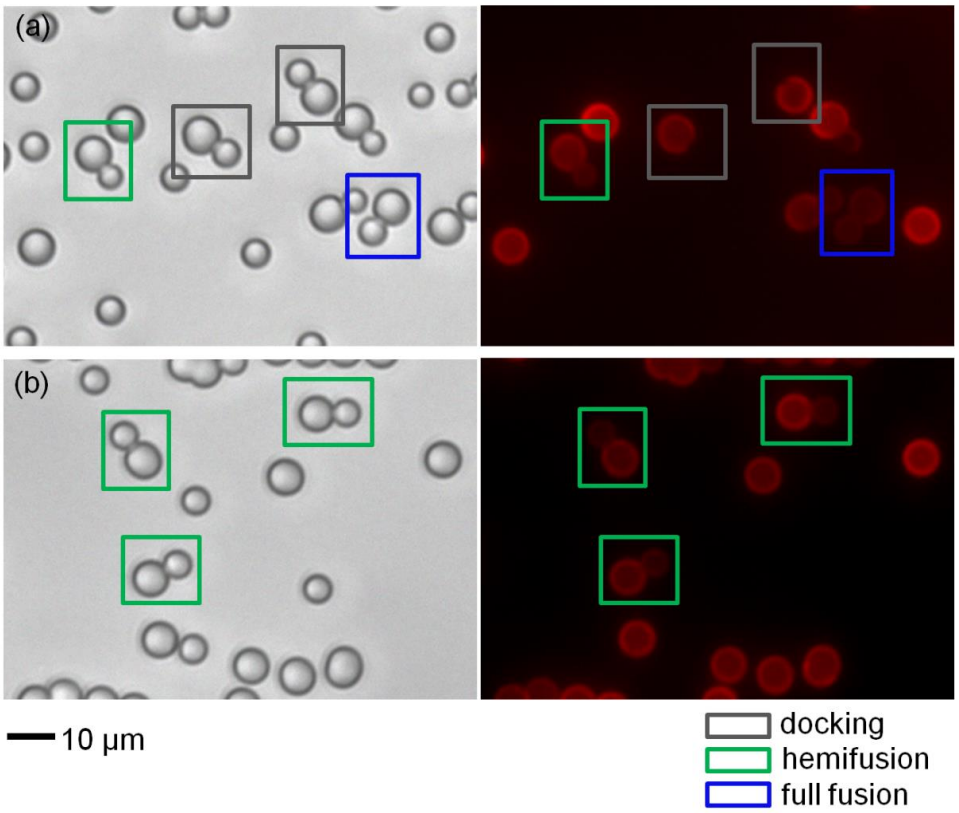

Figure 3-14 Bright field images (left) and corresponding fluorescence image (right) of LB-*i*-K3 and SB-*i*-E3 on a surface triggered by 12 mM Ca^{2+}. From the distribution of the fluorescent probe, docked pairs (gray rectangular box) and hemifused pairs (green rectangular box) as well as fully fused pairs (blue rectangular box) can be clearly distinguished. (a) and (b) were taken from different position of the sample.

3.3.3.2 FLUORESCENCE INTENSITY ANALYSIS

Fluorescence intensity analysis was used to analyze Ca^{2+} triggered full fusion events in images taken by CLSM. Figure 3-15 shows the normalized intensity of hemifused pair (Figure 3-15a) and a fully fused pair (Figure 3-15b), the relative intensities are 0.43 ± 0.045 and 0.99 ± 0.046 respectively, which are consistent with the observation in microscopy. Interestingly, a reduced intensity is found in the contact zone of the fully fused pairs, which is attributed to lipid depletion in the contact area. Combing the results of microscopy and intensity analysis, the conclusion can be drawn that all fusion events can be observed directly at the same time in one experiment, which is an important innovation of this 2D bead-based fusion assay.

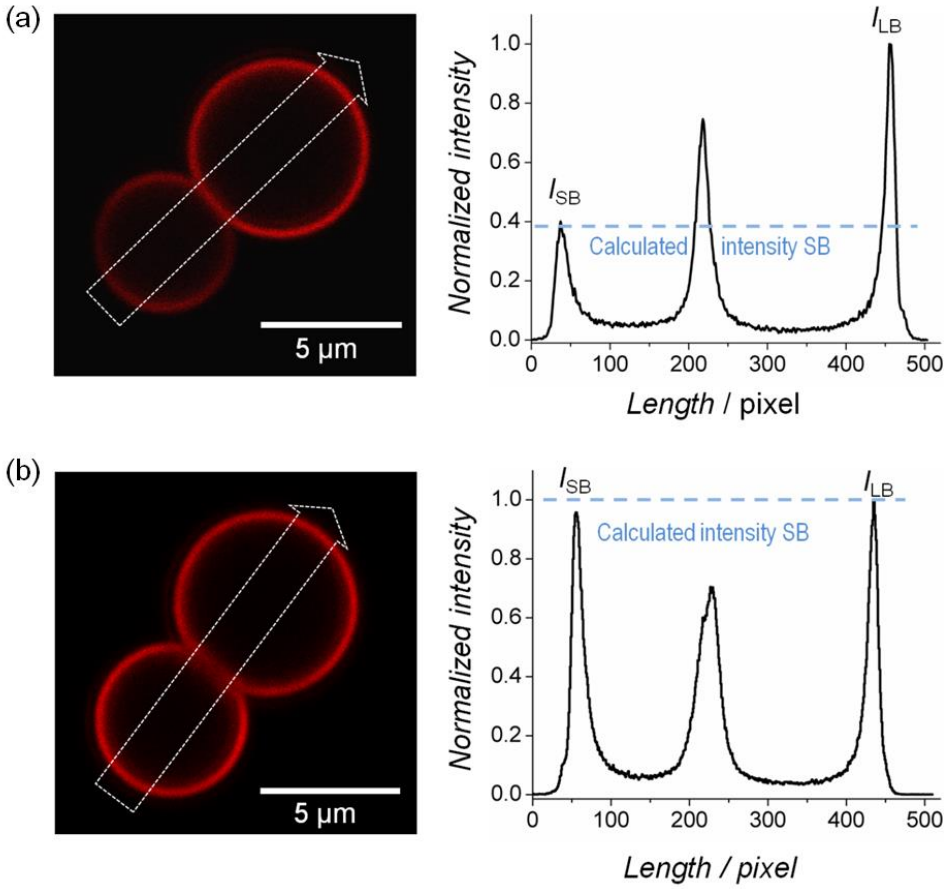

Figure 3-15 Classification and proof of principle considering membrane–membrane interaction triggered by coiled coil formation between LBs and SBs. Intensity analysis using a broad line profile (white arrow) across a pair consisting of LB-*i*-K3/SB-*i*-E3 imaged with a confocal laser scanning microscope. Peaks correspond to relative fluorescence intensity of SB-*i*-E3, merged area, and LB-*i*-K3. Scattered line shows calculated I_{SB}. Hemifusion is shown in (a) with a relative intensity ratio between SB and LB I_{Rel} 0.43 ± 0.045 as expected (16 pairs were considered), while (b) shows full fusion of both leaflets, I_{Rel} *is* 0.99 ± 0.046. (16 pairs were considered).

3.3.3.3 FRAP

FRAP experiments were performed on hemifused and fully fused pairs respectively (Figure 3-16). After bleaching the total SB-*i*-E3, the intensity recovery in both cases is very similar to the experiments performed in DI water (around 60% of the original intensity). In addition, the recovery time is up to 10 min, which is much longer than recovery times obtained from geometrically unrestricted membranes. Again, this is attributed to the tiny contact zone between the beads forming a bottleneck for lipid

diffusion. This experimental finding is supported by Monte Carlo simulations that are discussed in the following section.

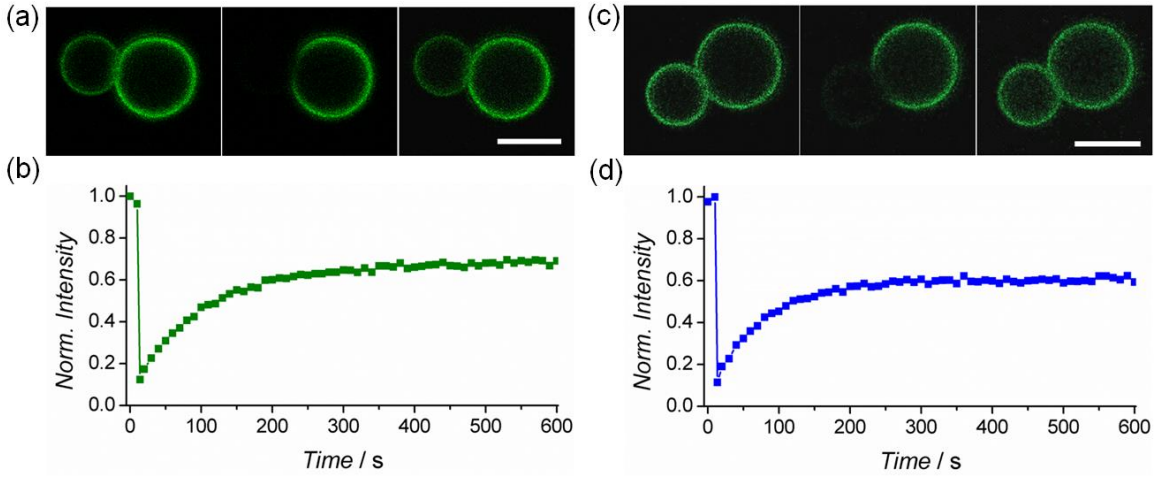

Figure 3-16 FRAP experiment proving membrane connection between LB-*i*-K3/SB-*i*-E3 trigged by $Ca^{2+.}$ (a, c) Fluorescence images of LB-*i*-K3/SB-*i*-E3 before, shortly after and 60 min after bleaching the entire SB-*i*-E3 (b. d) Corresponding normalized fluorescence recovery of bleached area as a function of time. (a, b) was performed on the pair that LB-*i*-K3 are brighter than SB-*i*-E3 while (c, d) was performed on the pair with similar brightness.

3.3.3.4 STATISTICAL ANALYSIS

Based on the above discussion of Ca^{2+} triggered full fusion, Figure 3-17a shows the schematic illustration of a scenario of the complete fusion process. After mixing of LB-*i*-K3 and SB-*i*-E3 in DI water, the recognition of peptides causing the plane docking of beads, due to the accumulated coiled coil formation, the majority of the docked pairs (92.2%) evolve into hemifusion, finally, upon the addition of Ca^{2+}, a small part (9.3%) of hemifused pairs transfer into full fused pairs (Figure 3-17b). Comparing to the values in DI water, the docking efficiency (7.8%) increases a bit (1.5% in DI water), this may be caused by the existence of ions (Ca^{2+}) which reduce the electronic double layer and allow more beads to get in close contact without being repelled.

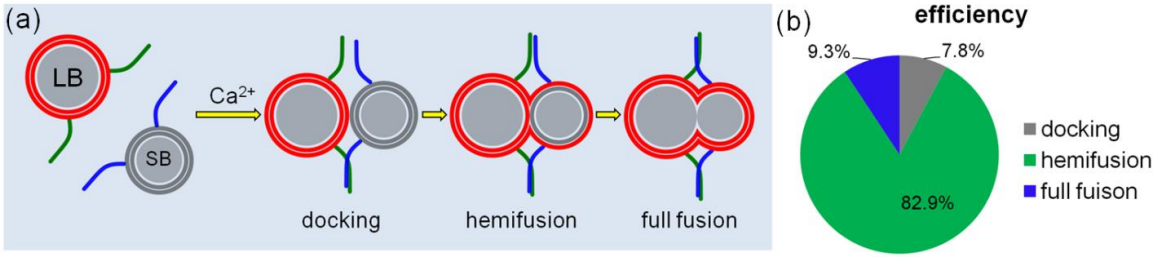

Figure 3-17 (a) Illustration of 2D fusion assay with LB-*i*-K3 and SB-*i*-E3 triggered by Ca^{2+} and (b) corresponding statistic analysis shows the efficiency of all fusion events including docking (grey), hemifusion (green) and full fusion (blue).

Only after administration of calcium ions, full fusion was observed in good accordance with a previous study employing liposome assays.[36] In this previous study, only observed fusion induced by E- and K-peptides in parallel orientation and in the presence of calcium ions. Even in this case, only 3% fusion efficiency was recorded, which is similar to what is found in this bead assay (7.8%). This implies that bead pairs as well as liposomes are mainly arrested in the hemifused state.

In liposome assays, fusion is driven by the gain in bending energy released by annihilation of one spherical bilayer structure. In this bead assay, the energy gain is inherently missing. However, the gain in energy could originate from the van der Waals attraction between the two silica beads, which come into close contact after fusion, removing all the water in between the two beads.

3.3.4 INHIBITION BY *I*-E3CYS

A general design of fusion inhibitors is that they can bind selectively to any conformation of the fusion protein during the fusion pathway.[37] Inhibition of viral fusion by preventing assembling of coiled coil complexes is a state key strategy to abolish viral infection in an early state.[38-41]

E3Cys peptides was used as a competitive inhibitor for the *i*-K3Cys displayed on LBs ($c_{i\text{-E3Cys}}$ = 15 μM added to the suspension of beads) in presence/absence of Ca^{2+}.[42] Efficiencies concerning docking, hemifusion and full fusion after incubating the two bead populations for 90 min at different conditions are shown in Figure 3-18. The (hemi)fusion efficiency is significantly decreased. When *i*-E3Cys was added into the fusion assay performed in water, the hemifusion efficiency was dramatically reduced from 98.5% to 11.5%, implying that the external *i*-E3Cys forms coiled coils with most of the surface bounded *i*-K3Cys (Figure 3-18a). More interestingly, in the presence of Ca^{2+}, full fusion event is absolutely abolished after adding *i*-E3Cys while hemifusion is also decreased a lot (from 82.9% to 33.2%). This suggests that *i*-E3Cys is a very efficient inhibitor for full fusion. It may block or change the zipping conformational of coiled coil structure, which is necessary for the viral infection of host cells.

However, the K_D value as determined by ellipsometry measurements is about 25 μM, but fusion is inhibited already at lower inhibitor concentrations (15 μM), probably because of limited lateral mobility after dimer formations.[1] The association of beads was attributed the to multivalency effects boosting the association constant of two beads attracting each other and nonspecific electrostatic interactions originating from the peptides themselves. The data show that indeed the assay allows classification and quantification of fusion inhibitors, thereby emphasizing its feasibility for high-throughput and high-content screening of potent viral fusion inhibitor.

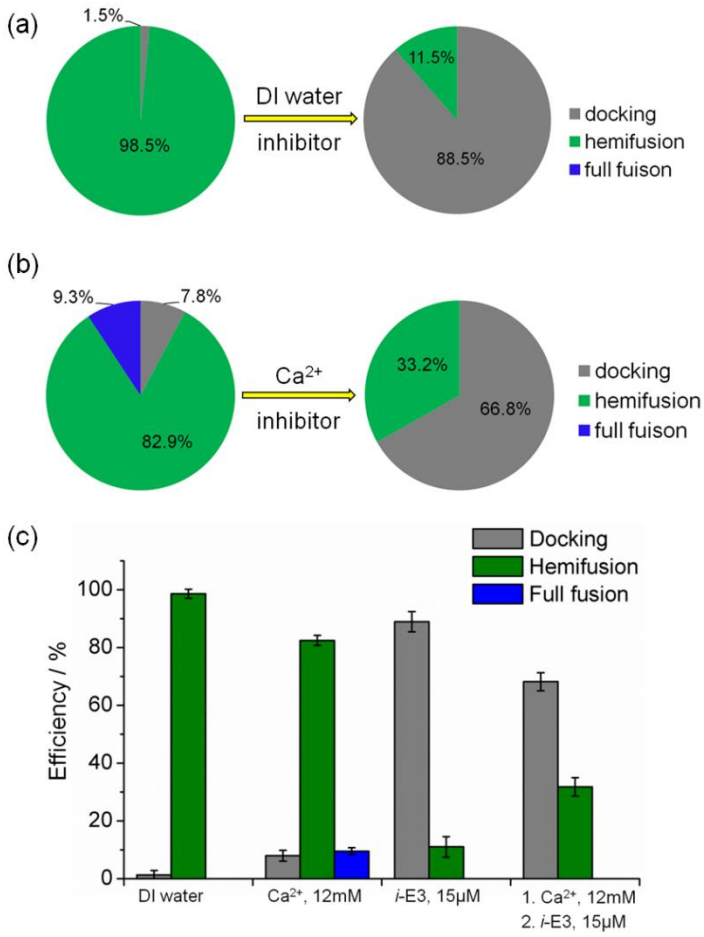

Figure 3-18 Statistical analysis of fusion events inhibited by 12 mM *i*-E3Cys in various conditions. Experiments were performed (a) without and with (b) Ca^{2+}. (c) Efficiency of docking (gray), hemifusion (green), and full fusion (blue) of LB-*i*-K3/SB-*i*-E3 pairs in the presence or absence of Ca^{2+} administration to trigger full fusion and presence of externally added inhibitor (*i*-E3Cys). Control experiments with membrane-coated beads in the absence of peptides attached to the membrane shell do not show fusion events and rarely show docking (beyond statistically formed pairs).

3.3.5 MULTIPLE FUSION

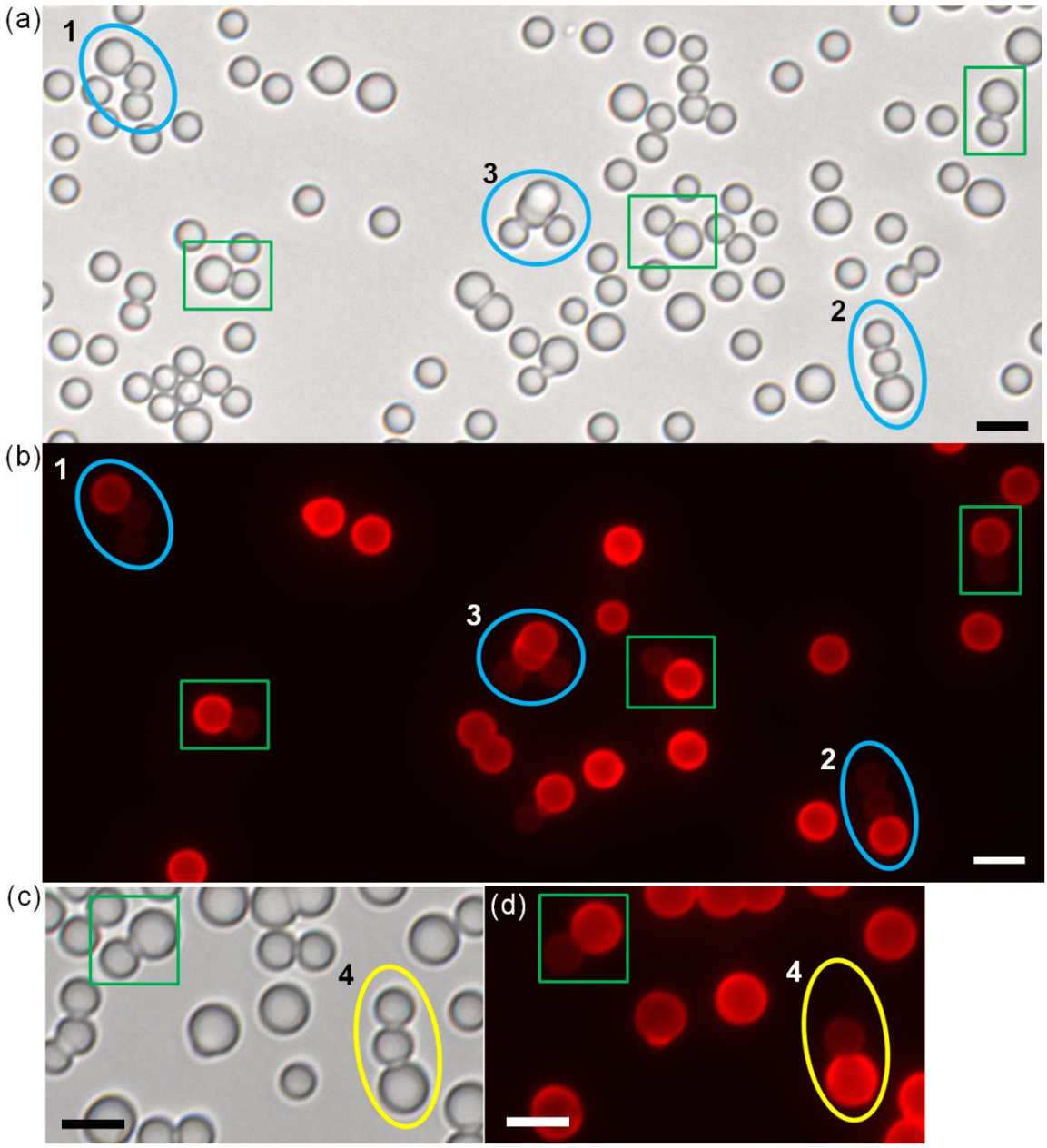

Figure 3-19 Multiple fusion of poly beads where lipid-mixing occurs at least twice results the poly beads, which contains at least three beads including at least one LB-*i*-K3 and one SB-*i*-E3. Bright field images (a), (c) and corresponding fluorescent images (b), (d) are taken from the mixture of on LB-*i*-K3 and SB-*i*-E3 in DI water but of different samples. The green box highlights the common hemifused pair, while the ellipses refer to poly beads. The scale bar is 10 μm.

In vitro fusion assays including traditional bulk vesicle assays and recent popular single vesicle assays reveal the molecular mechanism of fusion since they allow

manipulations and observations that are not possible *in vivo*. Although single-vesicle assay offer a powerful method to study the completely dynamic fusion process, observations of both kinds of assays are by means of fluorophore-fluorophore interaction no matter fluorescent spectrometry or fluorescent microscopy are used. For example, lipid mixing is usually monitored by FRET that is a distance-dependent interaction between donor and acceptor fluorophores.[43] From this perspective, the typical assays may cause problems when multiple fusions take place, since both of the assays are based on the assumption that the ratio of two fusogenic vesicles are 1:1 and the fusion occurs when two partner vesicles react. However, if one donor labeled vesicle react with more accepter labeled vesicles, the efficient FRET may not be observed due to the over dilution of fluorophore. In other word, these vesicle-based assays are indirect method for membrane fusion that cannot quantify multiple fusion in which fusion occurs at least twice simultaneously or in succession. However, the membrane-coated bead-based assay in this work overcomes the limitation due to its size-discrimination.

Figure 3-19 shows typical multiple fusion events as observed in this work by microscopy. Ellipse 1 and 2 (Figure 3-19a, b, blue) highlight hemifusion in which the hemifusion between LB-*i*-K3 and SB-*i*-E3 allows *i*-K3Cys crossing the contact zone to SB-*i*-E3 and react with *i*-E3Cys on the second SB-*i*-E3 hence inducing the second hemifuison and resulting a poly bead cluster. The bead cluster in ellipse 4 (Figure 3-19c and d, yellow) has the same "composition" (number of LB-*i*-K3 and SB-*i*-E3 in one poly bead cluster) and "configuration" (how the LB-*i*-K3 and SB-*i*-E3 connect) with this ellipse 1 and 2, but hemifusion occurs only once followed by docking. In ellipse 3 (Figure 3-19a and b, blue), poly bead cluster has the same composition but different configuration. Here, one LB-*i*-K3 is connected with two SB-*i*-E3 and hemifusion took place twice. Other bead clusters with various compositions and configurations were also observed (data not shown due to numerous combinations). Here as much hemifusion take place in majority of them like ellipse 1 and 3.

The bead-based assay can quantitatively (composition and configuration) and qualitatively (docking, hemifusion and full fusion) characterized by a poly bead cluster undergoes multiple fusion. The fusogenic populations can be distinguished by size-discrimination while the fusion events can be identified by fluorescence intensity of beads since only one fluorophore was used in this work and its intensity is proportional to

its concentration in the bilayer. Due to the complexity and diversity of multiple fusion, only tethered pairs containing exactly one LB and one SB were considered in this work.

3.3.6 ORIENTATION OF COILED COIL

Through the assembly of the SNAREs, the two opposing membrane are brought in proximity and could facilitates their fusion. According to the "zipper" model, the SNARE core complex zips from the *N*-terminal towards *C*-terminal and this stable "*trans"* structure containing a four-helix coiled coil motif which can overcome the repulsive forces between opposing membranes and induce membrane fusion.[29, 44, 45] Brunger and co-workers showed that antiparallel binding of SNAREs does not induce vesicle-membrane fusion.[46] Here, if the parallel orientation of the coiled coil is a prerequisite of membrane fusion was investigated based on the membrane-coated bead model system.

The strategy is based on the design of K3Cys that shares the opposite amino acid sequence with *i*-K3Cys, therefore, an antiparallel coiled coil arises when it reacts with *i*-E3Cys (Figure 3-20a). Interestingly, the hemifusion was induced even with these antiparallel coiled coil forming and the efficiency is extremely similar to parallel orientation when 10% MCC-DOPE is employed (Figure 3-20b). This demonstrates that the orientation of the coiled coil does not influence the fusion process in this membrane-coated bead model system. This conclusion is consistent with several studies where they used the reduced model system for membrane fusion such as Versluis' peptide-based model.[27] This may be due to the coiled coils in reduced models are much smaller than native SNARE proteins so that the spatial dimensions are likely too small for its orientation to play an important role.

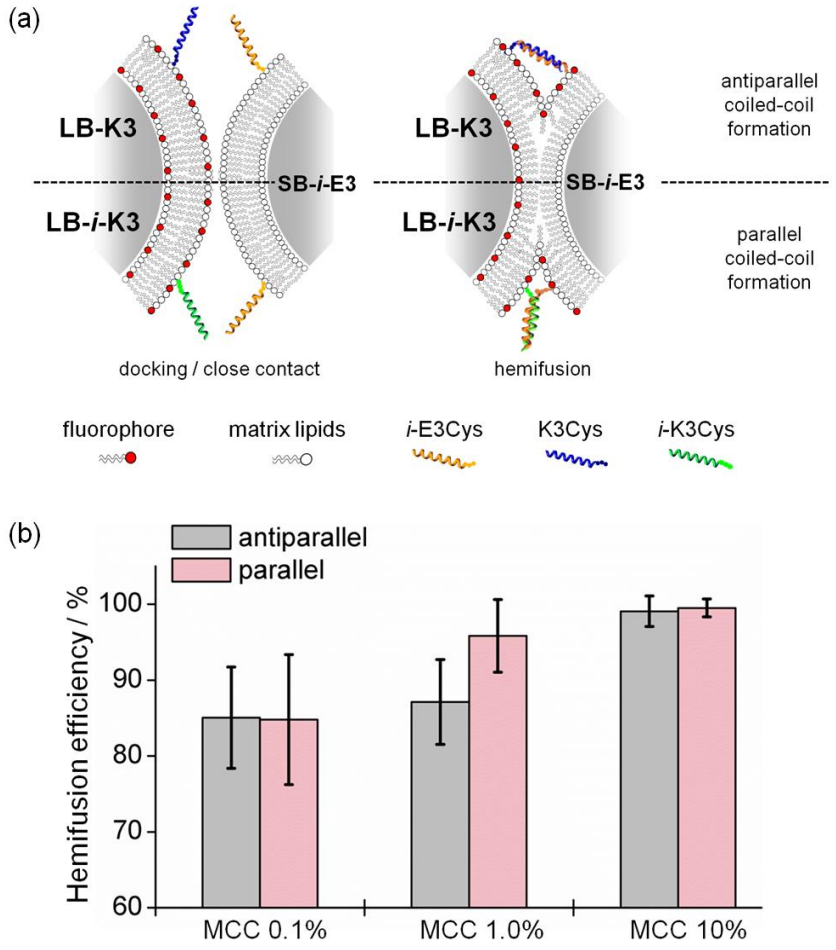

Figure 3-20 (a) Illustration of docking (left) and hemifusion (right) employing different peptide combinations that allows antiparallel (top) and parallel (bottom) coiled coil formation. (b) Quantification of membrane-membrane interaction depending on amount of used MCC-DOPE (0.1%, 1% and 10%) and different coiled coil orientation. LB-*i*-K3 and SB-*i*-E3 was used for parallel (pink) while LB-K3 and SB-*i*-E3 was used for antiparallel coiled coil formation.

Besides, other control experiments were performed by varying the number of fusogenic peptides decorating the membranes. Three orders of magnitude of the amount of MCC-DOPE (0.1%, 1% and 10%) were used in these experiments. Obviously, hemifusion efficiency increases as the number of fusogenic peptides raises due to higher possibility of coiled coil formation. However, the high value around 80-100% for both peptides geometries implies that the docking within the time regime leads to predominantly hemifusion (Figure 3-20b).

3.3.7 CONTACT ZONE OF LIPID FUSED PAIRS[29]

3.3.7.1 SIMULATION OF FRAP CONTACT ZONE

The ultimate proof that a continuous membrane has been formed after docking of two beads is provided by FRAP experiments. Moreover, the experiment also allows us to estimate the size of the contact zone by comparing the data to simulations assuming the same geometry.

Figure 3-21a (black curve) shows FRAP data acquired on a single LB, showing membrane fluidity as expected for solid supported lipid bilayers. After fully bleached the fluorophores on the SB-*i*-E3 that is in contact to a LB-*i*-K3 either hemifused or fully fused (Figure 3-21a, green and blue curves). The intensity recovery is slowed down by more than two orders of magnitude compared to the diffusion from geometrically unrestricted membranes (Figure 3-21a, black curve). This is attributed to the small contact zone between the beads forming a bottleneck for lipid diffusion. This experimental finding is supported by Monte Carlo simulations assuming identical geometry and initial conditions such as a fixed diffusion constant (Figure 3-21b). By assuming a contact angle of 10° corresponding to a contact radius of $a_{FRAP} \approx 1000$ nm, experimental findings such as the spread in time scales could be largely reproduced, assuming unaltered lipid diffusion constant.

[29] The simulation was done by Prof. Burkhard Geil, University of Göttingen, Germany

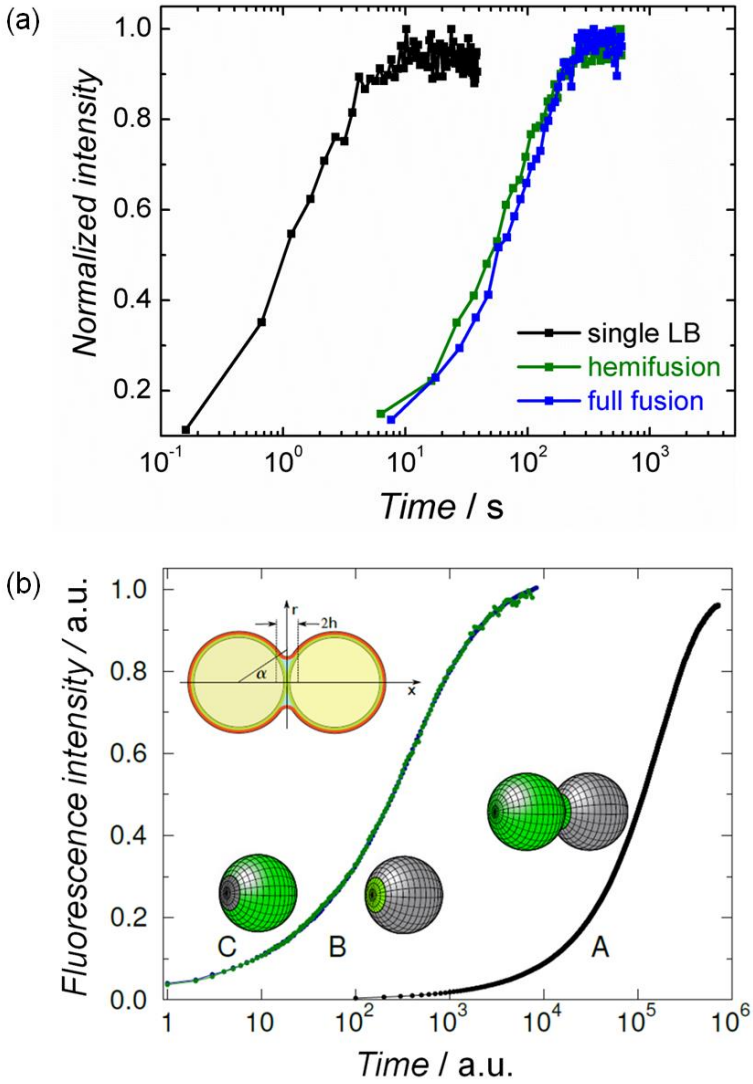

Figure 3-21 FRAP experiments/simulations proving membrane connection between LB-*i*-K3/SB-*i*-E3 through a small contact zone. (a) FRAP experiment of LB-*i*-K3/SB-*i*-E3 pairs after bleaching the entire SB-*i*-E3 (blue/green) compared to a reference experiment showing fluorescence recovery of a single LB after bleaching a spot on the bead (black). The green curve corresponds to the hemifused pair, while the blue graph represents data from the fully fused one. (b) Monte Carlo simulations of FRAP on a single bead (curves B and C) serving as a reference and dimers sharing one continuous membrane (curve A).

In these simulations of lipid diffusion, two beads are in contact and covered with a membrane (inset, top left). The membrane detaches from one bead at a "contact" angle α and spans a "belt" to the second bead. Initially, one of the beads is coated with a mobile fluorophore while the other "bleached" bead is label free. Figure 3-21b (curve A) shows the fluorescence recovery of this geometry using $\alpha = 10°$. As a reference, the diffusion of a

fluorophore on a single bead is also shown (same diffusion coefficient, same bead radius, and same "contact angle"). Curve B is the situation where the fluorophore initially covers most of the bead and only the contact area is photobleached. Both reference experiments demonstrate the FRAP on the surface of a single bead is 100 times (up to 1000 times, depending on α, the smaller the contact angle the slower the recovery) faster than the FRAP between the two tethered beads. This suggests that the slowing down in the fluorescence recovery is a pure geometric effect that arises from passing the bottleneck that forms the obstruction in the contact zone between the beads.

Interestingly, compared with the contact radius predicted by Hertzian contact mechanics ($a_{\text{Hertz}} \approx 37$ nm), a significant larger contact zone after hemifusion or full fusion was observed. The time delay between FRAP of single beads and dimers of beads can therefore be mapped directly to the contact area formed between the two beads. Notably, almost the same contact zone size for either hemifused or fully fused pairs was found. It is also important to mention that changing the contact angle from 0° to 90° (cylinder geometry) does not exceed the area dilatation beyond 5%, which is uncritical for bilayer integrity.

3.3.7.2 ESTIMATING THE SIZE OF CONTACT ZONE

Hertz's classical theory of contact mechanics is used to estimate the size of the contact zone. Hertzian mechanics assumes non-adhesive contact, small strains within the linear elastic limit, each body being considered as an elastic half-space with continuous and non-conforming surfaces, and the bodies being in frictionless contact. The theory of contact between elastic bodies can be used to easily find contact areas and penetration depths for simple indenter geometries. The contact radius a_{Hertz} can be calculated using:

$$a_{\text{Hertz}} = \sqrt[3]{\frac{3F}{4E_{\text{Y}}} R_{\text{eff}}}.$$

Assuming a Young's modulus E_{Y} of the membrane of 10 MPa, an effective bead radius R_{eff} of 2.73 µm and an adhesive force of F = 250 pN, a contact radius is arrived of a_{Hertz} = 37 nm, which is the lowest conceivable limit. FRAP analysis, *i.e.* comparison of experimental data with Monte Carlos simulations, suggests that the size of the contact

zone (contact radius) must exceed 1000 nm to explain the shift in time scales observed in recovery curves compared to bleaching a spot on a single sphere.

3.4 SIZE-DEPENDENT MEMBRANE FUSION

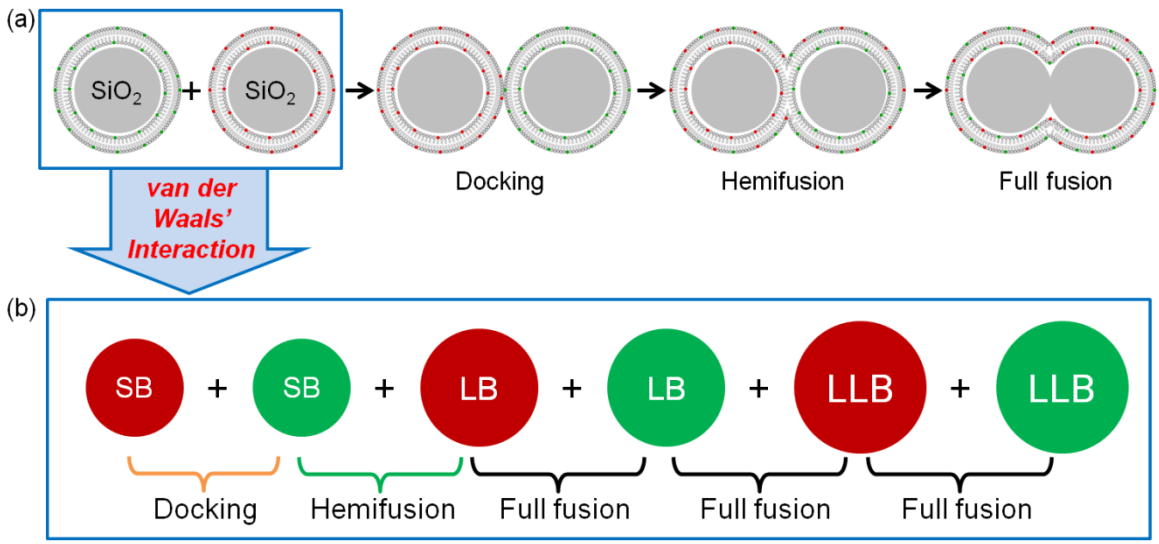

Figure 3-22 Schematic of size-dependent membrane fusion governed by van der Waals interaction. (a) Schematic illustration of scenarios after mixing membrane-coated beads, which are labeled with Texas Red (red) and NBD (green) respectively. Plain docking is followed by hemifusion and eventually by full fusion of the bilayer. All pairs consist of exactly two beads modified with complementary peptides. (b) Van der Waals interaction-controlled (size-dependent) fusion assays employed beads with different sizes. Five pairs of beads were investigated (from left to right) including SB-*i*-K3/LB-*i*-E3, LB-*i*-E3/LB-*i*-K3, LB-*i*-K3/LLB-*i*-E3 and LLB-*i*-K3/LLB-*i*-E3 with increasing van der Waals interaction. The diameters of SB, LB and LLB are 4.7 µm, 6.5 µm and 7.3 µm, respectively.

The DLVO theory, named after Derjaguin and Landau, Verwey and Overbeek, established the typical model towards interactions between colloidal particles that superimposes an attractive van der Waals interaction onto an electrostatic repulsion.[47] The electrostatic component of this theory, also termed electrical double layer force (F_{EDL}), originates from the surface charges and the repulsion between two charged particles. Salt concentration mainly affects the F_{EDL} (higher salt concentrations reduce the electrical double layer repulsion). The van der Waals interaction is determined by dielectric constants (Hamaker constant) and geometry of the system. According to Derjaguin approximation, F_{vdW} between two spheres can be calculated by the equation

$$F_{\mathrm{vdW}} = -\frac{A}{6D^2}\frac{R_1 R_2}{(R_1 + R_2)}$$

Where A is the Hamaker constant, D is the shortest distance between two surfaces and R_1, R_2 are the radii of two hard beads. The van der Waals interaction (F_{vdW}) is not influenced by presence of salt and but can be adjusted by the radius of particles.

In previous sections, membrane-coated beads were used to investigate membrane fusion driven by coiled coil formation. Full fusion was only achieved in the presence of Ca^{2+} when LB-*i*-K3 and SB-*i*-E3 were employed. In this section, the native interaction–van der Waals interaction–between charged membrane-coated beads was considered as a factor for affecting the membrane fusion. In addition to SBs and LBs, LLBs were used to adjust the van der Waals interaction. As the interaction increases, the main fusion event changes from docking to full fusion in the absence of Ca^{2+}. This size-dependent van der Waals force will provide a tool to manipulate the interaction between model membranes to study the influence on membrane fusion.

Five distinct pairs of beads with the increasing van der Waals interaction are employed including SB-*i*-E3/SB-*i*-K3, SB-*i*-K3/LB-*i*-E3, LB-*i*-E3/LB-*i*-K3, LB-*i*-K3/LLB-*i*-E3 and LLB-*i*-K3/LLB-*i*-E3 (Figure 3-22b). High concentrations of salts (50 mM HEPES, 150 mM KCl, pH 7.4) are introduced to efficiently reduce the F_{EDL}. *i*-K3Cys and *i*-E3Cys modified beads were labeled with NBD and Texas Red respectively, thus, the fusion events can be distinguished by fluorescent colors even when the same size of beads were used (Figure 3-22a). All experiments were characterized by CLSM including microscopy and FRAP. Only tethered pairs composed of different bead populations were considered for data collection and analysis.

3.4.1 MICROSCOPY AND INTENSITY ANALYSIS

Since the two bead populations were labeled with NBD and Texas Red respectively, green channel and red channel images are taken simultaneously (Figure 3-23, left) and fusion events can be determined by the corresponding intensity analysis (Figure 3-23, right).

Obviously, docking occurs upon SB-*i*-E3/SB-*i*-K3 mixing since only one bead can been observed in single channel images. Correspondingly, only one sharp peak appears at the position of the boarder of each bead (peak 1 and peak 3) in intensity curves. This means there is no lipid mixing (Figure 3-23a). The tiny red peak 1 is attributed to the cross talk of fluorophores due to the overlap of their emission spectra. In LB-*i*-E3/SB-*i*-K3 assays, as discussed in previous sections, hemifusion events were observed. Both beads can be observed in both channels but with less intensity (Figure 3-23b). Most interestingly, full fusion occurs in assays of LB-*i*-E3/LB-*i*-K3, LLB-*i*-E3/LB-*i*-K3 and LLB-*i*-E3/LLB-*i*-K3 mixtures. Both beads are observed with similar intensity in both channels, which indicates that both leaflets are merged and fluorophores are evenly distributed. This size-dependent membrane fusion from docking to full fusion is attributed to increasing van der Waals interactions.

The distance between intensity peaks of green and red channels (ΔPeak 1, ΔPeak 2 and ΔPeak 3) are calculated based on fluorescence intensity curves and summarized in Table 3-1. Although these values cannot represent the actual distance between lipid leaflets due to the limited resolution of CLSM, the comparison of ΔPeak is able to provide the relative distance under different fusion events. Especially ΔPeak 2 demonstrates the contact zone of the tethered pairs. For docked SB-*i*-E3/SB-*i*-K3, ΔPeak 2 is up to ten pixels (271.5 nm) while the value is maximal four pixels (104.1 nm) in the other cases. This indicates that the two opposed membranes are docked with a tiny separation and are not in close contact. However, these two cases are not distinguished in this work and collectively called docking.

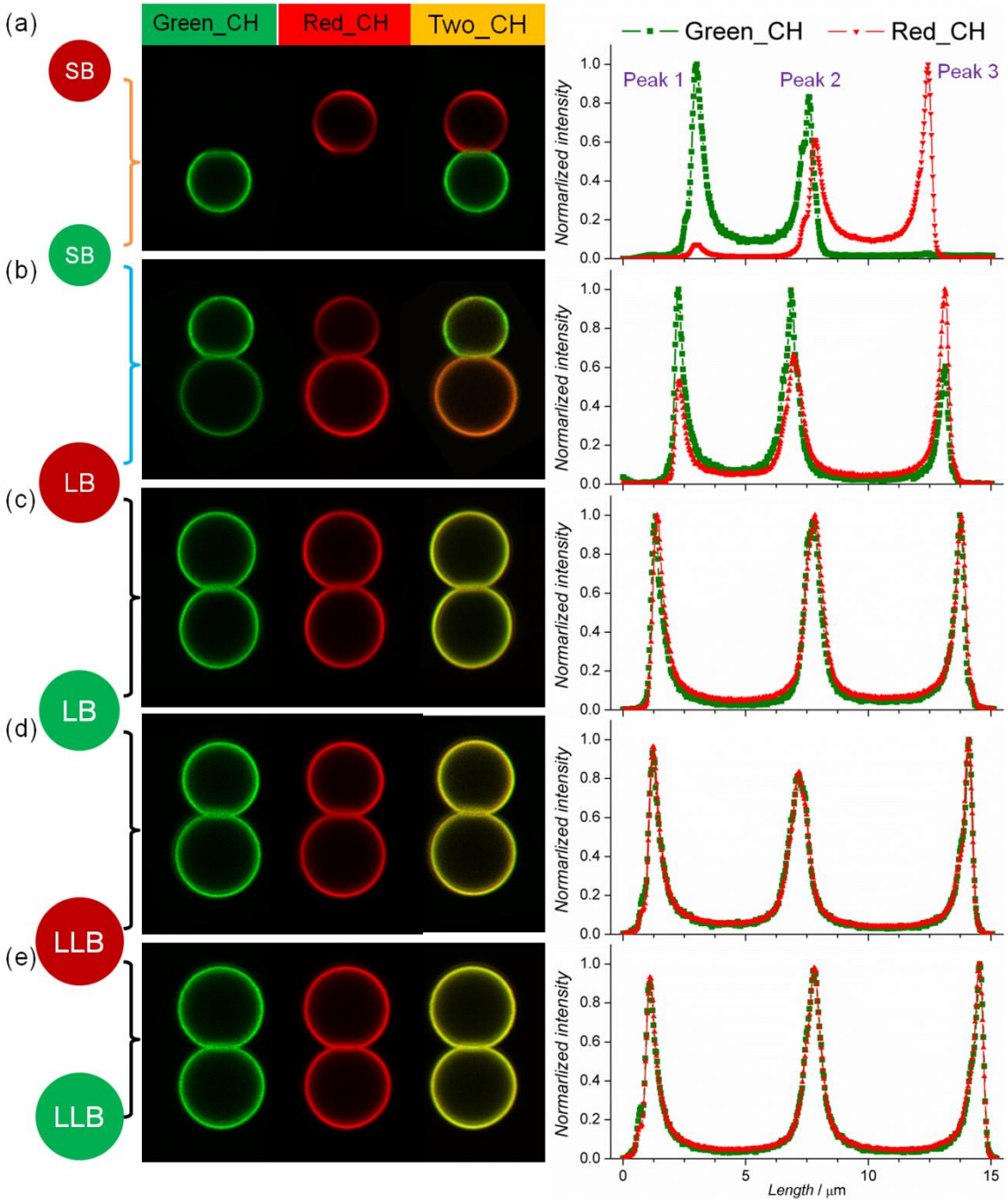

Figure 3-23 Images (left) and corresponding fluorescence intensity analysis (right) of size-dependent fusion assays including (a) SB-*i*-E3/SB-*i*-K3, (b) SB-*i*-K3/LB-*i*-E3, (c) LB-*i*-E3/LB-*i*-K3, (d) LB-*i*-K3/LLB-*i*-E3 and (e) LLB-*i*-K3/LLB-*i*-E3. The images from left to right are green channel image (NBD, excited by laser 488 nm), red channel image (Texas Red, excited by laser 595 nm) and combination of two channels. The intensity analysis is based on the two channel images and is normalized to the intensity of two channels at the same pixel. The three peaks correspond to the border of the first bead, contact zone of two beads and the border of the second bead.

Table 3-1 Peak difference between green channel and red channel for various sizes of fusogenic beads.

	Fusion events	Resolution of image	ΔPeak 1		ΔPeak 2 (contact zone)		ΔPeak 3	
		nm/pixel	nm	pixel	nm	pixel	nm	pixel
(a) SB/SB	docking	27.146	27.2	1	271.5	10	--	--
(b) LB/SB	hemifusion	26.020	26.0	1	104.1	4	52.1	2
(c) LB/LB	full fusion	30.929	61.8	2	92.8	3	61.9	2
(d) LB/LLB	full fusion	33.243	0	0	66.5	2	0	0
(d) LLB/LLB	full fusion	36.721	0	0	36.7	1	0	0

3.4.2 LIPID DIFFUSION IN FULLY FUSED PAIR

FRAP experiments were performed on the three full fused pairs (Figure 3-24). Arbitrary beads were bleached in LB-*i*-E3/LB-*i*-K3 and LLB-*i*-E3/LLB-*i*-K3 pairs while LB-*i*-K3 was bleached in LLB-*i*-E3/LB-*i*-K3. The fluorescence recovery of all three cases is extremely similar and is slowed down by more than two orders of magnitude compared to the diffusion in geometrically unrestricted membranes (single membrane-coated bead). This is consistent with the previous results of FRAP on hemifused and full fused SB-*i*-E3/LB-*i*-E3. These results indicate that the dynamic contact zone enlarging (fusion pore opening) of lipid mixing is independent on the size of the beads.

In addition, real-time monitoring of fluorescence intensity was performed on a fully fused LB-*i*-E3/LB-*i*-K3 pair to study the process of lipid diffusion (Figure 3-25). At t = 0 s, LB 1 and LB 2 are observed with high relative fluorescence intensity in both channels and their own fluorescence "flow" into each other as time goes by. Finally, lipid diffusion is "accomplished" (in equilibrium) at t = 6180 s where both beads show similar intensities in both channel images indicating a homogenous of both fluorophores in a continuous bilayer.

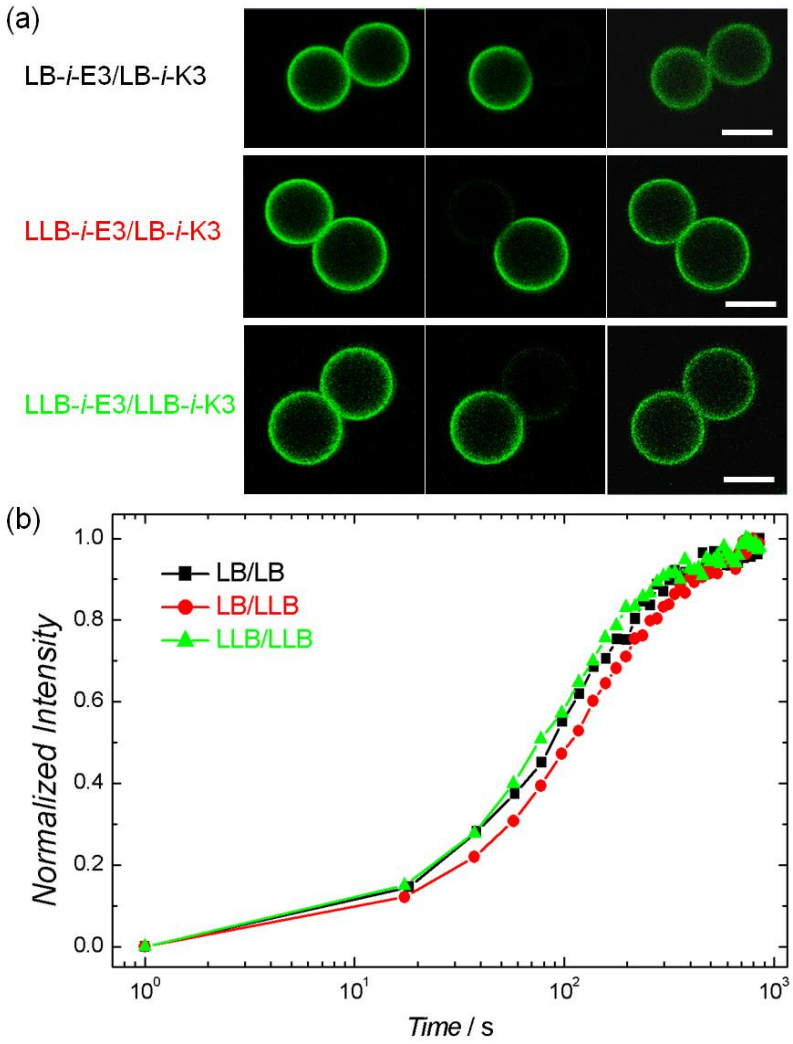

Figure 3-24 FRAP experiments proving membrane connection between two beads in a fused pair through a small contact zone. (a) Fluorescence micrographs prior to bleaching the NBD, directly after bleaching and after fluorescence recovery (from left to right) of fully fused LB-*i*-E3/LB-*i*-K3 (top), LLB-*i*-E3/LB-*i*-K3 (center) and LLB-*i*-E3/LLB-*i*-K3 (bottom). The scale bar is 5 µm. (b) FRAP experiments of fully fused pairs after bleaching the arbitrary LB of LLB-*i*-E3/LB-*i*-K3 pair (black curve), LB-*i*-K3 of LLB-*i*-E3/LB-*i*-K3 pair and arbitrary LLB of LLB-*i*-E3/LLB-*i*-K3 (green curve).

Comparing the time regime of FRAP (≈ 10 min) and real-time intensity analysis (≈ 100 min), conclusion can be drawn that the contact zone (fusion pore) is changing during lipid mixing.

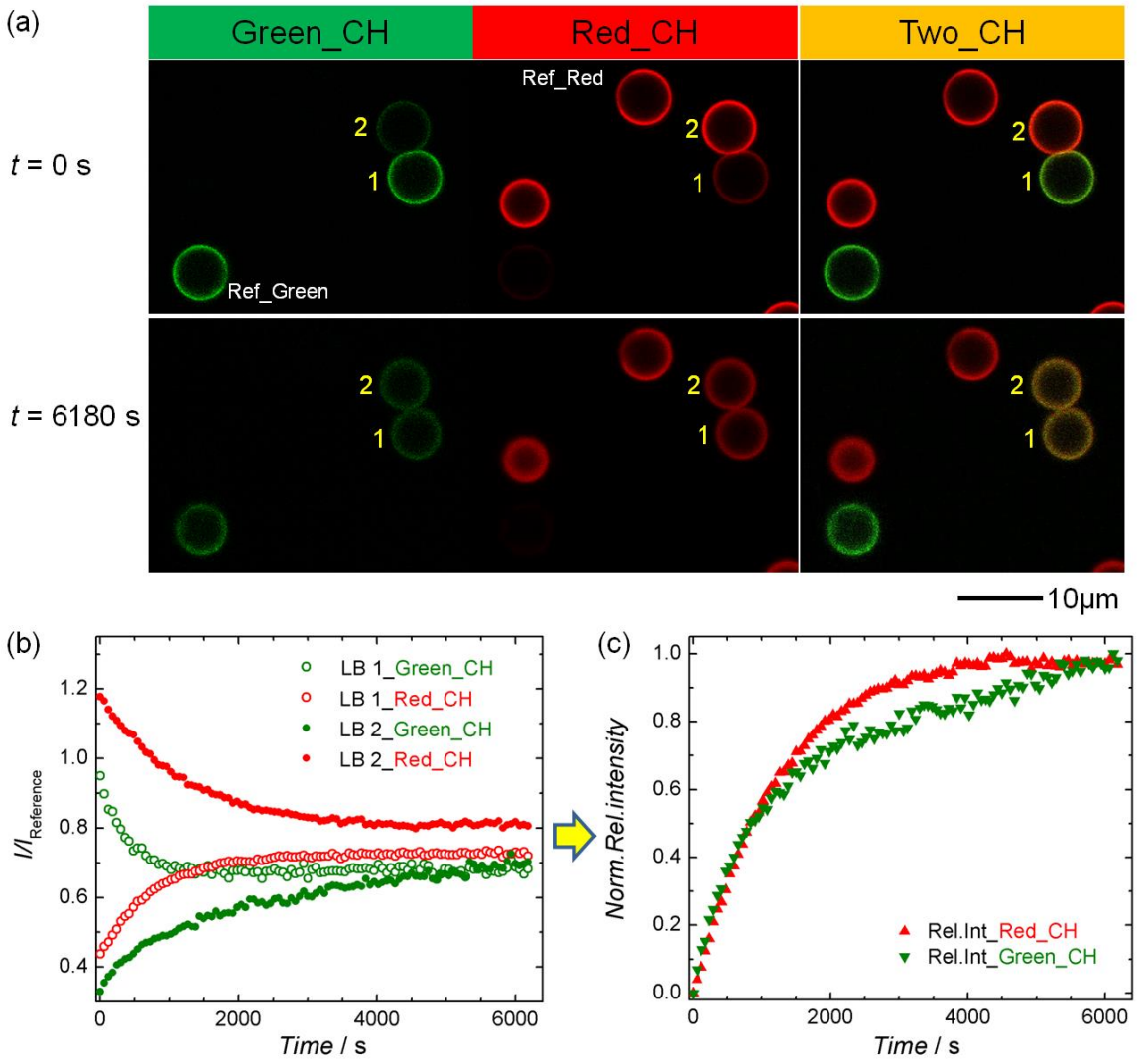

Figure 3-25 Real-time monitoring of lipid diffusion between LB-*i*-K3 and LB-*i*-E3 in a fully fused pair. A single Texas Red-labeled LB-*i*-E3 (Ref_Red) and NBD-labeled LB-*i*-K3 (Ref_Green) are chosen as references. (a) Fluorescence photographs of green channel (Green_CH, left), red channel (Red_CH, middle) and addition of two channels (Two_CH, right) at t = 0 s (top) and t = 6180 s (bottom), where LB-*i*-K3 is named LB 1 and LB-*i*-E3 is named LB 2, t = 0 s is defined 20 minutes after mixing the two populations of beads. (b) Curves of intensity vs time (left) of both beads (LB 1 and LB 2) with both channels (Green_CH and Red_CH) indicate the lipid diffusion between two beads. (c) Relative intensity curves that are obtained from curves in (b), where the relative intensity of the red channel (red triangle) is the ratio of LB 1_Red_CH and LB 2_Red_CH while the relative intensity of the green channel (green triangle) is the ratio of LB 2_Green_CH and LB 1_Green_CH.

3.4.3 STATISTICAL ANALYSIS OF I_{RI}

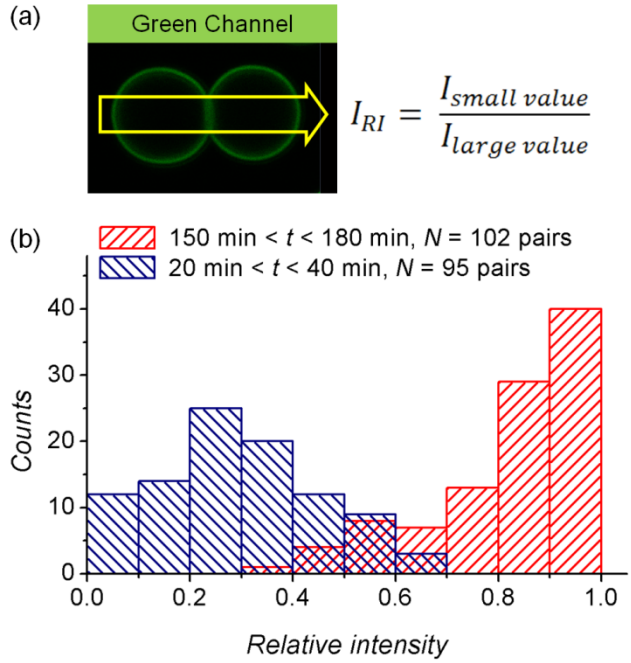

Figure 3-26 Relative intensity analysis of LB-*i*-K3/LB-*i*-E3 pairs at different periods. (a) Principle of relative intensity analysis based on green channel (NBD). Since the bead population is unable to identify when same sizes of beads are used, I_{RI} is the ratio of small value and large value. (b) Statistical analysis of I_{RI} during 20 min < t < 40 min (blue) and 150 min < t < 180 min (red), t is referred the time after mixing of the two populations of beads. 95 pairs and 102 pairs are counted, respectively.

Statistical analysis of relative intensity (I_{RI}) is performed on LB-*i*-K3/LB-*i*-E3 in different time regimes in order to evaluate the efficiency of fusion events (Figure 3-26). Different from the statistical method in SB-*i*-K3/LB-*i*-K3 assay, the histograms of I_{RI} provide distribution of I_{RI} of all tethered pairs other than classify the tethered pairs as docking, hemifuion and full fusion. Figure 3-26b shows the efficiency of full fusion of LB-*i*-K3/LB-*i*-E3 is up to 40% (if $0.9 < I_{RI} \leq 1.0$ is defined as full fusion). On the other hand, in SB-*i*-K3/LB-*i*-K3, only hemifusion occurs in the absence of Ca^{2+} while the efficiency of full fusion is 9.3% in the presence of Ca^{2+}. Again, this high efficiency of full fusion in LB-*i*-K3/LB-*i*-E3 mixture is attributed to van der Waals interaction between

charged membrane-coated beads, which contributes the additional energy needed for detachment of the supported membrane from the silica bead and thus facilitates full fusion.

3.5 PROS AND CONS

In the section, pros and cons of this 2D membrane-coated bead-based fusion assay are summarized comparing to the liposome-based assays including GUV-based assay and single vesicle assays. The disadvantages of bulk liposome-based assay are described in chapter one hence not be discussed here.

3.5.1 CONS

Obviously, there are two main disadvantages of this bead-based method. One is that it cannot measure content mixing, which is an important criterion for membrane fusion since lipid mixing can occur without or with notably delayed content mixing.[34, 48] For example, content mixing starts several seconds after lipid mixing in the process of influenza virus membrane.[49] This may be solved by using porous beads or polymer coated beads like the polymer cushion-supported bilayer used in single vesicle-SLB assay. The other disadvantage is that this bead-based assay do not allow the kinetic investigation of fusion process due to the tiny bottleneck contact zone, so that the lipid diffusion is extremely slow than in the native surroundings. This may be improved by the mechanism study of fusion pore opening and using microscope with higher resolution and sensitivity.

3.5.2 PROS

Albeit the limitations of bead-based assay, it also provides several advantages compared to liposome-based assays, such as simpler preparation, easy operation, direct observation and less labeling. Besides, this assay offers some information that the other method cannot offer, *e.g.* multiple fusion. Notably, it is advantageous in indentifying and screening inhibitors for inhibiting fusion in prefusion state.

In single vesicle assay, LUVs are always used for high encapsulated volume and lipid incorporation of fluorophore (up to four kinds of fluorophore with high concentrations).

To monitor the fusion process, sometimes a complicated TIRF with three-color excitation and two CCDs are employed.[34, 35] The extensive labeling and high intensity excitation might cause problems in the detection of fluorescence distinct for light-scattering artifacts and might compromise the fusogenic properties or peptides and proteins by altering the zeta potential of the liposomes and changing the microenvironment of the decisive constituents.[50] However, in bead-based assay, only one fluorophore (Texas Red) with 0.5% is necessary and the experiments can be easily performed in any standard biological laboratory. The populations of fusogenic membrane-coated beads can be clearly distinguished by size by normal optical microscopy.

GUVs are frequently used as a model membrane since their sizes are comparable to an entire cell.[51] They have been used for visualization of membrane fusion assays and conceivably as an attractive replacement for beads.[52, 53] However, this membrane-coated bead-based approach cannot be realized with GUVs. Firstly, GUVs are considerably more polydisperse and display thermally excited membrane undulations, which requires very strong attractive forces to overcome the barrier posed by the so-called Helfrich repulsion. Moreover, two GUVs merge into a single, larger vesicle, preventing the ability to reconstruct the history with only one fluorophore. This is because GUVs display large size differences and are hardly visible in conventional microscopy without labeling. Also often ignored are the inevitable osmotic gradients between the interior of the liposome and the external solution. Considering that area dilatation of lipid bilayers is limited to only few percent, a change in osmolarity of 5-10 mM is sufficient to rupture the GUVs in a size regime of 50-100 μm, not to mention that stress fosters fusion. Last but not least, GUVs need to be sedimented and fixed on the substrate as well as LUVs in single vesicle assay. This exerts pre-stress and requires sedimentation and attachment strategies that might interfere with fusion.[54] However, the fixation problem was perfectly solved in this bead assay by introducing ions.

3.6 REFERENCE

[1]. Pähler, G., Panse, C., Diederichsen, U., and Janshoff, A. (2012) Coiled-Coil Formation on Lipid Bilayers-Implications for Docking and Fusion Efficiency, *Biophys J 103*, 2295-2303.

[2]. Lorenz, B., Alvarez de Cienfuegos, L., Oelkers, M., Kriemen, E., Brand, C., *et al.* (2012) Model System for Cell Adhesion Mediated by Weak Carbohydrate-Carbohydrate Interactions, *J Am Chem Soc 134*, 3326-3329.

[3]. Schuy, S., Treutlein, B., Pietuch, A., and Janshoff, A. (2008) In Situ Synthesis of Lipopeptides as Versatile Receptors for the Specific Binding of Nanoparticles and Liposomes to Solid-Supported Membranes, *Small 4*, 970-981.

[4]. Schuy, S., Schäfer, E., Yoder, N. C., Kumar, K., Vogel, R., *et al.* (2009) Lipopeptides Derived from HIV and Siv Mimicking the Prehairpin Intermediate of Gp41 on Solid Supported Lipid Bilayers, *J Struct Biol 168*, 125-136.

[5]. Richter, R. P., Berat, R., and Brisson, A. R. (2006) Formation of Solid-Supported Lipid Bilayers: An Integrated View, *Langmuir 22*, 3497-3505.

[6]. Kasson, P. M., and Pande, V. S. (2004) Molecular Dynamics Simulation of Lipid Reorientation at Bilayer Edges, *Biophys J 86*, 3744-3749.

[7]. Jiang, F. Y., Bouret, Y., and Kindt, J. T. (2004) Molecular Dynamics Simulations of the Lipid Bilayer Edge, *Biophys J 87*, 182-192.

[8]. Richter, R., Mukhopadhyay, A., and Brisson, A. (2003) Pathways of Lipid Vesicle Deposition on Solid Surfaces: A Combined Qcm-D and Afm Study, *Biophys J 85*, 3035-3047.

[9]. Richter, R. P., and Brisson, A. R. (2005) Following the Formation of Supported Lipid Bilayers on Mica: A Study Combining Afm, Qcm-D, and Ellipsometry, *Biophys J 88*, 3422-3433.

[10]. Keller, C. A., and Kasemo, B. (1998) Surface Specific Kinetics of Lipid Vesicle Adsorption Measured with a Quartz Crystal Microbalance, *Biophys J 75*, 1397-1402.

[11]. Reviakine, I., Simon, A., and Brisson, A. (2000) Effect of Ca^{2+} on the Morphology of Mixed Dppc-Dops Supported Phospholipid Bilayers, *Langmuir 16*, 1473-1477.

[12]. Reimhult, E., Höök, F., and Kasemo, B. (2003) Intact Vesicle Adsorption and Supported Biomembrane Formation from Vesicles in Solution: Influence of Surface Chemistry, Vesicle Size, Temperature, and Osmotic Pressure, *Langmuir 19*, 1681-1691.

[13]. Radler, J., Strey, H., and Sackmann, E. (1995) Phenomenology and Kinetics of Lipid Bilayer Spreading on Hydrophilic Surfaces, *Langmuir 11*, 4539-4548.

[14]. Richter, R. P., Doctoral thesis (2004) The Formation of Solid-Supported Lipid Membranes and Two-Dimensional Assembly of Proteins., Université Bordeaux I,

[15]. Bao, C. X., Pähler, G., Geil, B., and Janshoff, A. (2013) Optical Fusion Assay Based on Membrane-Coated Spheres in a 2D Assembly, *J Am Chem Soc 135*, 12176-12179.

[16]. Lorenz, B., Keller, R., Sunnick, E., Geil, B., and Janshoff, A. (2010) Colloidal Probe Microscopy of Membrane-Membrane Interactions: From Ligand-Receptor Recognition to Fusion Events, *Biophys Chem 150*, 54-63.

[17]. Tamm, L. K., and Mcconnell, H. M. (1985) Supported Phospholipid-Bilayers, *Biophys J 47*, 105-113.

[18]. Seu, K. J., Pandey, A. P., Haque, F., Proctor, E. A., Ribbe, A. E., *et al.* (2007) Effect of Surface Treatment on Diffusion and Domain Formation in Supported Lipid Bilayers, *Biophys J 92*, 2445-2450.

[19]. Grakoui, A., Bromley, S. K., Sumen, C., Davis, M. M., Shaw, A. S., *et al.* (1999) The Immunological Synapse: A Molecular Machine Controlling T Cell Activation, *Science 285*, 221-227.

[20]. Otterstrom, J., and van Oijen, A. M. (2013) Visualization of Membrane Fusion, One Particle at a Time, *Biochemistry 52*, 1654-1668.

[21]. Diao, J. J., Su, Z. L., Ishitsuka, Y., Lu, B., Lee, K. S., *et al.* (2010) A Single-Vesicle Content Mixing Assay for SNARE-Mediated Membrane Fusion, *Nat Commum 1*, 1-6.

[22]. Diao, J. J., Ishitsuka, Y., Lee, H., Joo, C., Su, Z. L., *et al.* (2012) A Single Vesicle-Vesicle Fusion Assay for in Vitro Studies of SNAREs and Accessory Proteins, *Nat Protoc 7*, 921-934.

[23]. Domanska, M. K., Kiessling, V., Stein, A., Fasshauer, D., and Tamm, L. K. (2009) Single Vesicle Millisecond Fusion Kinetics Reveals Number of SNARE Complexes Optimal for Fast SNARE-Mediated Membrane Fusion, *J Biol Chem 284*, 32158-32166.

[24]. Christensen, S. M., Mortensen, M. W., and Stamou, D. G. (2011) Single Vesicle Assaying of SNARE-Synaptotagmin-Driven Fusion Reveals Fast and Slow Modes of Both Docking and Fusion and Intrasample Heterogeneity, *Biophys J 100*, 957-967.

[25]. Bowen, M. E., Weninger, K., Brunger, A. T., and Chu, S. (2004) Single Molecule Observation of Liposome-Bilayer Fusion Thermally Induced by Soluble N-Ethyl Maleimide Sensitive-Factor Attachment Protein Receptors (SNAREs), *Biophys J 87*, 3569-3584.

[26]. Marsden, H. R., Elbers, N. A., Bomans, P. H. H., Sommerdijk, N. A. J. M., and Kros, A. (2009) A Reduced SNARE Model for Membrane Fusion, *Angew Chem Int Ed 48*, 2330-2333.

[27]. Versluis, F., Dominguez, J., Voskuhl, J., and Kros, A. (2013) Coiled-Coil Driven Membrane Fusion: Zipperlike Vs. Non-Zipper-Like Peptide Orientation, *Faraday Discuss 166*, 349-359.

[28]. Versluis, F., Voskuhl, J., van Kolck, B., Zope, H., Bremmer, M., *et al.* (2013) In Situ Modification of Plain Liposomes with Lipidated Coiled Coil Forming Peptides Induces Membrane Fusion, *J Am Chem Soc 135*, 8057-8062.

[29]. Heidelberger, R., Heinemann, C., Neher, E., and Matthews, G. (1994) Calcium-Dependence of the Rate of Exocytosis in a Synaptic Terminal, *Nature 371*, 513-515.

[30]. Peters, C., and Mayer, A. (1998) Ca^{2+}/Calmodulin Signals the Completion Docking and Triggers a Late Step of Vacuole Fusion, *Nature 396*, 575-580.

[31]. Jahn, R., and Scheller, R. H. (2006) SNAREs-Engines for Membrane Fusion, *Nat Rev Mol Cell Biol 7*, 631-643.

[32]. Chapman, E. R. (2002) Synaptotagmin: A Ca^{2+} Sensor That Triggers Exocytosis?, *Nat Rev Mol Cell Bio 3*, 498-508.

[33]. Jahn, R., and Fasshauer, D. (2012) Molecular Machines Governing Exocytosis of Synaptic Vesicles, *Nature 490*, 201-207.

[34]. Kyoung, M., Srivastava, A., Zhang, Y. X., Diao, J. J., Vrljic, M., *et al.* (2011) In Vitro System Capable of Differentiating Fast Ca^{2+}-Triggered Content Mixing from Lipid Exchange for Mechanistic Studies of Neurotransmitter Release, *Proc Nat Acad Sci USA 108*, 304-313.

[35]. Kyoung, M. J., Zhang, Y. X., Diao, J. J., Chu, S., and Brunger, A. T. (2013) Studying Calcium-Triggered Vesicle Fusion in a Single Vesicle-Vesicle Content and Lipid-Mixing System, *Nat Protoc 8*, 1-16.

[36]. Pähler, G., Lorenz, B., and Janshoff, A. (2013) Impact of Peptide Clustering on Unbinding Forces in the Context of Fusion Mimetics, *Biochem Bioph Res Comm 430*, 938-943.

[37]. Harrison, S. C. (2008) Viral Membrane Fusion, *Nat Struct Mol Biol 15*, 690-698.

[38]. Frey, G., Rits-Volloch, S., Zhang, X. Q., Schooley, R. T., Chen, B., *et al.* (2006) Small Molecules That Bind the Inner Core of Gp41 and Inhibit HIV Envelope-Mediated Fusion, *Proc Nat Acad Sci USA 103*, 13938-13943.

[39]. Lin, P. F., Blair, W., Wang, T., Spicer, T., Guo, Q., *et al.* (2003) A Small Molecule HIV-1 Inhibitor That Targets the HIV-1 Envelope and Inhibits Cd4 Receptor Binding, *Proc Nat Acad Sci USA 100*, 11013-11018.

[40]. Schuy, S., Schäfer, E., Yoder, N. C., Hobe, S., Kumar, K., *et al.* (2009) Coiled-Coil Lipopeptides Mimicking the Prehairpin Intermediate of Glycoprotein Gp41, *Angew Chem Int Ed 48*, 751-754.

[41]. Colman, P. M., and Lawrence, M. C. (2003) The Structural Biology of Type I Viral Membrane Fusion, *Nat Rev Mol Cell Bio 4*, 309-319.

[42]. Apostolovic, B., and Klok, H. A. (2008) PH-Sensitivity of the E3/K3 Heterodimeric Coiled Coil, *Biomacromolecules 9*, 3173-3180.

[43]. Marsden, H. R., Tomatsu, I., and Kros, A. (2011) Model Systems for Membrane Fusion, *Chem Soc Rev 40*, 1572-1585.

[44]. Chen, Y. A., and Scheller, R. H. (2001) SNARE-Mediated Membrane Fusion, *Nat Rev Mol Cell Biol 2*, 98-106.

[45]. Lin, R. C., and Scheller, R. H. (1997) Structural Organization of the Synaptic Exocytosis Core Complex, *Neuron 19*, 1087-1094.

[46]. Weninger, K., Bowen, M. E., Chu, S., and Brunger, A. T. (2003) Single-Molecule Studies of SNARE Complex Assembly Reveal Parallel and Antiparallel Configurations, *Proc Nat Acad Sci USA 100*, 14800-14805.

[47]. Verwey, E. J. W. (1947) Theory of the Stability of Lyophobic Colloids, *J phys Colloid Chem 51*, 631-636.

[48]. Jun, Y., and Wickner, W. (2007) Assays of Vacuole Fusion Resolve the Stages of Docking, Lipid Mixing, and Content Mixing, *Proc Nat Acad Sci USA 104*, 13010-13015.

[49]. Floyd, D. L., Ragains, J. R., Skehel, J. J., Harrison, S. C., and van Oijen, A. M. (2008) Single-Particle Kinetics of Influenza Virus Membrane Fusion, *Proc Nat Acad Sci USA 105*, 15382-15387.

[50]. Düzgünes, N. (2003) Fluorescence Assays for Liposome Fusion, *Liposomes, Pt B 372*, 260-274.

[51]. Fenz, S. F., and Sengupta, K. (2012) Giant Vesicles as Cell Models, *Integr Biol 4*, 982-995.

[52]. Haluska, C. K., Riske, K. A., Marchi-Artzner, V., Lehn, J. M., Lipowsky, R., *et al.* (2006) Time Scales of Membrane Fusion Revealed by Direct Imaging of Vesicle Fusion with High Temporal Resolution, *Proc Nat Acad Sci USA 103*, 15841-15846.

[53]. Heuvingh, J., Pincet, F., and Cribier, S. (2004) Hemifusion and Fusion of Giant Vesicles Induced by Reduction of Inter-Membrane Distance, *Eur Phys J E 14*, 269-276.

[54]. Walde, P., Cosentino, K., Engel, H., and Stano, P. (2010) Giant Vesicles: Preparations and Applications, *Chembiochem 11*, 848-865.

4 CONCLUSION

A novel assay of membrane fusion is established based on membrane-coated beads in a 2D assembly. This assay allows identifying the different stages of the fusion process. Membrane fusion driven by heterodimeric coiled coil formation as a proof of concept using fusogenic K- and E-peptides provided results comparable to those obtained with conventional liposome assays, but with additional information on docking efficiency.[1]

In this fusion assay, LBs and SBs are modified with *i*-K3Cys (LB-*i*-K3) and *i*-E3Cys (SB-*i*-E3) respectively and LBs are fluorescent labeled. The populations of fusogenic beads can be distinguished by size discrimination. When LB-*i*-K3and SB-*i*-E3 are mixed in water, the fusion process terminates in hemifusion. Interestingly, all fusion events including docking, hemifusion and full fusion are observed in the presence of Ca^{2+} in one experiment. This may due to the bridging effect of calcium ions binding to PC and non-reacted negative MCC-DOPE.

Block or change the zipping conformational of coiled coil structure is necessary for the viral infection of host cells. In this bead-based assay, the introduction of inhibitors (*i*-E3Cys) efficiently decreases the hemifusion efficiency and abolishes full fusion (in the presence of Ca^{2+}). Therefore, this approach is expected to be an invaluable tool to identify small-molecule inhibitors of viral fusion with unprecedented accuracy in prefusion state.

Multiple fusion could be observed and distinguished, which takes place among more than two fusogenic membrane-coated beads. The orientations of coiled coil formation, including parallel and antiparallel orientations, are shown to have no effect on the fusion process in this bead-based assay. Most interestingly, size-dependent assays employed beads with increasing diameter scale, demonstrate that van der Waals interaction could provided energy for supported membrane detaching from the silica beads, hence promote membrane fusion.

In conclusion, comparing to the typical liposome-based assay, this bead-based assay can distinguish among docking, hemifusion and full fusion without interference from light scattering and use of a single fluorophore at very low concentration.[2, 3] In addition, the curvature of fusogenic membranes can be easily controlled and through variation of the

employed bead sizes, differences in fusogenity can be addressed. Furthermore, size-dependent assays open a door to controllable membrane fusion. At last, this bead-based assay, however, can be realized with ordinary laboratory, and is compliant with high-throughput multi-well techniques, *e.g.*, inhibitor screening.

Reference

[1]. Pähler, G., Panse, C., Diederichsen, U., and Janshoff, A. (2012) Coiled-Coil Formation on Lipid Bilayers-Implications for Docking and Fusion Efficiency, *Biophys J 103*, 2295-2303.

[2]. Lee, A. G. (2004) How Lipids Affect the Activities of Integral Membrane Proteins, *BBA-Biomembranes 1666*, 62-87.

[3]. Repakova, J., Holopainen, J. M., Karttunen, M., and Vattulainen, I. (2006) Influence of Pyrene-Labeling on Fluid Lipid Membranes, *J Phys Chem B 110*, 15403-15410.

ABBREVIATIONS

AFM	Atomic force microscopy
CD	Circular dichroism
CH	Cholesterol
CLSM	Confocal laser scanning microscopy
DOEPC	1,2-dioleoyl-*sn*-glycero-3-ethylphosphocholine
DMOPC	1,2-dimyristoleoyl-*sn*-glycero-3-phosphocholine
DOPC	1,2-dioleoyl-*sn*-glycero-3-phosphocholine
ESI-MS	Electrospray ionization mass spectrometry
FRAP	Fluorescence recovery after photobleaching
FRET	Fluorescence resonance energy transfer
GUV	Giant unilamellar vesicles
HEPES	4-(2-hydroxyethyl)-1-piperazineethanesulfonic acid
i-E3Cys	Peptide Ac-$(KELAAIE)_3$-GWGGGC-NH_2
i-K3Cys	Peptide Ac-WG-$(EKLAAIK)_3$-GGGGC-NH_2
K3Cys	Peptide Ac-WG-$(KIAALKE)_3$-GGGGC-NH_2
LB	Large beads (diameter 6.5 µm)
LLB	Larger beads (diameter 7.3 µm)
LUV	Large unilamellar vesicle
MCC-DOPE	1,2-dioleoyl-*sn*-glycero-3-phosphoethanolamine-N-[4-(pmaleimido methyl)cyclohexane-carboxamide
MLV	Multilamellar vesicle
MVV	Multivesicular vesicle
NBD	N-(7-nitro-2,1,3-benzoxadiazol-4-yl))
PC	Phosphatidylcholine
PE	Phosphatidylethanolamine
POPC	1-palmitoyl-2-oleoyl-*sn*-glycero-3-phosphocholine
POPE	1-palmitoyl-2-oleoyl-*sn*-glycero-3-phosphoethanolamine
PS	Phosphatidylserine
QCM	Quartz crystal microbalance

ROI	Region of interest
RP-HPLC	Reversed phase high-performance liquid chromatography
SB	Small beads (diameter 4.7 µm)
SLB	Solid supported bilayer
SNARE	Soluble *N*-ethylmaleimide-sensitive-factor attachment protein receptor
SPPS	Solid phase peptide synthesis
SPR	Surface plasmon resonance
SUV	Small unilamellar vesicle
Texas Red	Texas Red-1,2-dihexadecyl-*sn*-glycero-3-phosphoethanolamine
TIRF	Total internal reflection fluorescence
vdW	van der Waals (interaction)

ACKNOWLEDGEMENTS

I gratefully acknowledge the financial support of my work in Göttingen by Chinese Scholarship Council (CSC) and Fond der Chemischem In dustrie.

I have learned a tremendous amount about different aspects during my PhD study, for that I am indebted to my supervisor Prof. Dr. Andreas Janshoff. He gave me the opportunity to work in his lab and guided me for the research. I was always encouraged by his positive attitude tolerance and patience.

I am also very grateful to Prof. Dr. Philipp Vana for agreeing to be my second supervisor and sincerely appreciate his support. I also thank Prof. Burkhard Geil, Prof. Ulf Diederichsen, Prof. Bert de Groot and Dr. Thomas Burg for their interest in this manuscript and their agreement to be part of the thesis committee.

I thank Prof. Burkhard Geil for his kind cooperation, useful suggestion of my work and careful correction of this manuscript.

I thank Dr. Gesa Pähler for inducing me into this work environment, showing me various techniques, giving me suggestions, and always supporting me for research.

I think Frau Lappe for her patience the administrative support.

I thank Thilo Baronsky, Marieelen Oelkers and Hannes Witt for revising this manuscript.

I am deeply indebted to Weifeng for his support and having tolerated all my bad moods. I feel that we have grown together throughout this PhD study and hopefully continue to do so for the rest of our careers and life.

I wish to thank my parents and friends for their support and unquestioning faith, which helped and encouraged me in every stage of my life.

I thank all the very nice colleagues in both Janshoff and Steinem groups, for their kindly support and help, great activities, cheerful working environment, relaxed communication. I could never have made this amazing journey without them and I will always cherish their friendship!

CURRICULUM VITAE

Chunxiao Bao

Date of birth: 1983–03–31

Place of birth: China

Nationality: Chinese

Education

11/2009–Present	PhD candidate Supervisor: Prof. Andreas Janshoff Institute of Physical Chemistry, Georg-August-Universität Göttingen, Göttingen, Germany
09/2006–07/2009	Master of Science Supervisor: Prof. Bai Yang State Key Laboratory of Supramolecular Structure and Materials, Jilin University, Changchun, China
09/2002–07/2006	Bachelor of Science Supervisor: Prof. Bai Yang Institute of Chemistry, Jilin University, Changchun, China

Selected publication

Bao, C. X., Pähler, G., Geil, B., and Janshoff, A. (2013) Optical Fusion Assay Based on Membrane-Coated Spheres in a 2D Assembly, *J Am Chem Soc 135*, 12176-12179.

Poster-presentations

1. July 2012: Göttinger Chemie Forum, Göttingen, Germany
2. Sept 2012: Annual Meeting of the German Biophysical Society, Göttingen, Germany
3. July 2013: 9th European Biophysics Congress (EBSA2013), Lisbon, Protugal